POLITECHNIKA ŚLĄSKA

Wydział Mechaniczny Technologiczny

Katedra Materiałów Inżynierskich i Biomedycznych

PRACA DOKTORSKA

Wpływ składu chemicznego materiałów proszkowych na bazie żelaza na właściwości elementów spiekanych

mgr inż. Agnieszka Stanula

Dyscyplina: Inżynieria Materiałowa

Promotor:

dr hab. inż. Wirginia Pilarczyk, prof. PŚ

Gliwice, 2023 r.

W pierwszej kolejności słowa podziękowania kieruję
do ***pani dr hab. inż. Wirginii Pilarczyk, prof. PŚ, promotorki mojej pracy doktorskiej.***
Dziękuję za opiekę naukową oraz wsparcie merytoryczne,
które przyczyniło się do powstania tej pracy.

Moje podziękowania otrzymuje też ***Mark Jager****,* ***Assistant Professor and Program Director***
[adiunkt i kierownik projektu],
Welding and Metallurgical Engineering Technology, Wayne State University [Technologia
Inżynierii Metalurgicznej i Spawalnictwa z Uniwersytetu Stanowego Wayne]
za udzielanie konsultacji podczas pisania mojej pracy doktorskiej.

Szczególne podziękowania kieruję ***do rodziców***
za wspieranie mojej edukacji od najmłodszych lat.

Podziękowania kieruję także do ***moich najbliższych*** *– za cierpliwość.*

SILESIAN UNIVERSITY OF TECHNOLOGY

Faculty of Mechanical Engineering

Department of Engineering Materials and Biomaterials

DOCTORAL THESIS

Effect of the chemical composition of iron-based powder materials on the properties of sintered components

Ms. Agnieszka Stanula, M.Sc., Eng.

Discipline: Material engineering

Supervisor:

Wirginia Pilarczyk, Associate Professor, Ph.D., Professor of the Silesian University of Technology

Gliwice, 2023

In the first instance, I would like to thank
Ms Virginia Pilarczyk, Ph.D., Professor of the Silesian University of Technology, supervisor of my doctoral thesis. *Thank you for your scientific guidance and support, which has greatly contributed to this doctoral thesis.*

My thanks also go to ***Mark Jager, Assistant Professor and Program Director*** *[Assistant Professor and Project Manager],*
Welding and Metallurgical Engineering Technology, Wayne State University
for providing consultation during the writing of my thesis.

My special thanks go to ***my parents***
for supporting my education from an early age.

My thanks also go to ***my loved ones*** *- for their patience.*

Contents

Symbols

Ed compression module

σd0.2 yield strength in compression

σdM compressive strength

ƐdB (disproportionate (only plastic, permanent) relative shortening at failure)

ƐdtM (total relative shortening at compressive strength (at maximum force))[1]

Agnieszka Stanula

1. Introduction

A key in powder material manufacturing is the use of appropriate powder materials that fit the process conditions. Many parameters affect the production and the quality of the parts being built. An accurate assessment involves, besides other things, the powder flowability, which should be sufficient to create good-quality powder layers. [2]

Particle size, shape, and the physical characteristics of a metal powder (specific surface) have an effect on the behaviour of the powder during the compaction and sintering process.

The composition and surface contamination (the chemical properties) have a marked influence on the properties of the sintered metal.

The principal properties related to the powder particles themselves are:

1. Particle size and distribution.
2. Specific surface and particle density.
3. Particle shape.
4. Chemical properties.
5. Packaging and moulding properties. [3]

Powder Metallurgy parts formed by die compaction have inhomogeneous density distribution because of the friction between the powder compact, die wall and punches. Powder metallurgy is one of the most diverse manufacturing processes among the various metal forming technologies. The advantage of powder metallurgy is an ability to achieve near net shape forming. This production method saves material and energy, and in the production of structural parts, it offers higher precision. It eliminates most of the machining operations requires for casting and wrought products. It is more cost effective and environmentally friendly.

The powder metallurgy process is a fast, economical and high-volume method for producing precision parts from powder. There are a number of related consolidation techniques by which powders can be rolled into sheets, extruded into rods or isostatically compacted into parts with more complex geometries.

There are two main reasons for using a powder metallurgy product, cost savings compared to alternative processes and unique properties only achievable through powder metallurgy.

In about 80% of the production of structural parts from powder metallurgy, the main reason for choosing powder metallurgy is economic.

Components are designed to meet structural criteria in many applications. It is possible to produce sintered structural or mechanical parts with properties equal to or even better than parts produced by more traditional methods.

2. Literature review

2.1. Morphology and properties of iron-based powder metal.

Pore size measurements must be conducted on the raw materials used for powder metallurgy processes to ensure that the end-products yield the desirable mechanical properties. The strength, density, hardness and permeability of metal alloys produced from powder minerals depend upon the porosity of the raw constituents. [4]

The flowability of a powder is an important characteristic that depends on both the physical properties of the particle group and the testing method. The flowability is an indicator of the quality of the powder material itself and, therefore, the final component.

The principle of the Hall flow method (Figure 1) is very simple: 50 g of powder flows through a funnel and the time it takes is registered as the flow rate. The funnel has a standardised geometry with a 60°cone angle and ø2.5 mm outlet hole, (comparable standards ASTM B213, ISO 449). [5]
The principle of the Gustavsson Flow is that the 30° cone angle funnel has been established as ISO standard ISO 13517 and ø2.5 mm outlet hole. (Figure 2) [6]

The Hall Flowmeter (ISO 4490) is a standard used for determining flow in metallic powders including powders for hard metals. [7]
The Gustavsson Flowmeter (ISO 13517) is a new standard developed for determining flow in metallic powders including powders for hard metals and mixes of metallic powders and organic additives such as lubricants. The standard and horizontal vibration-free base, to support the funnel rigidly are indicated in Figure 3 and Figure 4. The difference between the Hall Flowmeter (ISO 4490)

and the Gustavsson Flowmeter (ISO 13517) is that the Hall Flowmeter has a 60° cone angle whereas the Gustavsson Flowmeter has a 30° cone angle. **[7]** There are arguments against the Hall Flowmeter method. One is that the method is not relevant for characterising the filling of tool dies.

Another problem that has been identified with the Hall Flowmeter method is that powder mixes, especially mixes with a high content of lubricant, graphite and/or other fine particulate additives, will not always freely flow through the funnel. In this situation, the idea of a modified funnel for the flow measurement of powder material mixes arose. [7]

Figure 1. Flow patterns in Hall Flowmeter [8]

Figure 2. Flow patterns in Gustavsson Flowmeter [8].

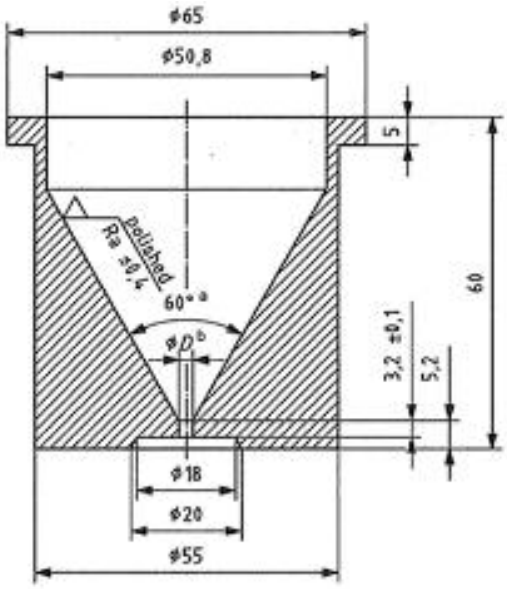

Figure 3. Hall Flowmeter Funnel [7]

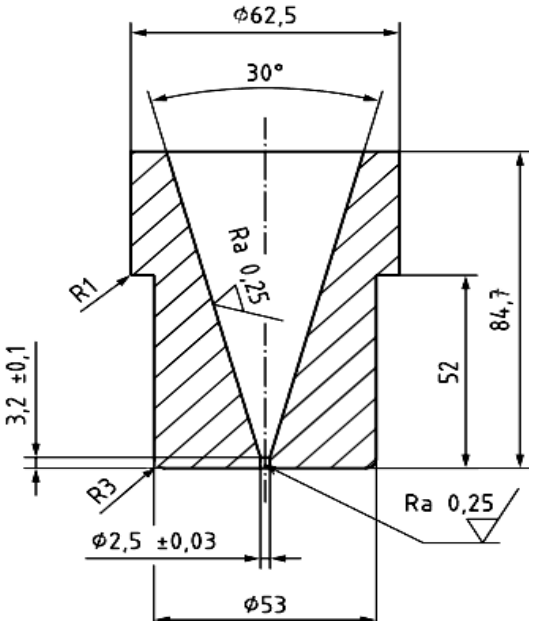

Figure 4. Gustavsson Flowmeter Funnel [6]

The Flow Test Methods is the ideal apparent density measurement instrument for research and quality management to efficiently evaluate the flow qualities and the apparent density of loose samples.

Apparent density - the ratio of the mass of porous material to the volume it occupies. Apart from the material itself, the calculations considers the volume of the pores between the grains of the material filled, for example, with air. [9]

The shape of powder grains can be determined by a descriptive or mathematical method. The descriptive method relies on norm PN-EN ISO 3253:2002 (Figure 5). The following nomenclature is adopted for powder grains. [10]

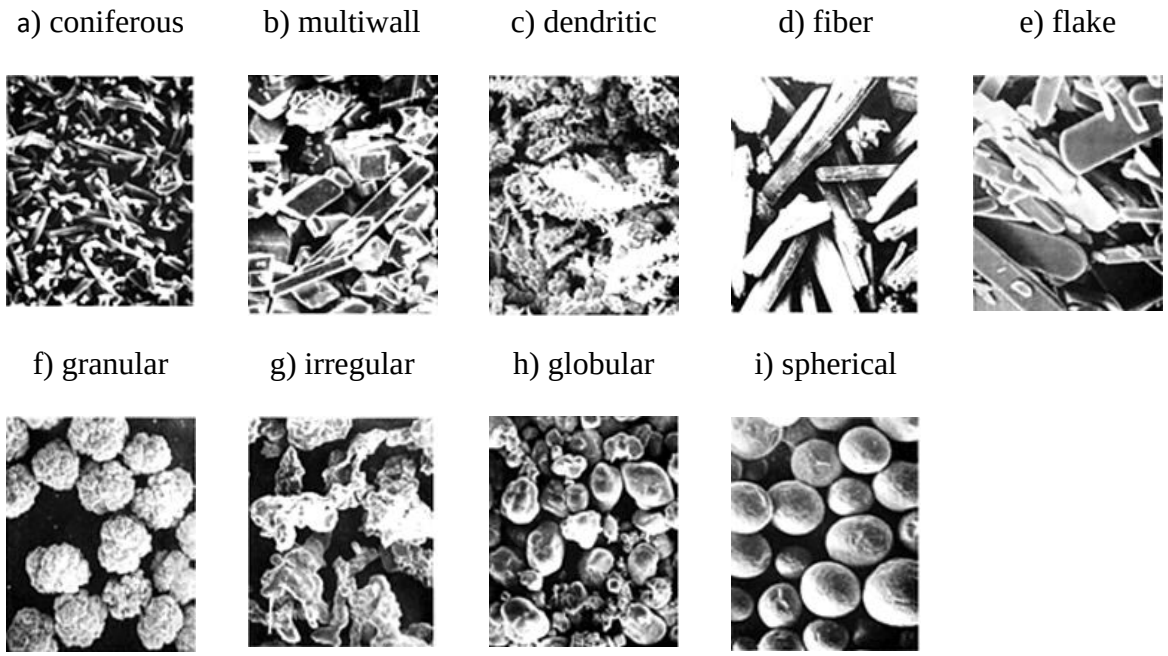

Figure 5. Nomenclature of the grain shape of powders by PN-EN ISO 3252 [10]

Powder materials manufactured from elemental iron powders that are essentially free of other alloying elements except carbon. The compacts are manufactured by pressing and sintering iron powder with or without graphite additions to introduce carbon. When the final density is to be 7.0 g/cm^3 or more, these materials may be processed by pressing, pre-sintering, repressing and sintering. Other processes such as warm-die compaction or warm compaction may also be used to achieve higher densities.

Powder Material carbon steel (F-0005) - Fe-C - materials are used primarily where moderate strength and hardness are desired (Table 1). Additionally, machinability might be required, such as drilling, tapping, lathe turning, milling, etc. They may also be steam treated for improved shelf life, pore closure and to increase hardness. The carbon content of a sintered structure can be calculated roughly from metallography form where 100% pearlite is equivalent to approximately 0.8% carbon. Carbon dissolves rapidly in iron, for example, after about five minutes at 1040°C. [11]

Table 1. Other Elements: 2% maximum may include other minor elements added for specific purposes. [11]

Material Designation	Fe	C	Element
F-0005	Balance	0.3	Minimum
	Balance	0.6	Maximum

Powder Material carbon steel (FC-0205 or FC-0208) - Fe-C-Cu are produced from admixtures of elemental iron powder and elemental copper powder with graphite powder (carbon) (Table 2). The proportions of each depend on the strength levels required and whether the material is to be used in the as-sintered or heat-treated condition. Because graphite diffuses readily into an iron powder matrix during sintering, a combined carbon of 0.8% or more is achievable. Copper powder is added to increase strength, hardness and wear resistance. Wear resistance can be improved by heat treatment. These materials find usage in medium strength structural applications. Admixed copper powder melts at approximately 1083°C. Copper dissolves in the iron and does not penetrate to the centre of the larger iron particles. During copper melting it diffuses or migrates leaving behind fairly large pores. These pores remain and can easily be seen in the microstructure.

Table 2. Other Elements: A 2% maximum may include other minor elements added for specific purposes. [11]

Material Designation	Fe	Cu	C	Element
FC-0205	Balance	1.5	0.3	Minimum
		3.9	0.6	Maximum
FC-0208	Balance	1.5	0.6	Minimum
		3.9	0.9	Maximum

The steam oxidation process consists of exposing ferrous material to a controlled superheated steam environment at 430-590°C for 1 to 4 hours. During the exposure the steam reacts with the ferrous material to produce an adherent blue-grey iron oxide (magnetite, Fe_3O_4):

$3Fe + 4H_2O$ (gas) -> $Fe_3O_4 + 4H_2$ (gas).

Both batch furnaces and continuous belt furnaces are used for the steam treatment of ferrous PM materials. The depth of penetration of the oxide into the part, product mass gain, oxide thickness and hardness of the finished products depends on the steam oxidation process parameters (time and temperature), the density of the material, the type of base powder used to create the part (atomised or sponge) and previous operations that could close-off the surface porosity. This additional process operation is applied in order to:

1. Seal the product to liquid or gas penetration, either for a subsequent process such as plating or for leak tightness in the product application.
2. Enhance the cosmetic appearance.
3. Increase apparent hardness to improve abrasive and adhesive wear resistance.
4. Increase corrosion resistance and improve shelf life.
5. Increase compressive yield strength results of these studies. [11]

Iron powder consists of several more iron particles. The particle size is in the range of 20 μm to 200 μm. The iron properties differ depending on the production method and source of a specific iron powder. There are two types of iron powders, sponge and atomised iron powder, and they are used in various applications based on their properties. The equilibrium phase diagram of the system Fe-C and an example of ferritic and pearlitic microstructure are presented on Figure 6-8.

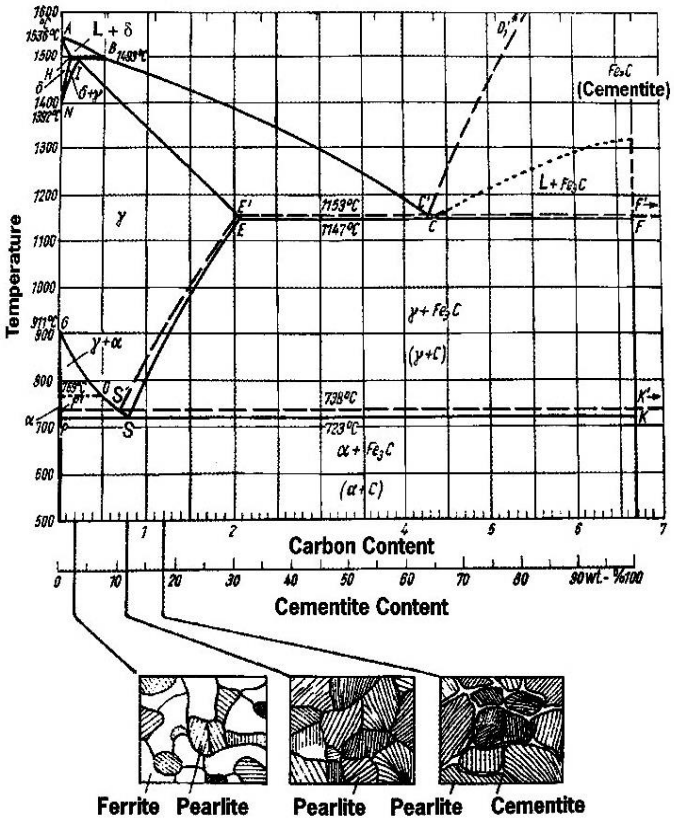

Figure 6. Equilibrium phase diagram of the system Fe-C (fully drawn lines = metastable system; dotted lines = stable system). [12]

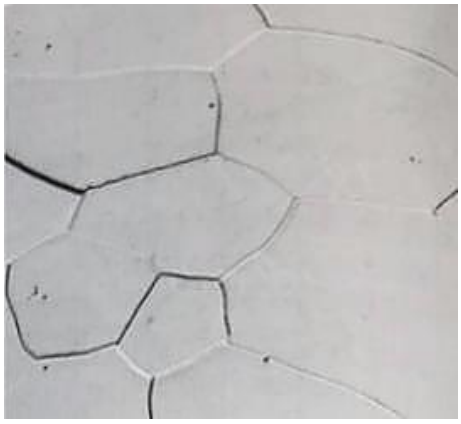

Figure 7. Example of ferritic microstructure [12]

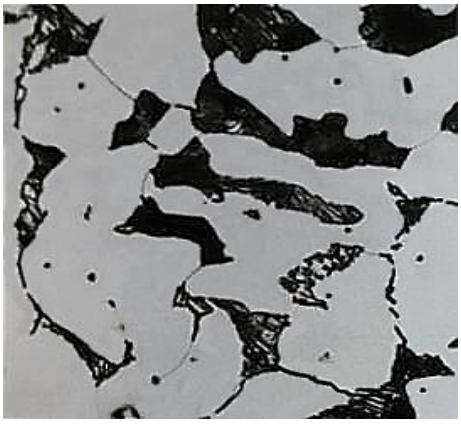

Figure 8. Example of pearlitic/ferritic microstructure [12]

Agnieszka Stanula

A crystal structure has three general properties: periodicity, directionality and completeness. Periodicity is the regular repetition in space of the atomic unit of the crystal. It is the basis of the remarkable plastic properties of crystals. Directionality of the crystal structure appears in the fact that properties like conductivity and elasticity vary with the direction of their measurement. Completeness is simply the filling of all crystal sites defined by the periodic structure with the required atoms.

The crystal structure presents graphically as a space lattice within which the sites of atoms are marked by points (or small circles). These points are referred to as lattice points. The basic unit of the crystal structure that repeats itself in all three directions of space is called the unit cell (Figure 9). The deforming edges of this cell are referred to as lattice constants, (usually a, b, c). [12]

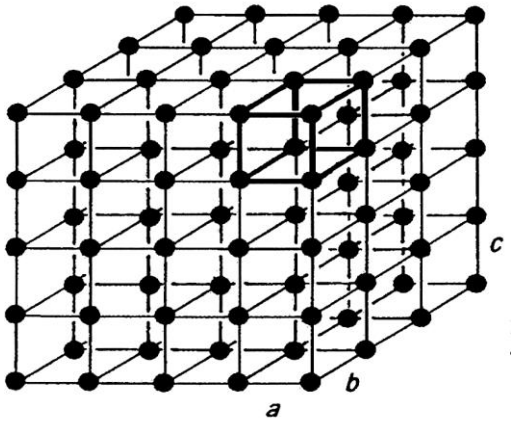

Figure 9. Unit cell in a crystal cell; lattice constants: a, b, c. [12]

The storage and handling of powders is a major challenge in the powder metallurgy industry. One of the major challenges with metallic powder is the pick-up of oxygen, which leads to oxide inclusions when considering materials with low oxygen solubility. The ductile fracture of metals generally occurs by nucleation, growth and coalescence of voids, and hard inclusions can act as nucleation sites for such voids thereby reducing fracture toughness. Hence oxygen pick-up needs to be kept to a minimum during powder handling and processing, especially for applications where the fracture toughness is crucial. Generally, a powder is kept in an inert atmosphere or vacuum to minimise oxygen pick-up, which makes powder storage

very expensive. An alternative strategy for controlling oxygen pick-up is to develop protective coatings on the powder as a part of the powder manufacturing process.

The flowability of a powder is another factor that particularly determines the reliability and quality of an additively manufactured product. The powder flow behaviour is generally influenced by the particle size and shape, surface roughness and interactions. In particular, surface cohesion due to the Van der Waals interaction can hinder powder flowability. The frictional behaviour of particles influenced by surface roughness also plays a role in powder flowability. Contact charging that results from friction leads to the transfer of an electric charge between powder particles, which in extreme cases and for some powders can result in fire and explosion hazards during storage and transport. [13]

2.2. Metal powder manufacturing methods

A wide variety of process may be used for the manufacture of metal powders each resulting in a product having its own particular characteristics in regard to the shape of the metal powder particles, the density of the particles themselves and the distribution of particle size. The particles may be dense, porous or hollow and, depending upon the process employed, may be spherical, flattened, angular and dendritic.

The choice of process is dictated by a number of considerations, including, of course, the economics of production and the commercial demand for a powder having the particular characteristics associated with its method of manufacture.

Not all metals and alloys necessarily lend themselves readily to manufacture by all of the methods available, and this is not surprising in view of the wide range of melting points covered by commercial metals and alloys, and because of the difference in reactivity between metals and the gases with which they may come into contact during the manufacturing process.

The primary production processes may be listed as follows:

1. Reduction of oxides. This is the oldest method for the manufacture of metallic materials, dating back to the charcoal fires of ancient history. It is the cheapest method for the production of powder. One of the cheapest iron powders produced utilises a carbon reduction of a high grade iron ore and this has been developed on a very large scale in Sweden, the Hoganas process

has been in operation since the early part of the present century. The product, which is known as Swedish sponge iron, is produced by reducing concentrates of iron ore with carbon in ceramic boxes or saggers that are charged into a tunnel kiln similar to that employed in the firing of bricks. The reducing agent used is either anthracite or coal dust, and, where necessary, limestone is used to absorb any sulphur. The product is a sintered cake of sponge iron of a fairly high level of purity (about 98%), and the sponge is subsequently broken down into powder by a form of pulverisation. It is understood that since the last war the newer grades of Swedish iron powders that have been introduced into the market result from the processing of the normal product with hydrogen, resulting in some degree of purification and, no doubt, a change in the characteristics of the final powder.

The reduction of oxides by hydrogen is probably the simplest of the methods employed in the manufacture of metal powders, and, provided that readily available and comparatively cheap sources of hydrogen and pure metal oxides exist, the process has a great deal in its favour. It is capable of yielding metal powders over a very wide range of particle sizes, which is controlled largely by the physical condition of the initial metal oxide and the reduction conditions, all of which are controllable features.

2. Reduction of salts. The most important process of this type so far developed is used for the production of copper, nickel and cobalt powders from ore concentrates or scrap metal. The raw material is leached with a suitable acid or alkali to obtain the metal in solution, this solution is then purified, and the metal powder participated using either hydrogen or carbon monoxide under pressure at an elevated temperature as the reducing agent. The scrap containing copper is treated with ammoniacal copper carbonate solution and then the copper powder is precipitated from the solution (after purification) by hydrogen under pressure at 175°C.

3. Thermal dissociation of metal compounds. Iron and nickel powders of high purity may be prepared from the massive metal and poor quality powder by the decomposition of the corresponding metal carbonyl. Iron powder is obtained by first passing carbon monoxide over iron at about 200°C and at atmospheric pressure when dissociation into carbon monoxide and iron takes place. The carbon monoxide is re-used. The preparation of nickel powder by the carbonyl process is very similar, differences being only in the required temperature and pressures. The powder obtained is spherical and during the growth of each particle from the gas phase, the metal is precipitated in layers, which on sectioning is indicated as centred rings. This structure is claimed to accelerate the sintering process.

4. Electrolysis. Metal either as a powder or in a form suitable for crushing may be obtained by the electrolysis of a wide range of solutions or fused salts. Sulphates, chlorides, cyanides, etc., are frequently used in solution either singly or as mixtures, and an organic reagent may also be added to promote the formation of the powder. Iron powder is produced commercially by the electrolysis of iron sulphate or chloride solution and a brittle deposit is obtained on the cathode, which must be removed at regular intervals. The deposit is then crushed into a powder, cleaned and dried, and then annealed prior to use. The purity of the iron powder is high and, although the costs of production are also high, it is frequently used for the production of high strength engineering components by powder metallurgy. The characteristics of the powder produced by electrolysis may be varied by controlling the bath composition and temperature, the current density, the shape of the electrodes, etc.

The current densities used for the preparation of powder are considerably higher than those required for plating and a slightly elevated bath temperature may be necessary. The shape of the particles prepared by electrolysis is usually dendritic and this causes the powder to have poor flow characteristics. However, if the powder is ground prior to use the angular nature of the particles will be destroyed. The preparation of alloy powders is possible by the use of baths containing more than one metal salt.

5. Atomisation. Atomisation consists of forcing a molten metal through an orifice and then breaking up this stream with a jet of gas or water. The particles of metal formed by the jet solidify extremely rapidly and, although the atmosphere may be air, only very superficial oxidation takes place. To completely prevent the oxidation an inert gas atmosphere is needed.

A wide range of different sizes of powder can be obtained by varying factors such as the temperature of the metal, the size of the orifice and the pressure and temperature of the jet fluid, but the particles formed are non-porous and frequently have poor compacting properties. It is the most important method of preparing powder due to the low costs of production and good quality of powder. [2]

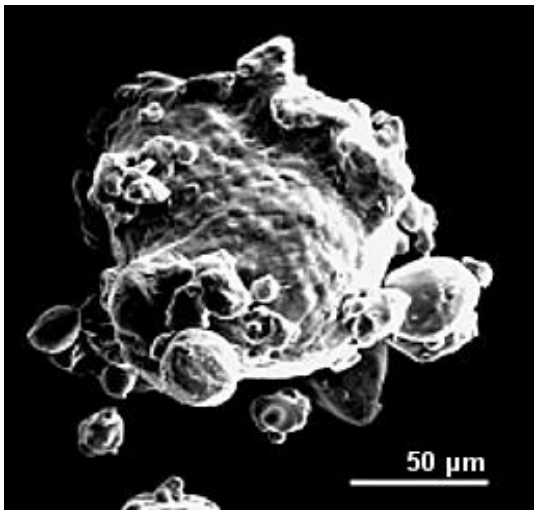

Figure 10. Atomised iron powder SEM [14]

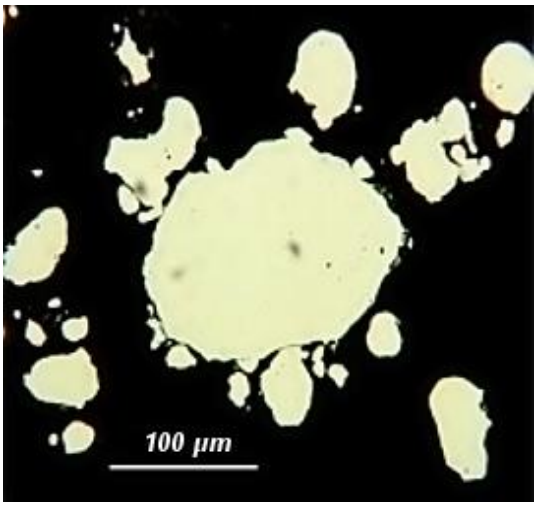

Figure 11. Atomised iron powder cross-section [14]

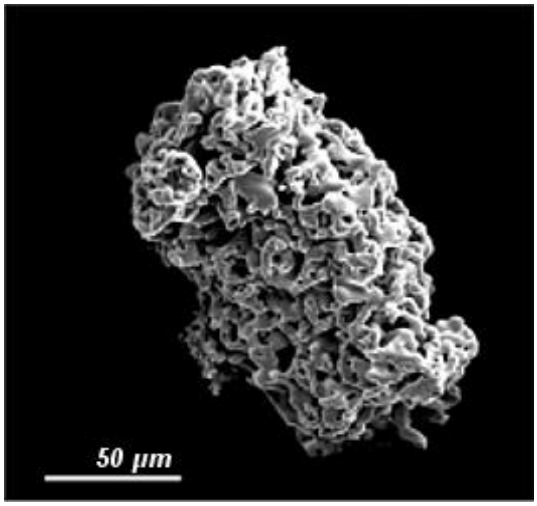

Figure 12. Sponge iron powder SEM [14]

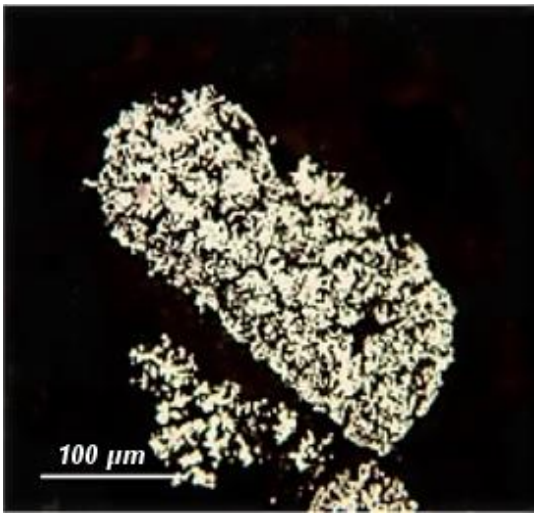

Figure 13. Sponge iron powder cross section [14]

An example of iron powder material is presented in Figure 10 – 13 and Figure 14, and Figure 15.

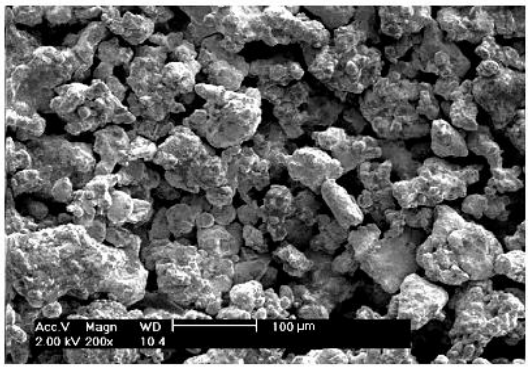

Figure 14. Scanning electron micrograph of iron powder. [15]

Powder characteristics (i.e. particle size, particle size distribution, particle shape, powder angle of repose, particle mechanical properties and particle aspect ratio). [16]

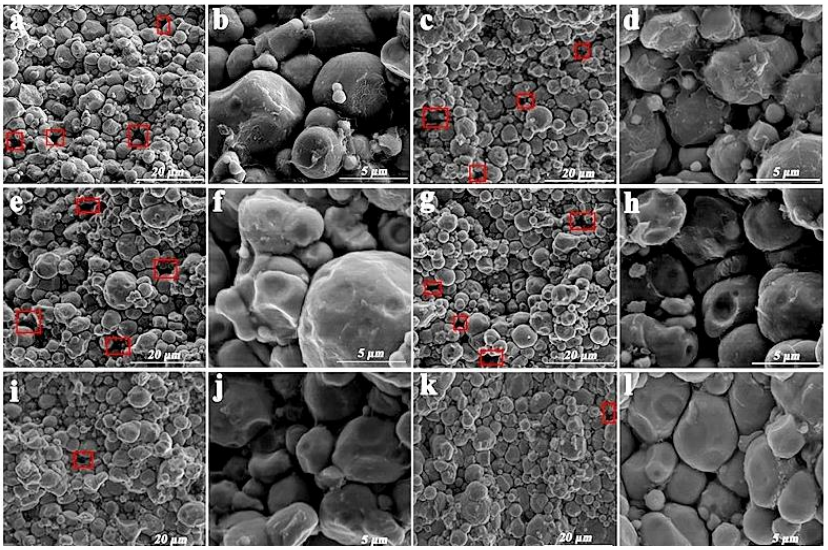

Figure 15. The SEM images of the iron powder cores prepared with different secondary particles with medium diameters of 356 µm (a and b), 265 µm (c and d), 94 µm (e and f), 52 µm (g and h), 265 µm (70vol%) + 94 (30vol%) (i and j), and 356 µm (70vol%) + 52 µm (30vol%) (k and l). [17]

The addition of metallic phosphate on the surface of bulk materials is able to improve the behaviour at machining. Figure 16 and Figure 17 below.

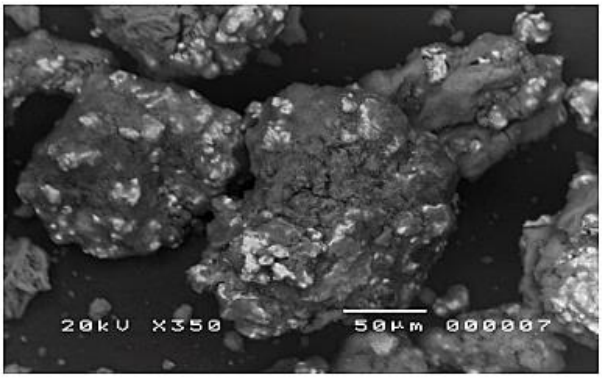

Figure 16. Backscattered SEM micrograph of phosphate iron powder. [18]

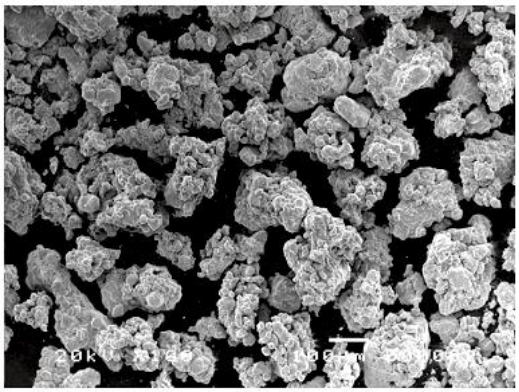

Figure 17. SEM micrograph of untreated iron powder. [18]

Water atomisation is an established technology for the production of metal powders for many commercial applications, including sintering and welding and metal injection moulding. It is also possible to use water atomised powders for additive manufacturing. Water atomised powders are often characterised as being irregular and covered with an oxide layer, which leads to a high oxygen content. The water atomisation has more advantages than gas atomisation. The production rate is several times higher, and it has a lower specific cost of powder and lower equipment cost. Microsegregation is caused by faster cooling and solidification, and it cause the irregular shape of powders.

Water atomised powders sometimes exhibit porosity inside the particles. This could be due to thermal contraction during solidification, the production of precipitates that fall out of the particle during analysis or the formation of gas bubbles inside the particles.

The choice of the appropriate method of powder production depends on the properties expected from the product and on economic calculations. Powders of one metal can differ significantly if they were prepared by different methods or if the production parameters were different. The physical, chemical and technological properties of powders have a significant impact on further technological processes and on the properties of finished products. [19]

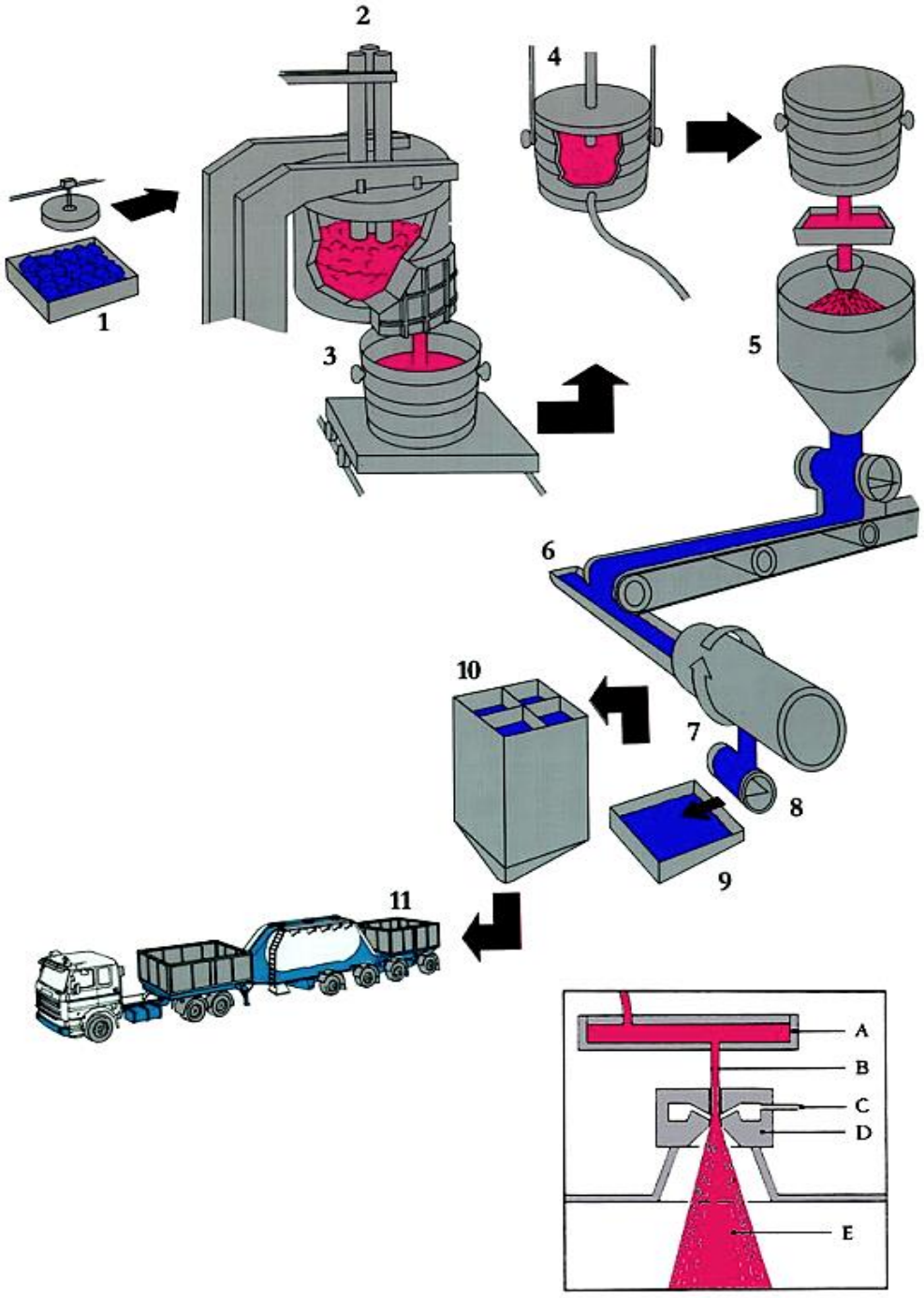

Figure 18. Flow-sheet for the Water-Atomising Process. [20]

The raw material for this process is a carefully selected iron scrap and sponge iron from the process described in the preceding paragraph (Figure 18).

1. Selected scrap - This raw material (1) is melted down in an electric arc furnace.

2. Arc furnace - An electric arc furnace of 50 tonnes capacity.

3. Liquid steel - Where, if desired, alloying elements can be added. The melt is teemed slag-free through a bottom hole into a ladle.

4. Injection - Where it is refined with an oxygen lance.

5. Atomising - The ladle is then transferred to the atomising station (5). Some of these droplets freeze immediately in to small spheres, others unite in small irregularly shaped agglomerates while freezing. Air, swept along by the water jet, and the water vapor arising in the atomising process, cause superficial oxidation of the small droplets. The solidified droplets and the atomising water are collected in a huge container, where they settle as a mud.

A. Tundish - The liquid iron (or steel) is teemed slag-free through a bottom hole in the ladle into a specially designed tundish (A).

B. Steel Stream - From there, the liquid iron (or steel) flows in a well-controlled stream (B)

C. High Pressure Water - Where it is hit by jets of highly pressurised water (C).

D. Nozzle - Through the centre of a ring-shaped nozzle (D)

E. Atomised Iron Powder - The stream of liquid iron (or steel) explodes into fine droplets (E).

6. Dewatering - This powder mud is de-watered (6)

7. Drying - This powder mud is dried (7).

8. Magnetic Separation - The dry powder is magnetically separated from slag particles (8)

9. Screening - The dry powder is screened (9)

10. Equalising - The dry powder is homogenised (10).

11. Transportation – It is eventually transported in special containers (11) to the works at Höganäs for further processing.

Routines for homogenising, quality checking, packaging and storing are the same as for sponge iron powders.

The Höganäs sponge iron process is essentially a chemical process in which finely divided iron ore is being reduced with coke breeze yielding a spongy mass of solid metallic iron, which can readily be comminuted to iron powder. The iron ore used at Höganäs is a magnetite slick (powdery Fe_3O_4) obtained by selective mining from mines in the north of Sweden and Norway. This magnetite slick, which by nature contains only very small amounts of gang and has extremely low contents of sulfur and phosphorus, is being dressed and concentrated while still at the mining location and then delivered to Höganäs in a highly pure state.

As shown in the flow-sheet in Figure 19, the process of transforming the magnetite slick to iron powder proceeds.

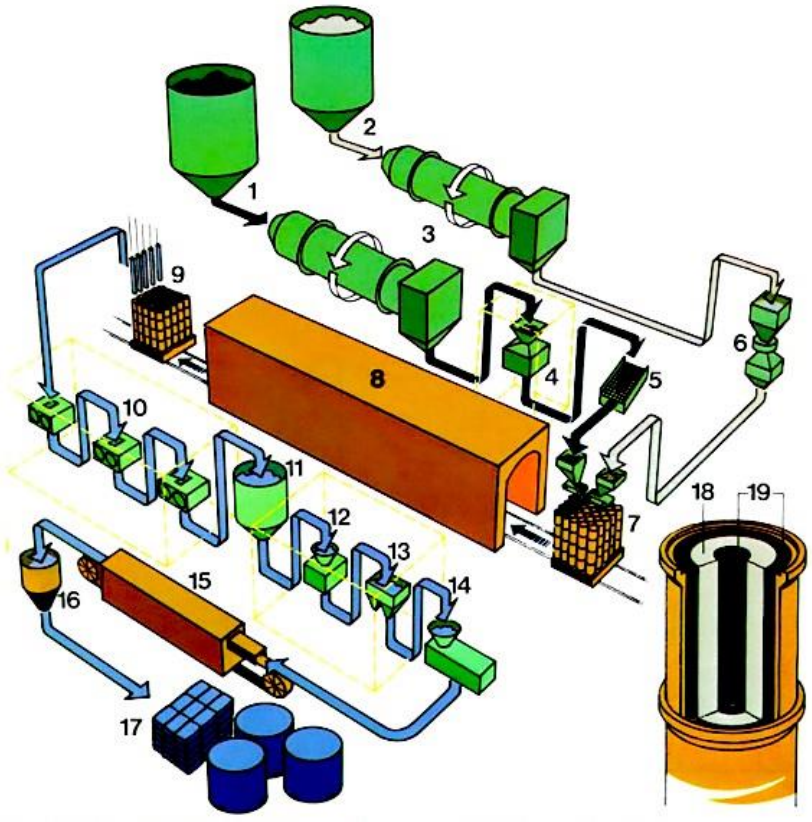

Figure 19. Flow-sheet for the Sponge Iron Process. [20]

The process starts with two raw materials:

1. Reduction mix of coke breeze and limestone - a “reduction mix” consisting of coke breeze blended with ground limestone (1),
2. Iron Ore - and a pre-processed magnetite slick (2).
3. Drying - The magnetite slick and the reduction mix are dried separately in two rotary ovens (3).
4. Crushing - The slightly agglomerated dried reduction mix is crushed (4).
5. Screening- The slightly agglomerated dried reduction mix is screened (5).
6. Magnetic Separation - The dried magnetite slick is passed through a magnetic separator (6).
7. Charging in Ceramic Tubes - Then, both materials are charged by means of an automatic charging device into tube-like ceramic retorts as illustrated (7), (18), (19).
8. Reduction in Tunnel Kilns, Approximately 1200°C - These retorts have an ID of 40 cm, are 2 m long, and consist of four tube segments of silicon carbide being stacked on top of each other. 25 of these retorts are stood on rail-bounded cars that are clad with a thick layer of refractory bricks. These cars travel slowly through a tunnel kiln of approx. 260 m length (8) within which the retorts are gradually heated to a maximum temperature of approx. 1200°C. As the temperature inside the retorts increases, the coke breeze begins to burn forming CO which, in turn, begins to reduce the magnetite to metallic iron while itself oxidising to CO_2. The CO_2 generated reacts with the remaining coke breeze forming new CO, which again reduces more magnetite to metallic iron. This reaction cycle continues until all magnetite has been reduced to metallic iron and a major part of coke breeze is burned up. Parallel to the reduction cycle, the limestone in the reduction mix binds the sulfur arising from the burning coke breeze. After the reduction is completed, the retorts are slowly cooled down again to approx. 250°C before leaving the kiln. Inside each retort, there is now a tube-like sponge iron cake with a porosity of about 75%, a residue of unburned coke breeze and a sulfur-rich ash.
9. Discharging - At an automatic discharging station (9), the sponge iron tubes are pulled out of the retorts, and the remaining coke breeze and ash are exhausted from the retorts.
10. Coarse Crushing - Thereafter, the retorts are ready to be charged again and go on a new trip through the tunnel kiln. The sponge iron tubes (after having been cleaned from

residual coke breeze and ash) are crushed in several steps and comminuted to a particle size below 3 mm (10).

11. Storage in Silos - This crude powder is intermediately ensilaged before further processing. From the intermediate silo (11).
12. Crushing - The crude powder is passed through a specially designed chain of mills (13) and screens (14), in order to be refined to a particle size below 150 μm (many belt furnaces are, of course, available to take care of the huge volume of iron powder to be treated).
13. Magnetic Separation - The crude powder is passed through a specially designed chain of magnetic separators (12).
14. Grinding and Screening - The crude powder is passed through a specially designed chain of mills (13) and screens (14), in order to be refined to a particle size below 150 μm (many belt furnaces are, of course, available to take care of the huge volume of iron powder to be treated).
15. Annealing in Belt Furnace, Approximately 800-900°C.
16. Equalising - These modern electrically heated belt furnaces are especially designed for the purpose, the belt width being 1500 mm. The powder from several belt furnaces is collected in a special silo (16), where it is homogenised in lots of 60 or 120 tonnes.
17. Automatic Packing - Each lot is carefully checked with respect to specified properties and – if okayed – packaged and stored, ready for shipment (17).
18. Iron Ore - Then, both materials are charged by means of an automatic charging device into tube-like ceramic retorts as illustrated (7), (18), (19).
19. Reduction Mix - Then, both materials are charged by means of an automatic charging device into tube-like ceramic retorts as illustrated (7), (18), (19). [20]

The most important property to evaluate the global quality of a powder bed is its packing density. [21] The properties of the final powder particles are presented in Figure 20 and in Figure 21.

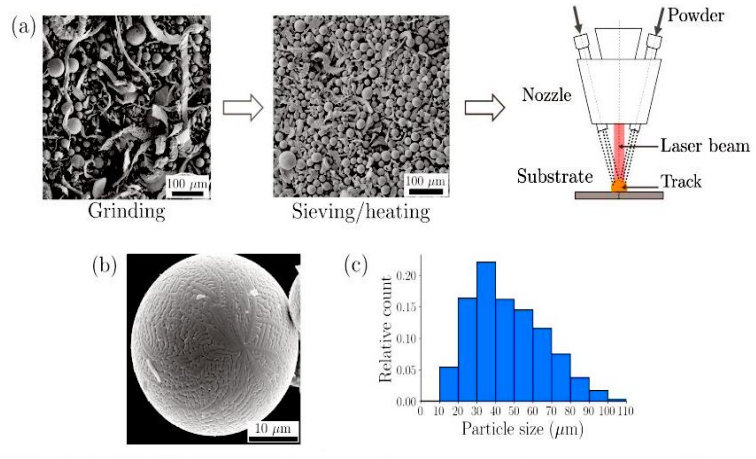

Figure 20. Schematic of the powder production method via grinding. (a) Material removed by surface grinding is collected, sieved and heated, prior to use in a DED process. The corresponding SEM images show the distribution of spherically-shaped particles in the resulting powder. (b) SEM image of a single particle showing the perfectly spherical shape and dendrites on the surface. (c) Particle size distribution in the final powder shows a size range ~ 20-100 μm. [22]

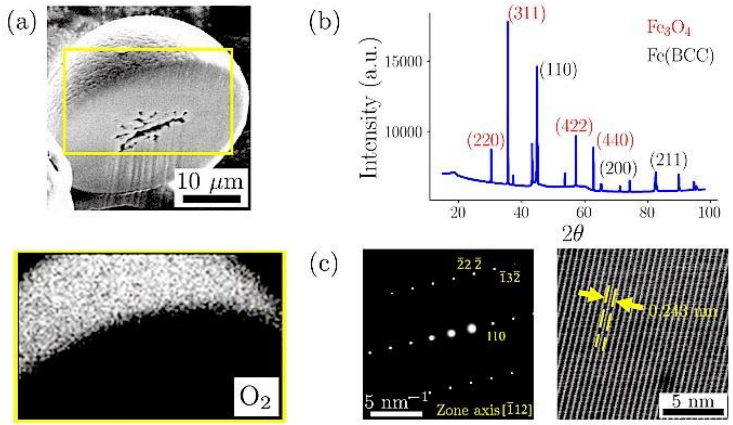

Figure 21. Properties of the final powder particles. (a) SEM image and associated EDS spectrum showing the presence of a thin oxide layer on the surface. (b) X-ray diffraction results on the powders show the occurrence of both alfa Fe and Fe_3O_4 peaks. (c) TEM SAD and HRTEM images of the section just below the surface show that the powder particles are indeed primarily alfa Fe. [22]

Agnieszka Stanula

The technological process of manufacturing products by powder metallurgy consists of the following main stages:

1) Obtaining a metallic powder or a mixture of powders
2) Pressing (forming)
3) Sintering (heat treatment)
4) Heat treatment

Pressing (forming)

Pressing is one of the main technological processes in the production of products from sintered metal powders. Its aim is to form compacts of specific dimensions, shape, appropriate density and physicochemical properties. The dies are used to have an exact shape. The weighed amount of powder is compacted by the pressure of the punch, and then pushed out of the matrix, after being poured into the matrix. The powder poured loosely into the matrix often reduces its volume two or three times, when is compacted.

The pressing process is divided into two stages:

a) Stage of pressing at low pressures – a collapse occurs and a liquidation of "bridges" created during backfilling, and close arrangement of grains due to mutual sliding and rotation of individual grains. The density of pressed mouldings when low pressures are used is very uneven, there are large differences, especially between the material adhering to the walls and the centre of the sample.
   Stage of pressing at higher pressures - plastic deformation of the powder grains takes place. [23]
b) Compacting involves pressing and compressing the powder mixture into the desired shape or die. The quality of the compacting step reduces potential voids and significantly increases the density of the product. Compacting pressure is between 80 MPa and 1600 MPa. Each type of metal powder requires a different amount of compacting pressure depending on its properties. In soft powder compacting, the pressure is between 100 MPa and 350 MPa. For more resilient and harder metals, such as steel and iron, the pressure is between 400 MPa and 700 MPa. The green compact is a final product and is formed by compacting. Sometimes, the green compact faces the possibility of cracking mainly due to the density gradient inside the green compact

resulting from the inhomogeneous density distribution, and friction between the powder particle and tooling. It has also been reported that the friction force is a strong function of compaction temperature. [24]

Sintering (heat treatment)

The key to the precision and success of powder metallurgy is the sintering process. During this step the compact is heated for bonding the powder particles. The temperature is marginally below the melting point of the primary metal. The green compact is sintered to decrease the porosity and to increase the density. The increase in density depends on the kind of powder materials and the sintering conditions such as temperature and time. [25] In addition the method of heating, the method of cooling after sintering, and protective atmosphere are taken into account in the sintering process.

The use of protective atmospheres (Table 3) is dictated by the need to protect sintered materials against oxidation, as well as the reduction of oxide coatings that could have been formed during the processing of the powder and its individual grains. Mechanical alloying of iron powders with nitrogen results in a highly refined microstructure.[26]

The process of sintering products made by powder metallurgy in large-series and mass production is most often carried out in continuous furnaces. These are tunnel kilns and depending on the method of moving the moulded parts, placed in baskets or on pallets, there are belt kilns and pusher kilns. [23]

Table 3. Types of protective atmospheres

Protective atmospheres		
Reducing	indifferent	oxidising

The chemical interaction of the sintered material with the atmosphere in the furnace shall be taken during the choice of the protective atmosphere. (Table 4)

Table 4. The dependence of the choice of the protective atmosphere

The choice of protective atmosphere		
Chemical composition of the sintered material	Furnace type	Economic factors

The gases used as the protective atmosphere are listed below:

- Endothermic
- Exothermic
- Converter
- Dissociated ammonia
- Hydrogen
- Sintering in a vacuum
- Protective backfills

In general, with the onset of grain growth there is a decrease in the shrinkage rate. As the sintering temperature increase, grain growth begins to play a major role in the densification process. [27]

Heat treatment

To improve the surface properties of powder material parts the thermal processes are applied (for example, carbo-nitriding, carburising treatment, steam treatment, scaling or oxidation).

Carbo-nitriding is a high temperature modified carburisation treatment in an ammonia based atmosphere that promotes both carbon and nitrogen diffusion into the component surface for hardening, usually followed by quenching.

The carburising treatment consists of introducing carbon to the surface of the pieces at a temperature where the austenite is stable. Hardness is obtained by quenching and it depends on carbon potential on the surface of the material. The carbo-nitriding process can be explained as a carburising gas where ammonia is added to the atmosphere. The temperature and the time

are lower than in the carburising treatment, therefore less dimensional change are produced. Due to the stabilising effect of the nitrogen over the austenite, carbo-nitriding confers more hardenability than carburising.

Steam treatment consists of tempering the steel in super-heated steam, adopted as an additional treatment for conventionally hardened and tempered tools. These treatments are typically heat treatments above 500°C in an atmosphere containing steam, used to grow a blue–black Fe_3O_4 tenacious surface oxide on steels The holding time is between 30 and 60 min. Recommended pressure for steam tempering is 100 MPa water column. The blue–black iron oxide Fe_3O_4 that is deposited on the component during steam treatment is a hard porous oxide that is usually about 0.005 mm thick and is very receptive to coolants. The treatment is adopted for steels, iron based and sintered products because it increase the life of components. [28]

Scaling or oxidation - electrolytically produced iron powder has these physical characteristics and would provide the required material for oxidation. [29] At high temperature (700–1250°C), the growth rate of the oxide scales follows a parabolic law, showing that the limiting step of the reaction is the ion diffusion through the oxide layers. The mobility of iron cations is larger that of oxygen anions during the oxidation process, thus the rate-limiting step of solid-state oxidation of pure iron is the outward diffusion of iron cations. [30]

The conventional sintering process (Figure 22) follows each of the steps of basic powder metallurgy: Obtaining a metallic powder or a mixture of powders, pressing (forming) and sintering (heat treatment). It is much like the ancient method of powder metallurgy with the added benefit of modern technology. The conventional sintering process takes a long time and needs a high temperature. There is a very high demand to improve the sintering technique in reducing the sintering temperature and shortening the sintering time, and thus reducing the energy cost.

The sintering temperature has a significant effect on the densification degree of iron powder compact during intensified sintering. Sintering time has some effect on the densification degree of iron powder compact in intensified sintering, and there is also an optimum sintering time in which the sintered compact can reach the highest densification degree. [31]

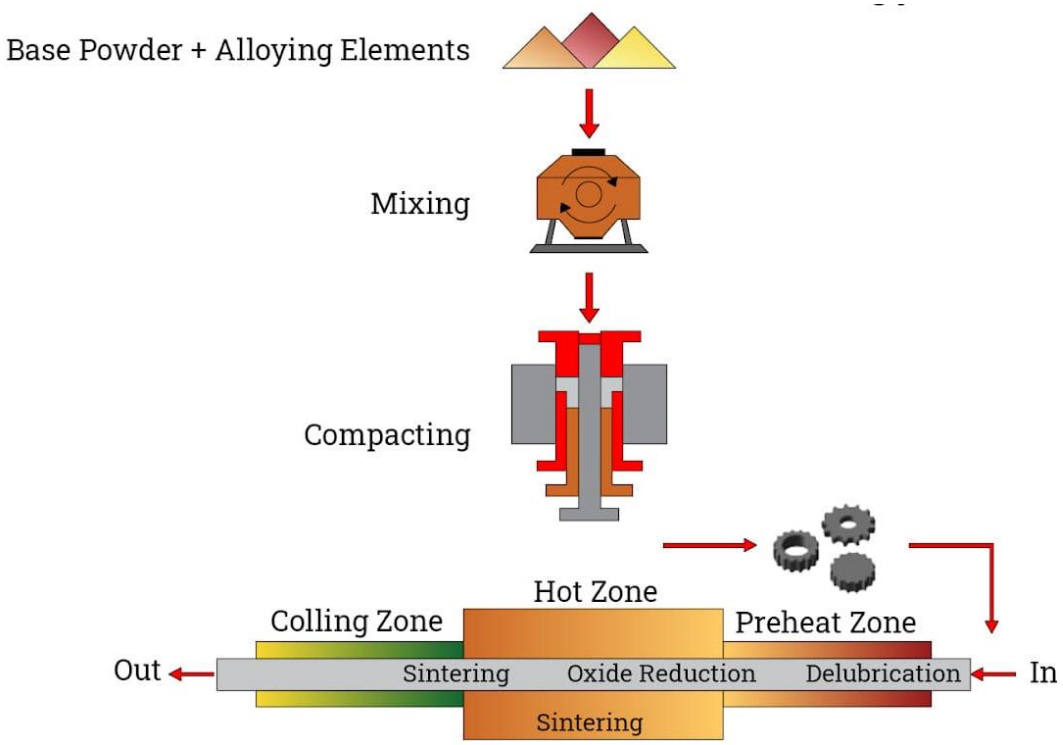

Figure 22. Conventional Powder Metallurgy Process [32]

The model of sintering between two similar spheres is presented in Figure 23.

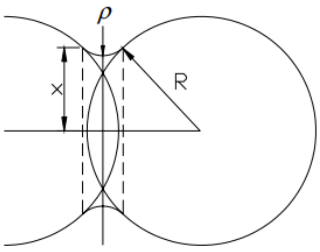

Figure 23. The model of sintering between two similar spheres [33]

The use of copper and phosphorus provides a liquid-phase sintering with increased strength of the sintered components. [34]

The origins of material strain during sintering are related to:

(1) dimensional changes due to temperature change dependent upon the coefficient of thermal expansion (a) of the material;

(2) phase transformation during heating, for example, ferrite to austenite transformation;

(3) diffusion and dissolution of alloying elements in the matrix;

(4) sintering phenomena including shrinkage and swelling. The sintering effect and the dissolution of the alloying elements should have a vital role on the contact pressure and thus on the bond strength. It is well known that Fe–Cu powder compacts usually swell during the sintering period that is known as "copper growth".

In fact, during the sintering cycle, copper melts and penetrates between the solid particles and grain boundaries. Also, copper diffuses into the iron lattice through the surface of the particles and the grain boundaries. These phenomena cause significant swelling of the Fe–Cu powder compact during sintering.

The swelling of the Fe–Cu parts induces a mismatched strain between them, leading to a high contact pressure. This pressure, which arises at high temperatures, provides a diffusion bond between two components. The surface area of the iron powder influences the swelling in Fe–Cu powder compacts. As the iron particle size increases, swelling goes through a peak. It is known that the swelling of Fe–Cu powder compacts is affected by the presence of carbon. [35]

Actually, carbon has a high solubility in iron and decreases swelling due to grain boundary penetration by molten copper. It has been shown previously that dissolution of graphite into the iron particles at 1000°C is completed in a few seconds, indicating a very high diffusivity of carbon inside the c-iron lattice. Before the melting of the copper, diffusion of carbon from the solid steel to the powder compact should have taken place. This results in carbon depletion from the interface area inside the solid steel and inversely, it causes carbon enrichment in the powder compact. Additionally, the presence of alloying elements with a high diffusion coefficient such as carbon is also useful as they speed up the diffusion process itself. Therefore, although carbon diffusion may decrease swelling of Fe–Cu, it increases the hardness of the powder compact and contributes to rapid diffusion bonding. Thus, the diffusion of carbon can enhance the strength of the bonded zone. The optimum condition would be that the diffusion of carbon takes place, but it should not be so high as to hinder the copper growth. [35]

The density of the sintered compacts and as-sintered hardness increase with increasing compaction pressure and are influenced by the powder structural characteristics. During steam treatment the type of powder and compaction pressure have an important influence on the extent of pore closure and weight gain. Surface pore closure and oxidation resistance of the steam-treated components are improved with increasing compaction pressure. This layer always plays an important role in the industrial applications as well as in laboratory experiments for abrasive wear as they used atomised and different sizes iron powders.[28].

The literature example of microstructure of iron based sinter compacts are presented in Figure 24 and Figure 25.

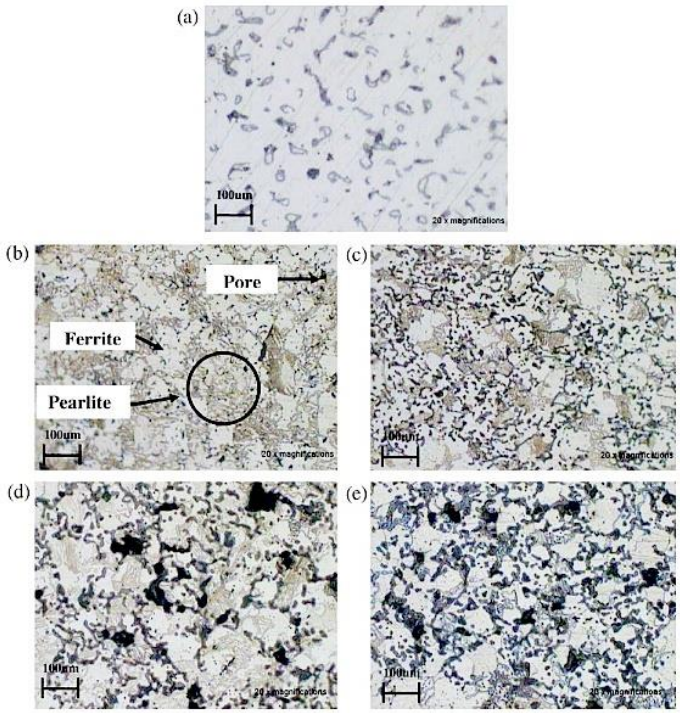

Figure 24. Optical microscope image of (a) pure iron and Fe-1%C alloy with different melting time (b) 4h, sintering at 1150°C, (c) 6h, sintering at 1150°C, (d) 8h, sintering at 1150°C; Magnification 200X [36]

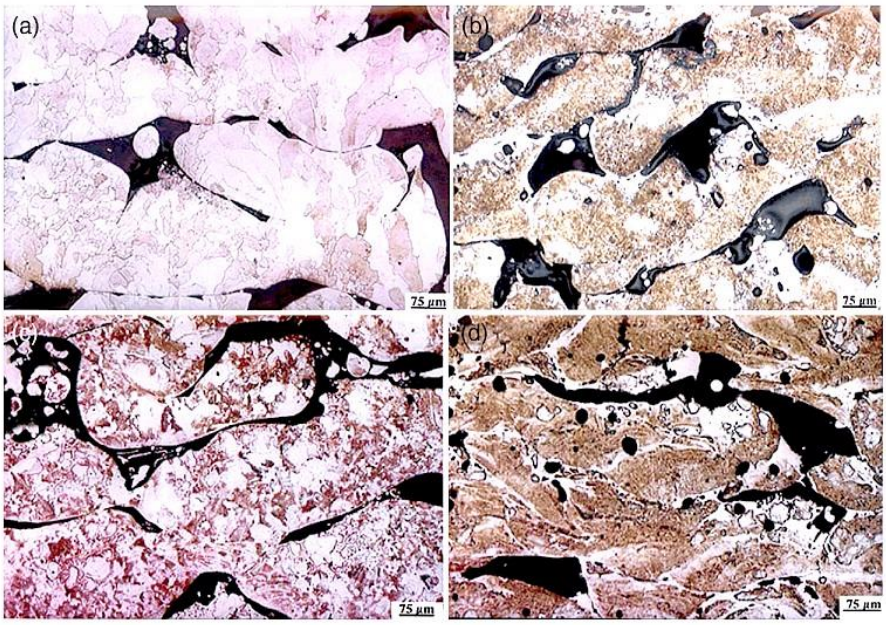

Figure 25. Microstructure of laser-sintered Fe (a), Fe-4Cu (b), Fe-0.8C (c), and Fe-0.8C-4Cu-0.35P (d). [37]

2.3. Mechanical properties

The strength of materials is a part of technical mechanics, based mostly on the laws of statics, changing not with a rigid body, but with a deformed body (changing its shape under the action of external forces).

The strength of materials is a science that provides methods and ways of testing construction materials and giving these materials certain shapes in various structures. The changes in the body under the influence of external forces are interesting. If under the influence of these forces the body has assumed a certain deformation and is already in equilibrium, then there must be some system of external forces of the body that would not balance the action of these forces. [40]

There are two types of forces:

1) The system of external forces causing deformation of the body

2) A system of internal forces that opposes a system of external forces.

From the tensile diagram of brittle metal, after the proportional period, there is a rapid increase in stress with a slight elongation of the sample, and then the sample breaks. This is a reason that brittle metals do not reveal the yield point when they are stretched.

Elongation during stretching does not usually exceed 1%. The value of elongations is calculated as a percentage. It is the ratio of the length of the measuring part to its diameter. [38] The tensile test is invalidated according to the PN-62/H-04310 standard if: [39]

(a) More than one neck is formed on the sample.

b) The sample tore beyond the gauge length and the calculated elongation does not meet the requirements for the material.

c) The specimen tore at the mark and does not exhibit the required elongation or contraction [40]

In addition, the strength properties of materials are influenced by:

1. Temperature - at high temperatures, the strength of materials is reduced. [38] Concretes and natural stones are generally not very sensitive to temperature changes, with the exception of very high temperatures, in which a sintering processes may occur. [40]
2. Time - a phenomenon called material creep occurs when structural metals subjected to constant stress over a long period of time begin to elongate. The creep phenomenon is visible only at higher temperatures.
3. Types of metal loads - there are three types of loads, variable loads can lead to material failure faster than permanent loads.
4. Influence of metal fatigue - fatigue strength is the highest value of alternating stress at which the material can work for any length of time without the appearance of fatigue cracks.

TENSILE

The tensile, compression, bending and torsion fatigue strength is determined. This strength is influenced by the smoothness of the surface of the object, the size of its cross-section, the shape of the object and the influence of corrosion. [38] In metals, the value of the coefficient E depends on the chemical composition and heat treatment, and on the load. The bend test has found wide applications in the study of brittle metals, whose mechanical properties are not clearly emphasised during the tensile test. This applies in particular to the sensitivity of these metals to eccentric fixation of the sample. The lack of plastic deformation makes it impossible to equalise additional stresses and leads to early rupture of the sample. [40]

There are several features that distinguish the mechanical properties of plastic and brittle materials.

1. The main difference is that brittle materials are destroyed with small deformations, while a fairly large change in shape is needed to destroy a plastic material. Brittle materials are easily damaged by impact due to the fact that their specific work of deformation is very small.

2. The second difference is that for plastic materials in the initial stages of deformation, the course of stretching and compression can be assumed to be unidirectional. Because most brittle materials offer much less resistance to stretching than to compression. This fact limits the scope of applicability of brittle materials or causes the use of special protection when working with their tensile strength.

3. In brittle materials, there are no large deformations until failure, the picture of stress distribution will take place in tension and compression, until the greatest stress does not exceed the strength of the material. The greater the stiffness of a given element; i.e. the smaller its length and the larger its cross-sectional area and modulus of elasticity, the greater forces it takes on itself [41].

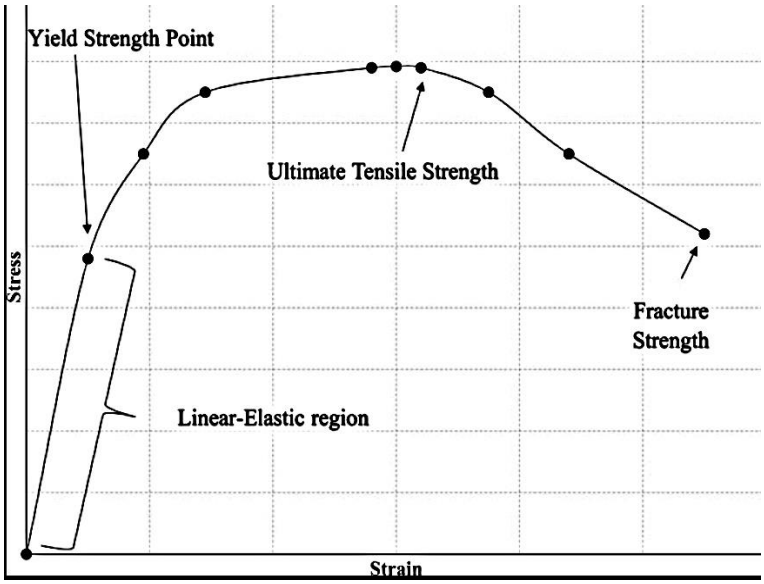

Figure 26. A typical stress-strain curve for metal. [42]

From the stress - strain curves Figure 26, the yield stress, the elastic modulus and the fracture load can be determined. On a displacement curve, the initial level corresponds to the positioning of the system and especially to the crossbar on the support points. The active parts of the load–displacement curves only start with the linear increase corresponding to elastic strain. This behaviour stops and the material deforms itself irreversibly. Finally, the load decreases until the sample is broken. Then, the fracture morphology of the different compacts is analysed by scanning. [42].

Tensile tests are used to determine the following mechanical properties: Young's modulus, Poisson's ratio, ultimate tensile strength, yield strength, etc. The primary curve produced from a tensile test is a direct stress-strain curve. Figure 26 shows a typical stress-strain curve for metal foams. The curve includes two points of interest: the yield strength and ultimate tensile strength, and the quasi elastic initial stiffness. [42].

To describe elastic behaviour of components under load, the known edge of stiffness constants is needed. Isotropic materials can be described by Young's modulus E, shear modulus G and Poisson's ratio m.

Since elastic moduli represent metallic bonds stiffness, for the sintered metallic, models for predicting the porosity dependent effective values of elastic moduli are needed. Young's and shear moduli follow similar models of degradation, so researchers deal mainly with E modulus.

In granular materials like metal powder, the cohesive frictional behaviour of the material and inhomogeneity within the powder compact will have a significant influence on the type of fracture. The failure of metal powder during compaction has always been related to the shearing and friction behaviour of the material, where the yield criteria of the powder material model have been developed based on the solid mechanics material model. [42].

Therefore, it is believed that a fracture in metal powder compaction will most likely be due to shear fracture, rather than an opening fracture due to the mechanical behaviour of the powder material in closed die compaction.

COMPRESSION

During compressive testing a material experiences opposing uniaxial forces that press the sample from opposite sides. The loading forces in compressive testing are the opposite of those in typical tensile tests. The tensile and compression tests are done on the same machine. [44] The stress – strain behaviour of rock in compression is presented in Figure 27.

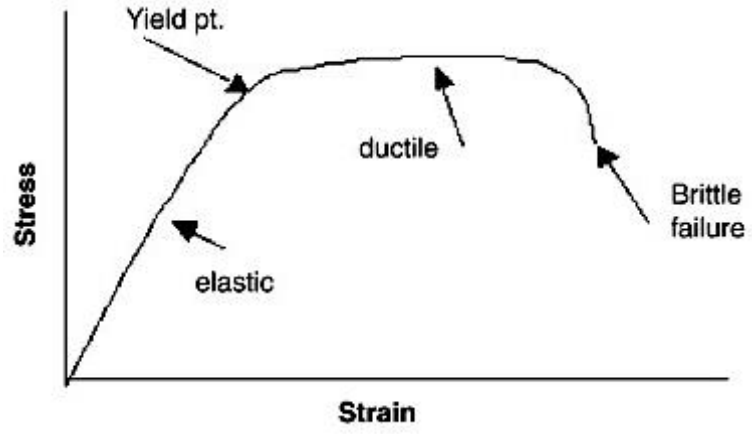

Figure 27. Stress-strain behaviour in compression. [43]

The goal of compression tests is to detect the behaviour or response of materials and obtain the corresponding compressive properties (ultimate compressive strength, yield strength, elongation) when it experiences compressive loads. The generally applicable standards for compressive testing are ASTM E9–19 and ASTM E209–18, which are specific to the compression of cylinder-shaped metallic materials at room temperatures and elevated temperatures (beyond 538°C), respectively. [45]

Compression tests are also used to determine the modulus of elasticity, compressive yield strength, and compressive strength. These properties are important to determine if the material is appropriate for the particular application. [46]

Compressive testing is relatively more difficult than tensile testing. The mode of failure involves some type of buckling. The compression specimen geometry and method of load introduction should be relevant to the actual application for which the data is being generated. [47]

The purpose of the compression test is:

- the determination of the diagram or work of strain

- determining the value of stresses causing the destruction of the sample.

The purpose of the standard test is to determine:

a) compressive strength in the event that the metal sample fails during the test

b) a pronounced yield point

c) relative shortening

d) a stress curve as a function of shortening

The purpose of the strict test is to determine:

a) modulus of elasticity (Young's modulus in compression)

b) conventional elastic limit

c) the yield strength. [48]

Material samples (Figure 28) intended for compression tests are in the shape of rods or cubes.

1. samples in the form of rods at a certain length may, in addition to compression, also undergo warping (buckling), which may change the test results.
2. in cube samples, in relation to their size the contact surfaces with the plates of the compression machine are too large, as a result the friction generated between these surfaces and the plates distorts the results of the experiment.

There is a strict proportionality between stresses and unit strains ε. The numerical value of the proportionality coefficient does not differ from the value of this coefficient when stretched. Hooke's law shall be applied. By increasing the load on the sample made of ductile materials, the shape changes to barrel-shaped, and then the sample flattens out.

The barrel-shaped shape of the crushed sample is explained by the friction of the front surfaces of the plate of the pressing machine. This friction inhibits the expansion of layers of material lying close to the plates; the effect of friction forces decreases as one moves away from the surface of the plates, and therefore the thickening is greatest in the middle of the sample. For mild (forgeable) steel, both the proportional limit and the yield point can be observed.

In the case of samples made of brittle materials, samples in the shape of cubic are tested for compression. They show a very low proportionality limit. The parts cracked after the test. Compressive strength is the stress that causes the samples to crack. The value of Young's modulus E does not differ from the value of this modulus in tensile strength.

End loaded specimens tend to broom or split from the end, and so indirect loading by means of shear is often used. This gives rise to stress concentrations, and failures usually initiate where the specimens are gripped. High shear stresses in this area may also interact with compressive stresses, and this type of test tends to underestimate the intrinsic compressive strength. [49]

The test method is an ASTM or other standard is not in itself a dominant selection criterion. Often the laboratory equipment available, and the skill of the person performing the test, have to be taken into consideration when selecting a procedure. The right test method can be strongly dependent on many factors, not all of which are completely technical. [50]

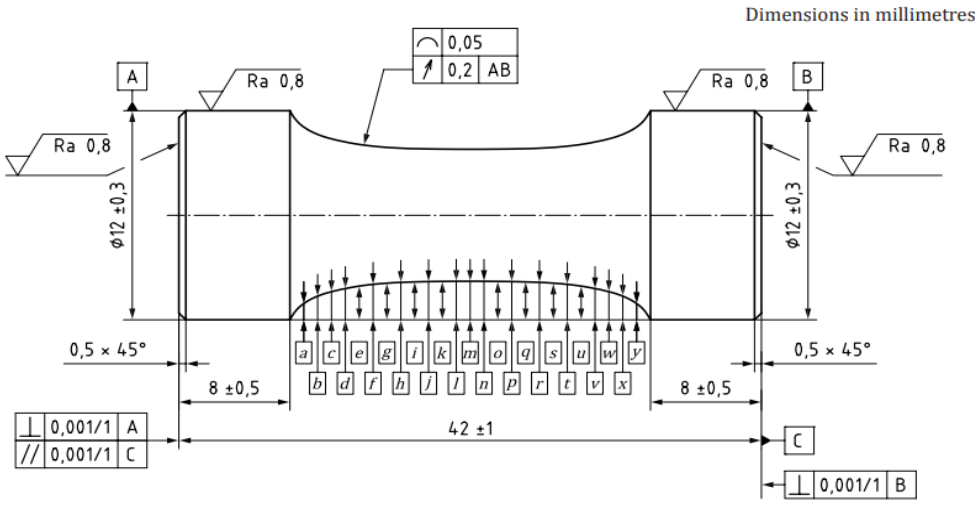

Figure 28. Compression sample [51]

a	b	c	d	e	f	g	h	i	j	k	l
1.21	1.90	2.29	2.54	2.69	2.79	2.86	2.91	2.94	2.96	2.98	2.99

m	n	o	p	q	r	s	t	u	v	w	x	y
3.00	2.99	2.98	2.96	2.94	2.91	2.86	2.79	2.69	2.54	2.29	1.90	1.21

Note The 25 coordinate a to y are at 1 mm intervals. [51]

2.4. Numerical methods FEA, Drucker-Prager model

Finite element analysis (FEA) is a numerical modelling method that splits a problem into finite parts and solved computationally using the modern day computer processor. This technique is applied to solve different complex problems using theoretical fundamentals, such as classical mechanics, solid mechanics, thermodynamics and fluid mechanics. FEA is a technique with a broad range of applications, however as with any modelling method, the quality of the analysis is dependent on the validity of the assumptions made. [48]

The choice of model to be used depends on the analysis type, the material type and the data available for calibration of the model parameters, and the range of pressure stress values that the material is likely to experience.

The hyperbolic model is useful for brittle materials for which both triaxial compression and triaxial tension data are available, which is a common situation for materials such as rocks.

DRUCKER – PRAGER MODEL

When using the Drucker-Prager material model, Abaqus allows you to prescribe initial hardening by defining initial equivalent plastic strain values, as discussed below along with other details regarding the use of initial conditions. [48]

The Drucker-Prager yield criterion is a pressure-dependent model for determining whether a material has failed or undergone plastic yielding. The criterion was introduced to deal with the plastic deformation of soils. It and its many variants have been applied to rock, concrete, polymers, foams, and other pressure-dependent materials. [52]

The extended Drucker-Prager models are used to model frictional materials in which the compressive yield strength is greater than the tensile yield strength. The Drucker-Prager failure criterion is a three-dimensional pressure-dependent model to estimate the stress state at which the rock reaches its ultimate strength. The criterion is based on the assumption that the octahedral shear stress at failure depends linearly on the octahedral normal stress through material constants. [53]

The shortcomings of the Drucker-Prager failure criterion in reproducing polyaxial laboratory experiments are illustrated in Figure 29.

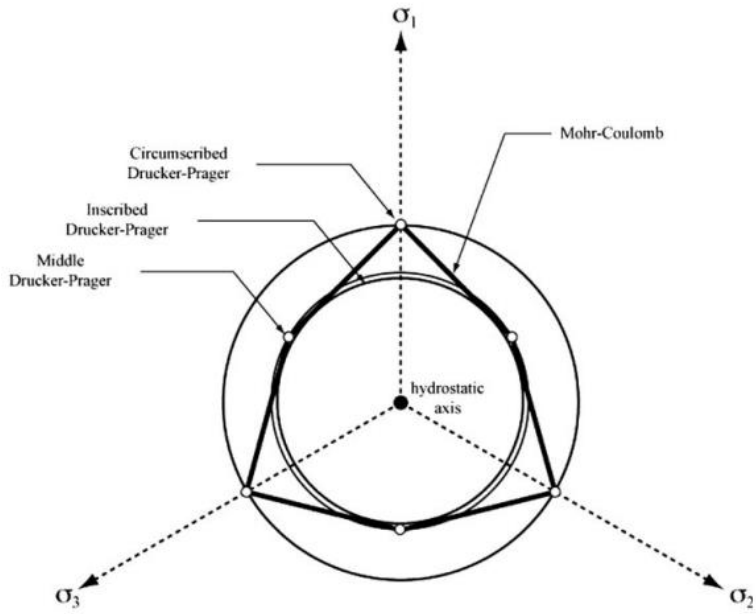

Figure 29. Drucker-Prager and Mohr-Coulomb failure criteria in stress space. [53]

CAST IRON PLASTICITY MODEL

It describes the mechanical behaviour of grey cast iron, a material with a microstructure consisting of a distribution of graphite flakes in a steel matrix. In tension the graphite flakes act as stress concentrators, resulting in yielding as a function of the maximum principal stress, followed by brittle behaviour. In compression the graphite flakes do not have an appreciable effect on the macroscopic response, resulting in a ductile behaviour similar to that of many steels.

The cast iron plasticity model is used to provide the value of the plastic “Poisson’s ratio”, which is the absolute value of the ratio of the transverse to the longitudinal plastic strain under uniaxial tension.

CONCRETE PLASTICITY MODEL

Concrete plasticity models are generally based on the same framework of plasticity theory for metals, but it includes the special properties of concrete.

The key aspects of a plasticity model include the yield surface, the flow rule and the hardening/softening rule. The initial yield surface shows the beginning of the plastic

deformation. The flow rule shows the tendency of plastic deformation. the hardening/softening rule defines how the yield surface evolves with plastic deformation. Many yield functions have been proposed for concrete. The Drucker-Prager (D-P) criterion has been widely adopted for the modelling of concrete because of its simplicity (involving only two parameters) and its capability to capture shear strength increases as a result of hydrostatic pressure increases, which is a unique property of concrete under confinement.

The shear strength of concrete under equal biaxial compression, which refers to concrete subjected to equal stresses in two principal directions and a zero stress in the third principal direction, and that under triaxial compression are different, even when the first stress invariant of the two cases is the same. Based on the plasticity theory, the stress states of concrete under equal biaxial compression and triaxial compression correspond to different circumferential positions on the deviatoric plane. (Figure 30) [54]

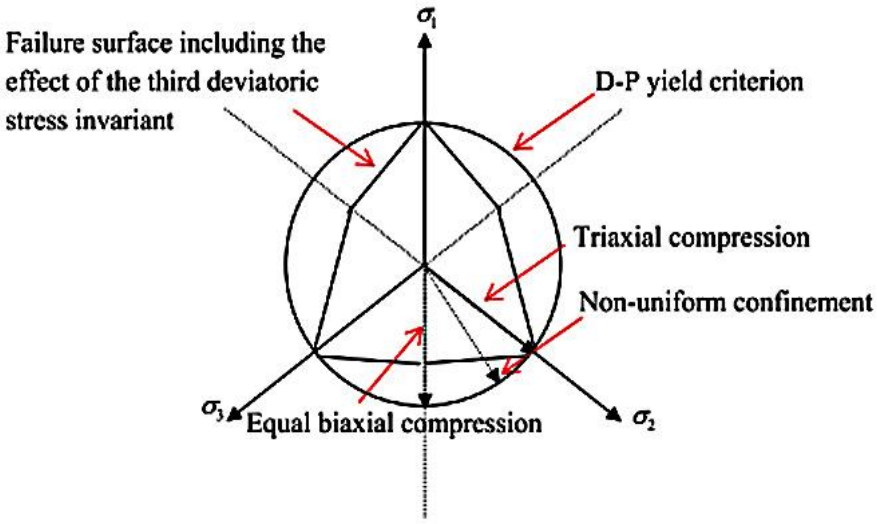

Figure 30. Failure surface in the deviatoric plane. [55]

It is a constitutive model that is based on a combination of the theory of plasticity and the theory of damage mechanics. [55]

The damage concrete plasticity model is widely used. This model is employed in the ABAQUS manual. [56]

This model is one of the most popular concrete damage-plasticity models in the literature and engineering practices. The determinations of many critical model parameters and calibration are challenging. [57]

The ongoing increase of computational resources, and advances in the development of numerical methods, in particular the finite element method, damage plasticity models have become a crucial tool in modern engineering practice and science for analysing the mechanical pre- and post-peak response of structures. [17] This model is able to simulate tensile and compressive behaviour of concrete under quasi-static loading quite well and it has been extensively used in a lot of research for different applications. [58]

2.5. Iron based sintered used in the automotive industry

The term powder metallurgy may be considered according to norm PN-EN ISO 3252:2019-12 as field of technology involving the production and fusion of powders of a metallic nature, as well as merging them with non-metallic powders, without liquefying the entire product. [10]

Powder metallurgy was developed and researched by different scientists starting by the Egyptians from 300 BCE through P. G. Sobolewski (1782-1841), Wollaston William Hyde (1766-1828), Henry Bessemer (1813-1898). [59-61]

Iron based material is used in steering components, car suspensions - parts of shock absorbers, doors, brakes, etc. (Figure 31 - 34). The analysed material is directly applied to the components of shock absorbers, such as piston cylinder ends, strut rod guides and compression valves.

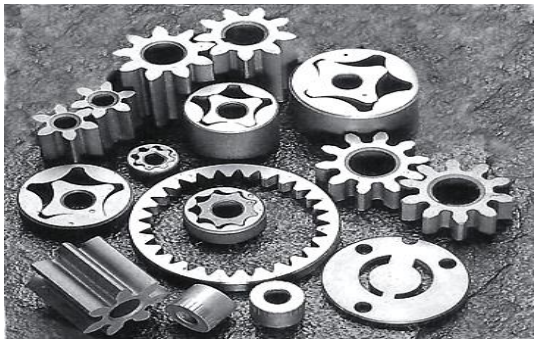

Figure 31. Oil pump rotors and gears [62]

Figure 32 Scooter/motorcycle parts. [62]

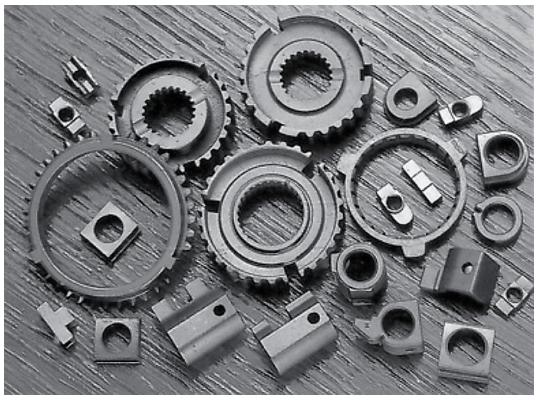

Figure 33. Gear box/transmission (clutch hub, gear shifting yokes etc.). [62]

Figure 34. Shock absorber parts. [62]

Powder materials are used in different applications, for example, porous bearings. The advantage of porous bearings is that the pores can be filled with lubricating oil. This is a reason that the bearings do not require any additional lubrication during the whole life of the machine in which it is used. This feature accounts for the use of the term ‘self-lubricating bearings’, but increasingly the term ‘oil-retaining’ bearings seems to be preferred. The porosity should lie between 20% and 35% by volume, the upper limit being imposed by strength considerations that varies inversely with its porosity [62]

The sintered powder mixtures Fe-C-Cu are applied in powder forged connecting rods, crankshaft belt drives, camshaft sprockets, camshaft pulleys, valve seat inserts, clutch adjustment rings, converter turbine sleeves, oil pump gears etc. [63]

Agnieszka Stanula

Iron powders have applications in the manufacture of a variety of magnetic dielectric components for radio-equipment. The use of metallic powders with a high specific surface is often limited by their oxidation sensitivity. Therefore, one of the key requirements for the powders is that each particle must be provided with an adherent insulating surface film. [35]

Fe powder is a kind of prerequisite friction component and shows pronounced influence on the friction and wear properties of brake pad materials In mild test conditions, the friction coefficient increases with the increase of Fe content, which is attributed to the increased surface roughness by the addition of Fe. [64] Based on demands of high-speed rail applications, the iron based pads are suitable for disc. [65]

Iron based powders are the most used in the production of automobile components. They are included in:

- Steering components
- Transmission components
- Connecting rods
- Main bearing caps
- Variable valve timing
- Seating applications
- Exhaust applications
- Catalytic reduction systems
- Fuel system components
- Engine components

The example of powder material parts used in shock absorbers are presented in Figure 35.

Figure 35. Powder Materials parts used in shock absorbers. [66]

Inside a pressure cylinder filled with hydraulic oil, a piston attached to a piston rod moves on one end. The hydraulic oil is pushed through the small slots in the piston when the piston is moved up and down. These openings allow only a small amount of oil to pass through the piston. This slows down the movement of the piston, which in turn slows down the movement of the spring and suspension.

Figures 36-38 show the double-tube absorber, piston valve and base valve assemblies. And on the drawing (Figure 39) the design principle of the energy-harvesting shock absorber, in general.

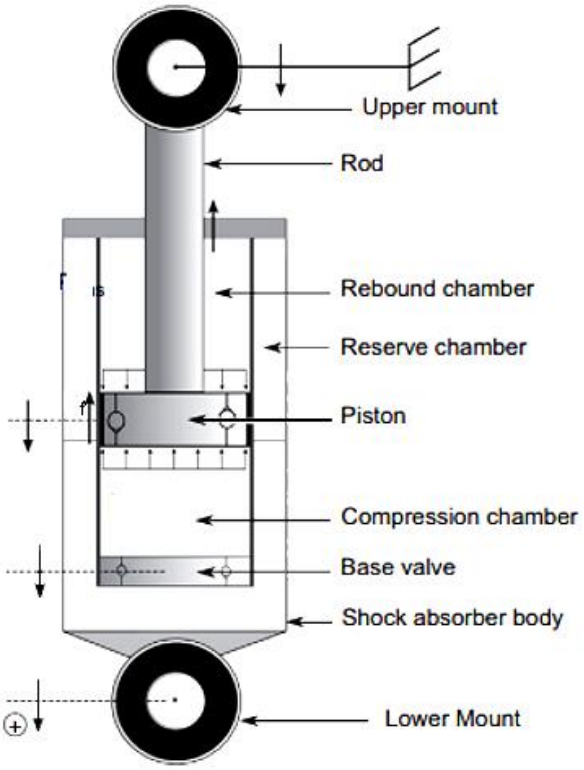

Figure 36. Double- tube shock absorber. [67]

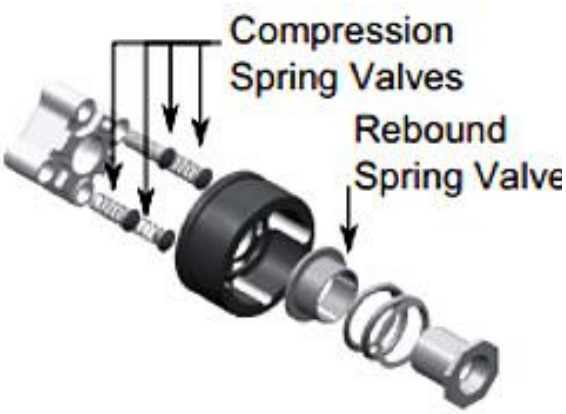

Figure 37. Piston valve [67]

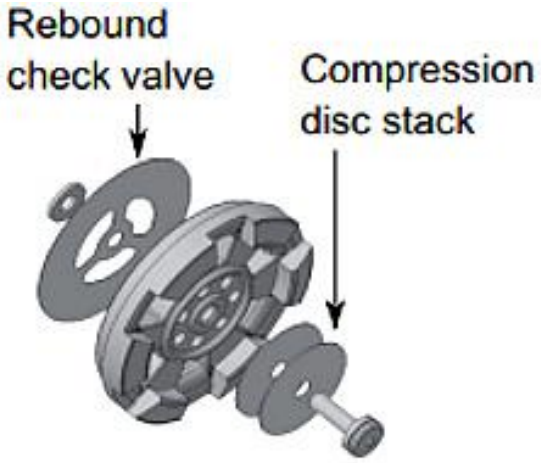

Figure 38. Base valve [67]

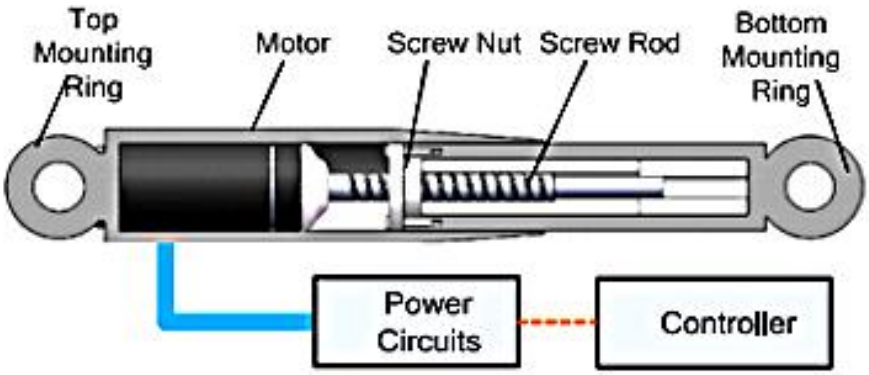

Figure 39. Design principle of the energy-harvesting shock absorber [68]

The most important task of the shock absorber is to ensure contact between the vehicle tires and the road surface.

They:

• Control the movement of the spring and suspension.

• Ensure the smooth driving and braking of the vehicle.

• Prevent premature tire wear.

• Make it easier to keep tires in contact with the road surface.

• Maintain dynamic wheel alignment.

• Control undesirable body movements such as bouncing, rocking (lateral and vertical), pitching (body dives when braking and rear end bottoms when accelerating).

• Reduce wear of other components.

• Facilitate even tire and brake wear. [69]

An example of a shock absorber, wheel suspension and steering system are presented in Figures 40-42. As an integral part of the suspension system, shock absorbers cushion vibrations and contribute to a car's comfort and safety. Shock absorber parts have to perform their function while enduring constant impacts and temperatures of up to 120°C. Materials used in shock absorbers therefore have to meet specific requirements, particularly in terms of durability and heat resistance. [70,71] The future trends of the regenerative shock absorber would be:

1) High power to weight ratio
2) Better mechanical-electrical energy conversion efficiency
3) High compatibility with the vehicle [72]

Figure 40. Shock absorber [73]

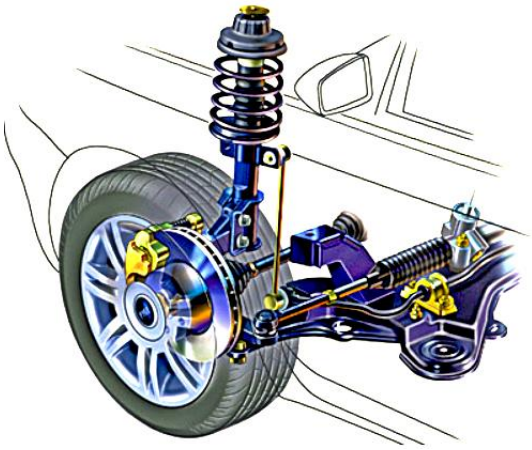

Figure 41. MacPherson strut suspension [74]

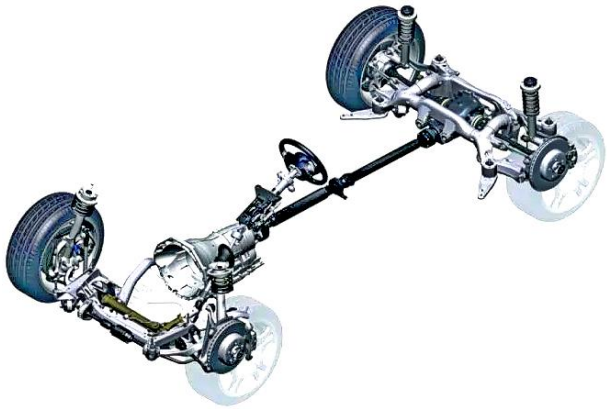

Figure 42. Steering system [75]

The areas of application for powder metallurgy in a car are presented in Figure 43.

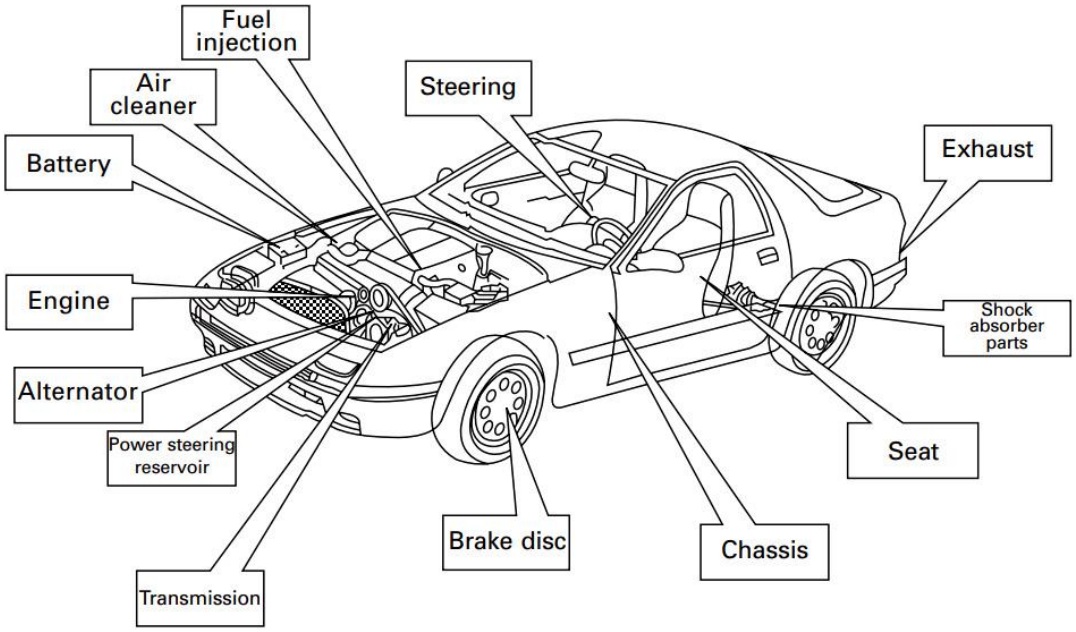

Figure 43. Powder metallurgy application areas in a car. [62]

2.6. Six Sigma and IATF

The global automotive industry demands world-class product quality, productivity and competitiveness, as well as continuous improvement. To accomplish this, vehicle manufacturers require suppliers to certify the quality management standard for suppliers in the automotive sector, known since October as IATF 16949:2016 (formerly ISO/TS 16949).

It is an ISO technical specification that combines the requirements of existing American, German, French and Italian standards for management systems within the global automotive industry. It defines the quality requirements of the quality management system in related companies with the automotive industry. It was defined to improve both quality within the supply chain and the certification process itself. [76,77,78]

In order to carry out the tasks and achieve the goals of each enterprise, especially in the period of progressing globalisation, it is necessary to have a reserve of resources to shape the quality of the product at all stages of its life cycle.

The basic principles as quality management instruments include:

a) Quality management principles
b) Quality management methods
c) Quality management tools

Quality management methods allow tasks to be solved throughout the product life cycle. Their characteristic features are planning and repeatability and are based on science. [79]

Toyota Production System (TPS) – TPS is the first of the Japanese methods known in the West. There are four principles that underpin the TPS method:

- each operation should be defined in detail in terms of the necessary equipment, time to perform and the final result

- any customer-supplier relationship must be clearly targeted and there must be an appropriate route for requests and responses.

- there must be a clearly defined flow path for each product and service.

- each improvement project must be implemented in accordance with the guidelines of a given method, under the guidance of a teacher (mentor) at the lowest possible level of the company.

Six Sigma is a method of quality management that measures the effectiveness of activities and increases efficiency. A characteristic feature of the Six Sigma method is the pursuit of the lowest possible number of defects. A lower defect rate means better quality, but in the Six Sigma method, improving quality is also supposed to improve the profitability of the company.

Six Sigma principles:

a) Principle 1 - customer direction. The customer's needs change.
b) Principle 2 - information-driven management.
c) Principle 3 - process, manage and improve.
d) Principle 4 - active management.
e) Principle 5 - unlimited cooperation.
f) Principle 6 – excellence, tolerance of failure.

The Six Sigma method is currently one of the most advanced quality management techniques that combines all previous methods.

Six Sigma is a philosophy described as the full focus of all activities on the customer, the constant increase in the ability to meet customer needs and the reduction of prime costs. [79]

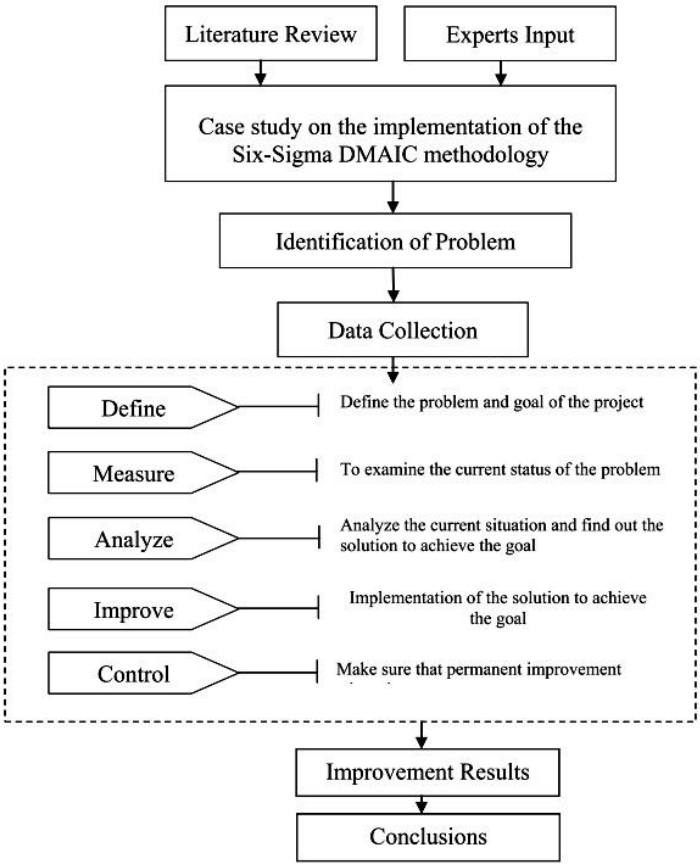

Figure 44. Research methodology Flowchart [80]

DMAIC is a data-driven problem-solving technique designed to identify and address inefficiencies in a process (Figure 44). It is divided into five basic phases:

- Define the problem and goal of the project.
- Measure to examine the current status of the problem.
- Analyse the current situation and find out the solution to achieve the goal.
- Improve - implementation of the solution to achieve the goal.
- Control - make sure that permanent improvement takes place. [80]

3.Research part

3.1. Thesis statement

The chemical composition of powder material, the density of the moulded parts and the type of material from various technological processes has an impact on the properties of sintered components include hardness and compression, tensile strength values.

3.2. Goal

The scientific objective of the doctoral dissertation is examination of the impact of the influence of the chemical composition of iron-based powder materials, as Fe-C, Fe-C-Cu on the properties of sintered components.

Based on the formulated research postulate, the following implementation goals of the dissertation were determined:

1. selection of powder material to determine the strength properties of sintered components
2. reduction of large research amounts under laboratory conditions by the development of an appropriate scientific knowledge base and verification of the implementation of new powder metallurgy products
3. the Digital Twin concept - a comparison of real and literature parameters used for the finite element analysis (FEA)
4. design and construction of a suitable test stand to study the density of sintered components.

3.3. Scope

The thematic scope of the dissertation, including the definition of the research topic, includes defining the relationship between copper and carbon content and the density parameter for sintered components that are components of vehicle suspension. Using the right chemical composition and a technological process, it is possible to find relationships among the chemical composition, density and mechanical properties of the components (tensile and compression strength, yield strength, elongation and hardness).

Metallographic studies carry information about the effects of a crack in a sintered component on a potential failure in the entire car suspension system. Production costs may be reduced by the calculation and determination of carbon losses in the production process.

The scope of scientific studies requires verification of the following issues:

1. the properties of powder materials
2. the structures of manufactured sintered components
3. the mechanical properties of sintered components

For that purpose, an optical microscope, a scanning and a transmission electron microscope were used. Studies of mechanical properties require hardness, tensile and compressive strength tests and density.

The scope included a comprehensive study of a compact structure, built from FC-0208 material (22). Tensile and compressive strengths were tested for various combinations. The test data yielded compression and tensile test results for the tests conducted at 23°C and 120°C, for sintered components of different densities, and for the sintering process, either with or without additional heat treatment. The breakthroughs were analysed, using SEM and TEM microscopy. A Drucker-Prager mathematical model was developed to simulate the behaviour of the compacts during compression and tension tests and the appearance of potential cracks.

The scope of the dissertation included checks of the behaviour of sintered components produced from Fe-C iron-based powder material and from Fe-C-Cu copper-doped and iron-based powder material. Their compression and tensile strengths were tested. Their microstructure was also tested for different density samples of the sintered component.

3.4. Powder material properties

The material suppliers indicated the chemical composition of the bulk powder. The chemical composition of the powder and the measurement uncertainties are given in Table 6 – 9. Figure 45-56 shows the SEM image revealing the morphology of as-received powder.

Fe-C and Fe-C-Cu powders were used for the tests. There was sponge and atomised powder.

Sponge powder - porous, reduced powder produced by grinding metal sponge with a high porosity

Atomised powder - powder produced by atomising liquid metals and alloys into droplets, which solidify to form individual particles.

The outer shapes of both particles are irregular and quite similar to each other, but the sponge iron particle, as the name suggests, is spongy internally, while the water atomised particle is internally compact.

In the dissertation,

powder A was designated as 22

powder B was designated as 18

powder C was designated as 4

powder D was designated as 26

powder E was designated as 2

powder F was designated as 17

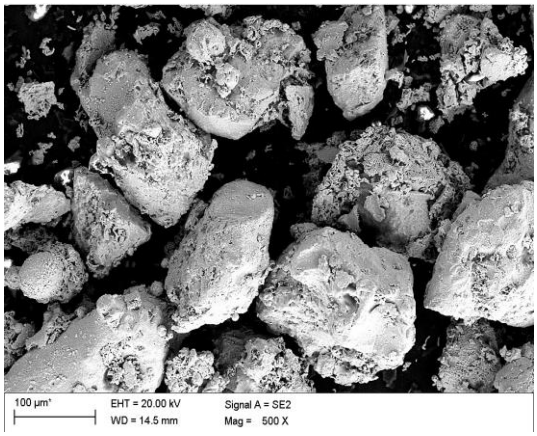

Figure 45. SEM picture of powder metal PN 22, atomised, Magnification 500X,

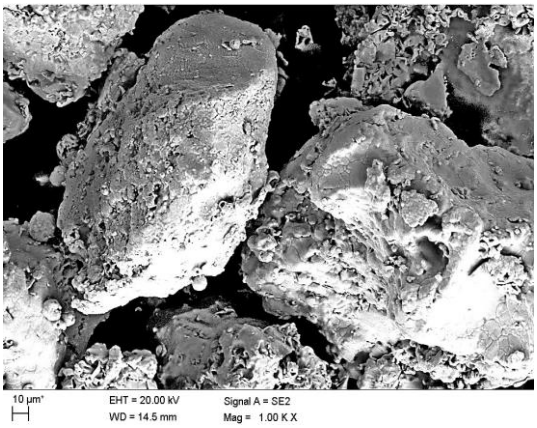

Figure 46. SEM picture of powder metal PN 22, atomised, Magnification 1000 X,

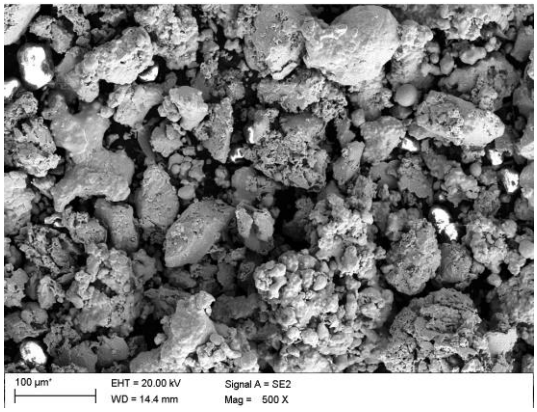

Figure 47. SEM picture of powder metal material PN 18, atomised, Magnification 500X

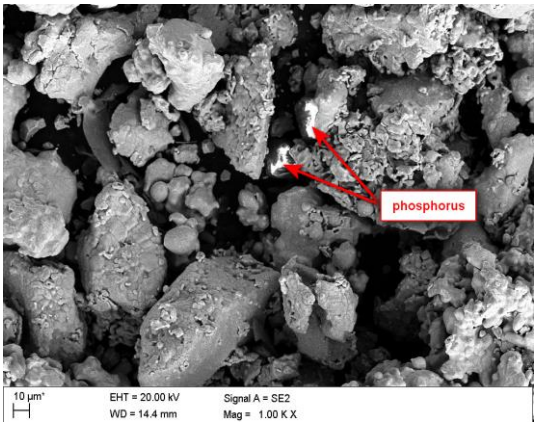

Figure 48. SEM picture of powder metal material PN 18, atomised, Magnification 1000X

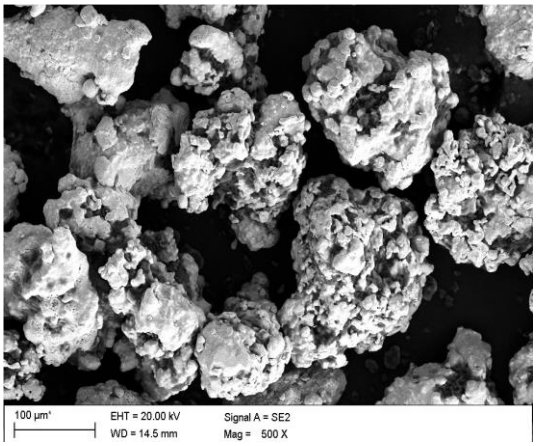

Figure 49. SEM picture powder metal of material PN 4, atomised, Magnification 500X

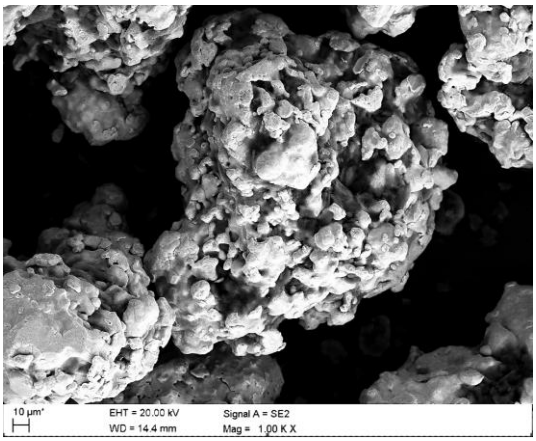

Figure 50. SEM picture powder metal of material PN 4, atomised, Magnification 1000X

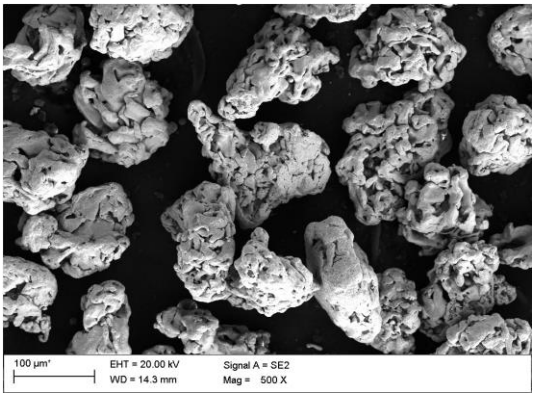

Figure 51. SEM picture of powder metal material PN 26, sponge, Magnification 500X

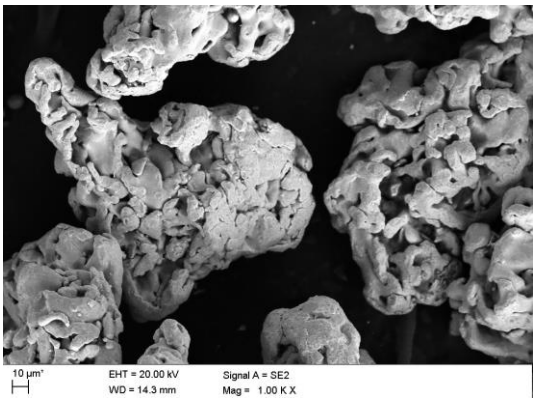

Figure 52. SEM picture of powder metal material PN 26, sponge, Magnification 1000X

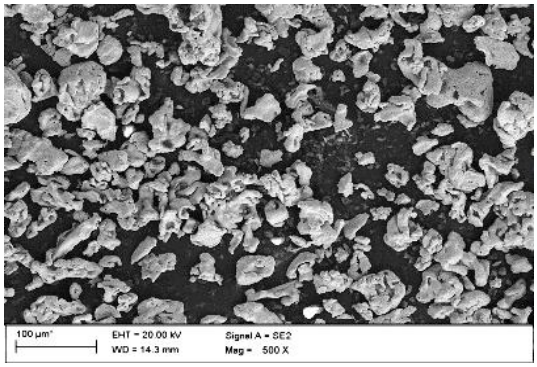

Figure 53. SEM picture of powder metal material PN 2, sponge, Magnification 500X

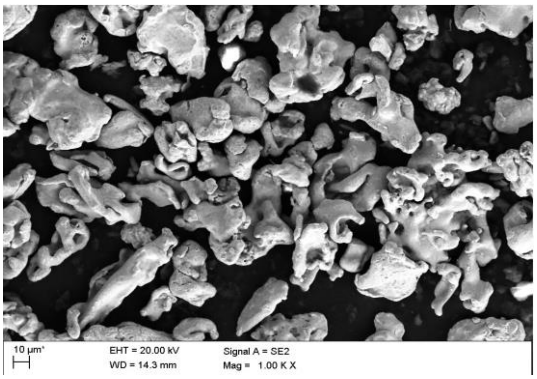

Figure 54. SEM picture of powder metal material PN 2, sponge, Magnification 1000X

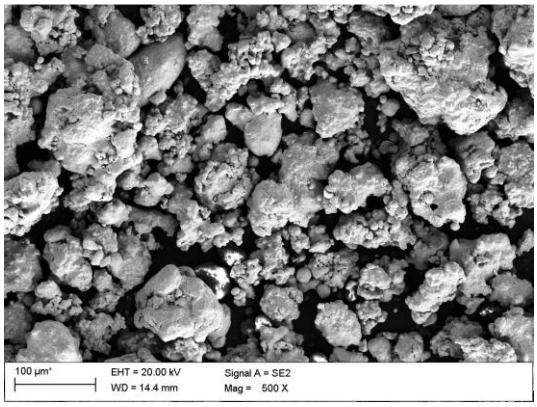

Figure 55. SEM picture of powder metal material PN 17, atomised, Magnification 500X

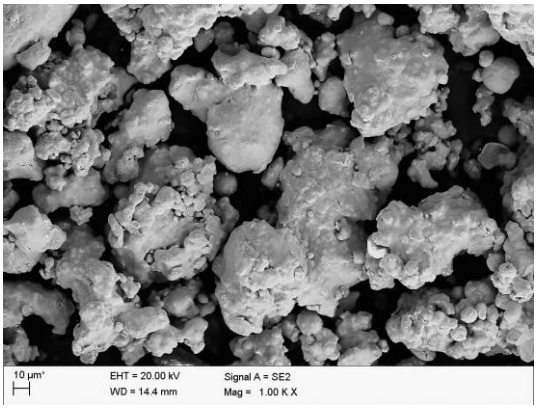

Figure 56. SEM picture of powder metal material PN 17, atomized, Magnification 1000X

The material classification according to the MPIF 35 standard is presented in Table 5.

Table 5. Classification of materials according to the MPIF 35 standard; % Iron-Copper and Copper steel [11]

Powder Metal Number	Material Designation	C	Cu	Fe	Element
2	F-0005	0.3-0.6	/	balance	min-max
4	FC-0208	0.6-0.9	1.5-3.9	balance	min-max
17	F-0005	0.3-0.6	/	balance	min-max
18	FC-0205	0.3-0.6	1.5-3.9	balance	min-max
22	FC-0208	0.6-0.9	1.5-3.9	balance	min-max
26	FC-0208	0.6-0.9	1.5-3.9	balance	min-max

Other Elements: 2.0% maximum may include other minor elements added for specific purposes.

The detailed chemical composition is given in the material card from the powder supplier. Table 6 – 9.

Table 6. Chemical composition from Material Safety Data Sheet from Source 1.

Chemical Composition of powder material	Powder Material 2	Powder Material 4	Powder Material 17	Powder Material 26
S [%]	/	/	/	1.62-1.99
Ni [%]	/	/	0.42-0.57	/
Mo [%]	/	/	0.45-0.55	/
Cu [%]	/	2.70-3.33	/	1.62-1.99
C-Graphite [%]	1.08-1.32	0.90-1.10	0.35-0.45	0.72-0.88
Zn-stearate [%]	0.72-0.88	/	/	/
Lubricant [%]	/	0.88-0.99	/	0.81-0.99
Lube E [%]	/	/	0.54-0.66	/
Fe is base [%]	/	/	/	/

Table 7. Physical Properties from Material Safety Data Sheet from source 1.

Physical Properties of powder material	**Powder Material 2**	**Powder Material 4**	**Powder Material 17**	**Powder Material 26**
AD Gustavsson [g/cm^3]	2.72-2.84	3.23-3.43	2.95-3.15	max. 5.00
Flow Gustavsson (+24 h) [70 sec/50 g]	max. 70	max. 35	max. 42)	max. 90
GD Green Density (3.5 tonne/cm^2) [g/cm^3]	min. 6.30	min. 7.04	min 7.04	6.74

Table 8. Chemical properties composition from the Material Safety Data Sheet from Source 2.

Chemical Composition of powder material	**Powder 18**	**Powder 22**
Iron ATOMET 24 [%]	54.03	/
Iron ATOMET 1001 [%]	42.42	/
Iron ATOMET 28 [%]	/	97.45
Copper [%]	2.00	4.65
Graphite [%]	0.60	0.90
Lubricant (Acrawax Powdered) [%]	0.80	0.75
Lubricant EBS Wax [%]	/	/
Phosphorus [%]	0.45	/

Table 9. Physical Properties from the Material Safety Data Sheet from source 2.

Physical Properties of powder material	**Powder 18**	**Powder 22**
Apparent Density [g/cm^3]	2.70-2.80	2.60-2.80
Flow rate ISO 4490 [s/50 g]	max. 40	max. 55
Compacting pressure (MPa)	max. 480	/
Green density at 400 MPa,	/	min. 6.45
Green strength at 400 MPa	/	11.51
Dimensional change from die size, % (acc. to ISO 4492)	/	0.10
Transverse rupture strength, MPa; acc. to ISO 3325	/	733
Hardness [HRB]	/	74

3.5. Conventional sintering method

Powder materials with properties shown in Table 6 and Table 9 were subjected to the conventional sintering method pressed at 400 MPA, sintered 25 minutes at 1121°C in N_2/H_2: 90/10 atmosphere.

From the materials listed above, oar-shaped mouldings were produced in accordance with the MPIF 10 standard [81]. The samples were prepared according to the norm BS EN ISO 2740:2009 = MPIF 10. The compacts, apart from the chemical composition, differed in density in the range (5.9 - 6.9 g/cm^3).

Two different stages of production were used for specimens shaped in accordance with MPIF 10 for tensile strength testing:

1) Compaction process → Sintering step
2) Compaction process → Sintering step → Steaming step

The atomised and sponge iron based powder used in the automotive industry were used to produce the powder metal compacts. All powders were mixed with different lubricants as presented in Tables 6 and Table 8. The general chemical composition of the Powder Metal

compacts was given in Table 5. These powders were compacted by the conventional sintering process using a furnace at 1120°C for 30 min. The N_2/H_2 gas was introduced into the furnace to create the sintering environment. After the sintering process some compacts were additionally steamed. [28].

3.6. Testing Methods

PARTICLE SIZE MEASUREMENT

Metal powder samples were measured without any restrictions using a HELOS laser diffraction system using the measurement procedure presented in Table 10.

The particle size distributions of the samples were measured with a HELOS laser diffraction instrument. Samples were measured 3 times each to prove the reproducibility and repeatability of the HELOS system and the quality of applied dispersing technique.

Table 10. Selected measuring range of the HELOS instrument

Measuring range	**Focus length f [mm]**	**Measuring range [µm]**
R5	500	0.5 - 875

The dispersion of the particles was carried out with the dry disperser RODOS/M. The cumulative distribution Qr(x) indicates the normalised fraction of particles that are smaller than the particle diameter x. Usually in the graphical presentation of the results for the particle size analysis the value of the cumulative distribution Qr is plotted along the linearly subdivided ordinate whilst the particle diameter x is plotted in µm along the logarithmically subdivided abscissa.

Density distribution curve and frequency distribution curve respectively, indicating the ratio of a class, that is, the fraction for a particle size interval, to its class width.

The graphical presentation of the curves is often executed on a double linear grid, which means both the ordinate and the abscissa are subdivided linearly.

TENSILE TEST

For the purpose of the tensile test samples were prepared according to the norm BS EN ISO 2740:2009 = MPIF 10. The test specimens were pressed in dies with the dimensions in Figure 57 and Figure 58 (conventional flat test specimen).

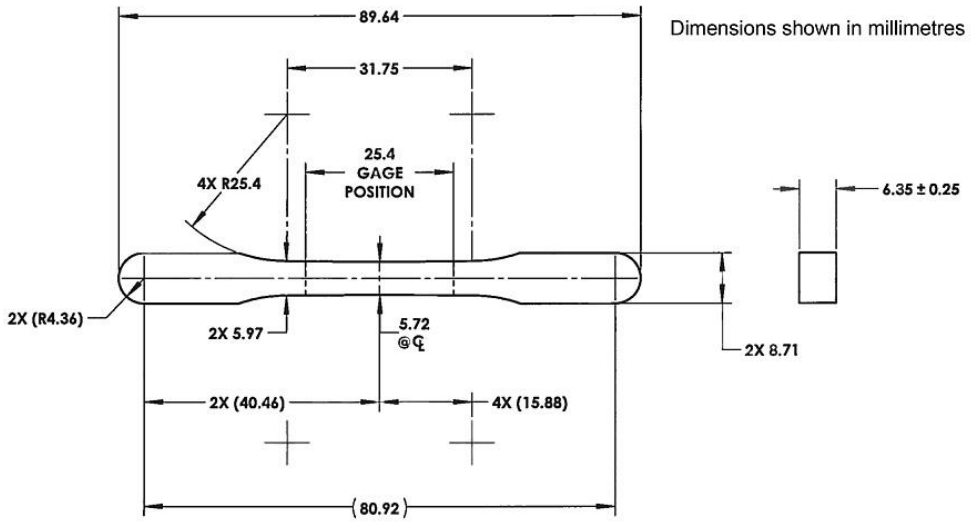

Figure 57. Conventional flat test specimen according to drawing [81]

Figure 58. Conventional flat test specimen – real after production process.

The tensile test was performed on the ZWICK Z250 tensile machine (Figure 59). This testing machine is able to perform all static strength tests required in the assessment of the examined materials. This machine offers the ability to carry out the static tensile test at room temperature, with the determination of the values required by PN-EN ISO 6892-1 standard [39]; static compression and bend test; and the determination of Young's E module.

The repeated tensile test was performed on an MTS insight System machine, MTS Insight System 10kN (Figure 60). It is a multi-purpose testing machine by MTS, equipped with specialized instrumentation enabling the performance of tests and measurements in a wide range, (maximum load 10kN, available force heads 10kN, 500N), with MTS TestWorks and FlexTest software.

Figure 59. The ZWICK Z250 tensile machine [82]

Figure 60. MTS Insight System 10kN [83]

The tensile test were performed at a temperature of 23° and a temperature of 120°C, see Figure 61 below.

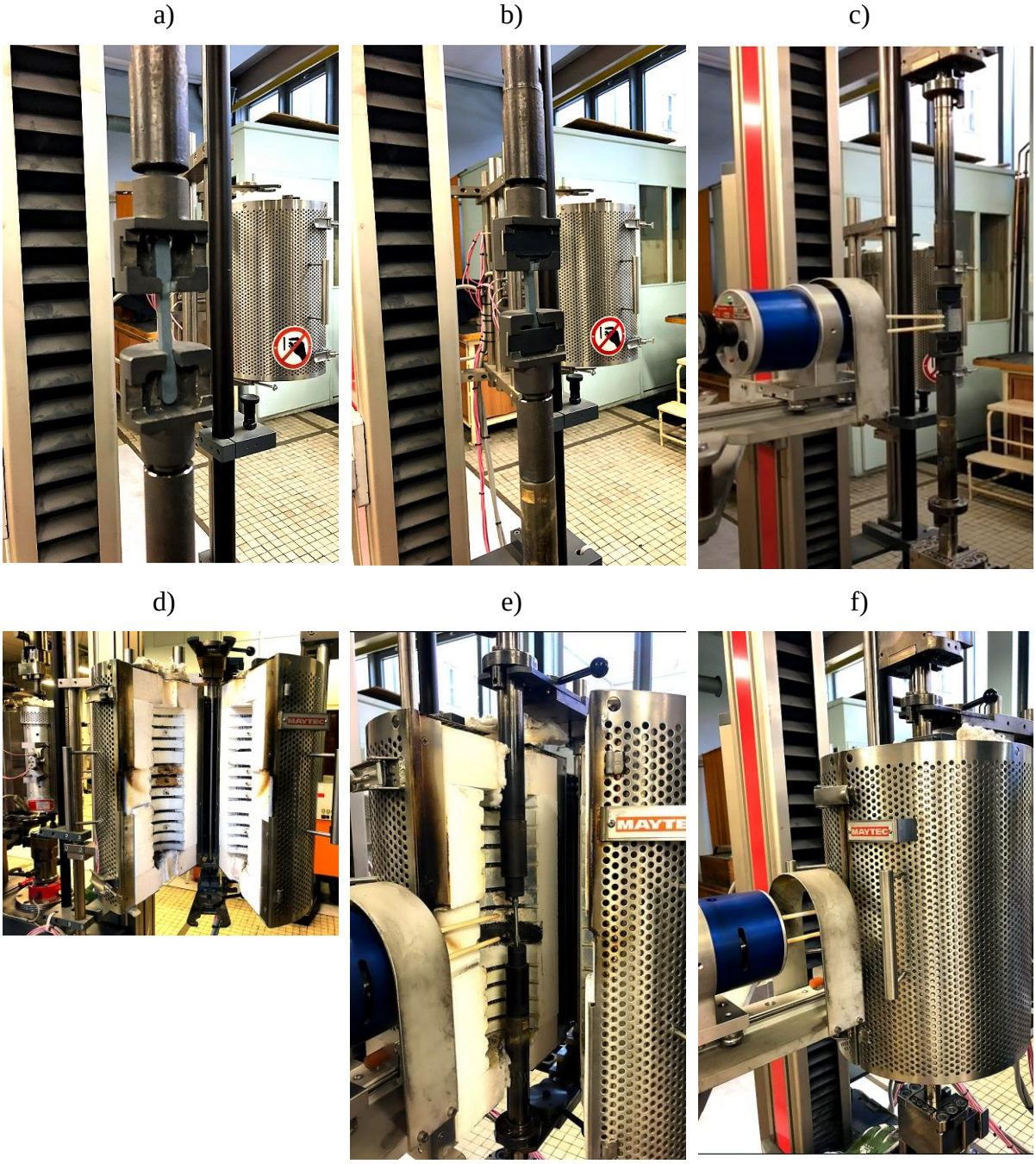

Figure 61. Tensile test machine a) - c) at 23°C, and d)-f) 120°C, with the extensometer.

COMPRESSION TEST

The compression test was performed on the INSTRON 5585H machine with a force measurement range of up to 250kN according to the PN-EN ISO 4506:2018-05 standard [51].

For FEA analyses there were produced the special samples were produced with the shape presented in the drawing below (Figure 62).

a) b)

Figure 62. The produced compact for compression strength test according to norm [51]

The remaining compacts 2, 4, 17, 18, 22, 26 were subjected to a compression test on a ZWICK Z250 machine with two heads (250kN and 10kN, Figure 62) and two furnaces (temperature range from 120°C to 200°C, Figure 63). The size of the compacts used for compression test was 5.8 mm × 6 mm × 10 mm. The compressive strength of the specimen is calculated by using the compressive strength, the maximum load before fracture and the minimum cross-sectional area of the sample, respectively [65].

a) b)

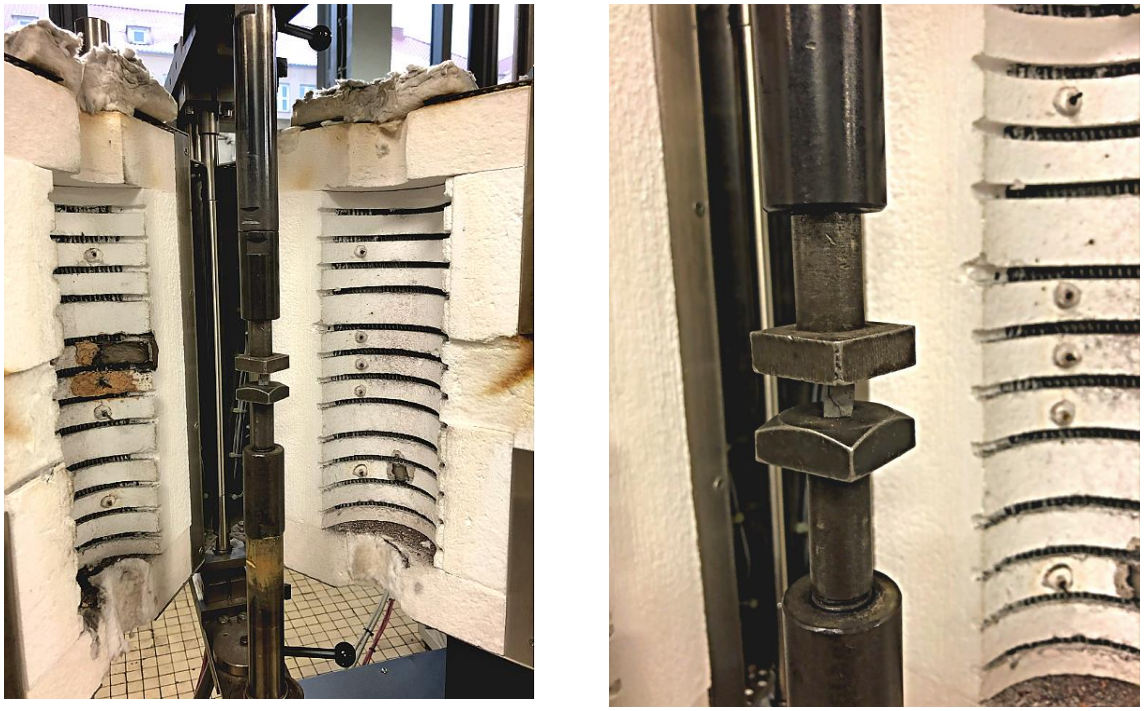

Figure 63. The compression test machine a) - b) at 120°C, and the compact sample ready for testing.

HARDNESS TEST

The Rockwell hardness tester, manufactured by INNOVATEST, model VERZUS 710RS was used for hardness measurements (Figure 64). It was checked by Scale HRB [84] , and 1/16" Ball Holder [85]

Figure 64. Rockwell hardness tester, manufacturer INNOVATEST, model VERZUS 710RS [86]

The advantages of the Rockwell method are:

- very fast hardness reading, which makes it possible to use it in mass tests,
- minor damage to the tested element,
- universality of testing in terms of hardness of materials,
- ease of use of the hardness tester.

The disadvantages include:

- a large number of measurement scales, making it difficult to compare results,
- small indentations make it impossible to measure inhomogeneous materials.

OPTICAL MICROSCOPE

The compacts were cut on Abrasimatic 300 Buehler, tan mouldings using the Mecapress 3 machine, and ground and polished with the Metkon Digiprep 251 machine.

The samples for the metallographic investigations were prepared under identical conditions followed by chemical etching with nital 5%. The special prepared mould samples were observed with an Optical Microscope. An Eclipse MA200 NIKON (LOM) light microscope was used to check the structure, with magnification up to 1000x, 2D image. (Figure 65 below).

Figure 65. The optical microscope Eclipse MA200 NIKON [87]

Figure 66. Carbon and sulphur content analyser - CS600 by LECO. [88]

The CS carbon analyser (Figure 66) is designed for a wide-range of measurement of carbon content in powder metals. A weighed sample of 1 gram is combusted in a stream of oxygen using RF induction to heat the sample. Carbon present in the sample is oxidized to carbon dioxide (CO_2), and swept by the oxygen carrier through a drying reagent. The gas flow continues past a heated catalyst, where carbon monoxide (CO) is converted to CO_2, which is subsequently removed by a filter. Carbon is then detected as CO_2 by another NDIR cell. A pressure controller is used to maintain constant pressure in the NDIR cells to reduce interference from natural variations in atmospheric pressure. The final component in the flow stream is an electronic flow sensor, which is used for diagnostic purposes to monitor the carrier flow. Non-dispersive infrared cells are based on the principle that CO_2 absorbs infrared (IR) energy at unique wavelengths within the IR spectrum. [89]

Agnieszka Stanula

SEM (SCANNING ELECTRON MICROSCOPE)

The Scanning Electron Microscope (SEM) was used for observation, analysis and characterization of the surface and surface layer of the tested objects/materials. It was used for the analysis of the particle shape and size of the powder metal. And for the compacts the SEM was able to check the material structure (grains, fractography, etc).

Using the SEM/EDS the chemical composition (copper content) was also checked. Energy Dispersive Spectroscopy (EDS) allows for a rapid qualitative and quantitative determination of the elemental composition of the tested materials.

The direct SEM microscope was used, MERLIN with the GEMINI II (Figure 67) where the column and FEG electron source offers high resolution imaging using advanced detection modes, including InLens (SE), InLens (EsB), Angle Selective back-scattered detector (AsB), 3DSM and STEM. Gemini II optics imaging settings, such as voltage or probe current, can be adjusted without realignment. Parallel on-axis in-lens secondary electron (SE) and energy selective backscattered (EsB) detection can easily identify the smallest differences in materials composition.

Figure 67. SEM Merlin Gemini II (ZEISS) [90]

Agnieszka Stanula

TRANSMISION ELECTRON MICROSCOPY

In addition, the tests were performed on the Transmission Microscope, unique on a global scale, a high-resolution analytical transmission electron microscope Titan Cubed G2 60-300 (FEI) with a unique instrumentation for studying the micro/nanostructure of materials with high resolution (70 pm) (Figure 68,69). A transmission microscope records electrons passing through a sample (very thin plate). For this purpose a sample was prepared using the Focused Ion Beam (FIB) method (Figure 70).

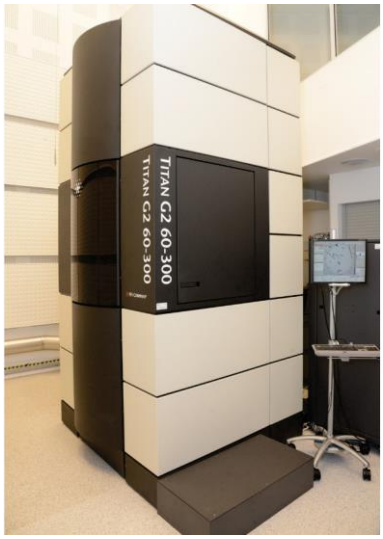

Figure 68. The Transmission Microscope Titan Cubed G2 60-300 (FEI) [91]

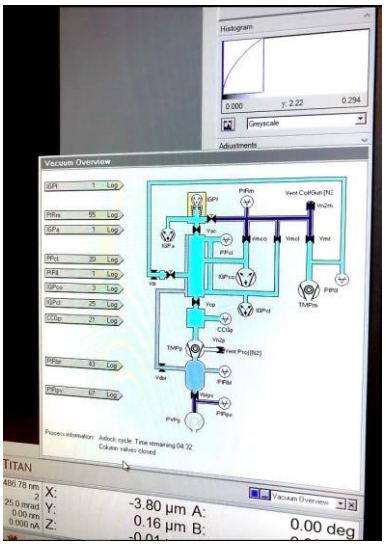

Figure 69. The software for the observation of samples under a Transmission Microscope.

Figure 70. The samples for observation prepared using the FIB method.

DENSITY AND POROSITY MEASUREMENT

The density and open porosity of the compacts were measured by the Archimedes method. An analytical balance (Figure 72) - Advanced Level Analytical Balance with an accuracy of 0.0001 g was used to weigh the samples. [65] For density checks, an analytical balance, a container with water, and a vacuum system (Figure 71) were used. The test was performed according to norm MPIF 42. (Figure 73,74)

Figure 71. Vacuum Inclusion system Cast N' Vac 1000 [92]

Figure 72. Advanced Level Analytical Balance [93]

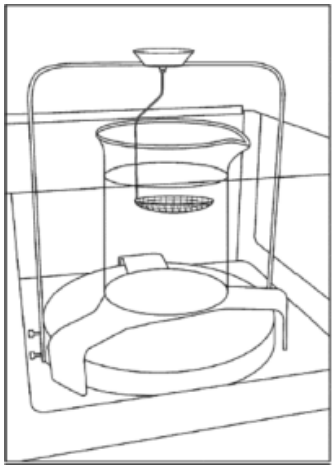

Figure 73. Beaker support above balance drawing. [94]

Figure 74. Beaker support above balance real.

3.7. Description of the results of testing of sintered elements from material FC-0208 (22) with discussion

The compacts made of FC-0208, powder material 22 were produced by material with particle size values from 11 – 236 μm. [95]

It was confirmed by Figure 4 that the particles have irregular or a near spherical shape, which conforms to the morphological features of water atomized powders. [96]

The carbon combined content of the sintered part is 0.62±0.03% - for powder 22, steamed with density 6.3 g/cm^3 with a porosity range of 5-10%.

The characteristic values of the particle size distributions and the averaged distribution curves presented as cumulative distribution Qr(x) and distribution density, the shape factors and particle pictures are shown in Figure 75,76.

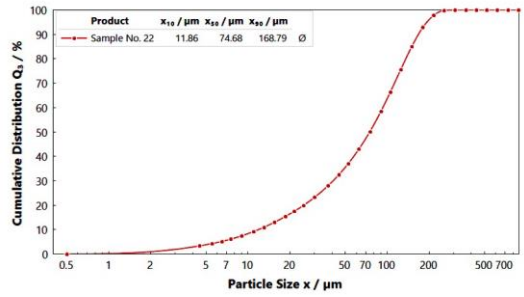

Figure 75. Cumulative distribution Q3/% of sample No. 22

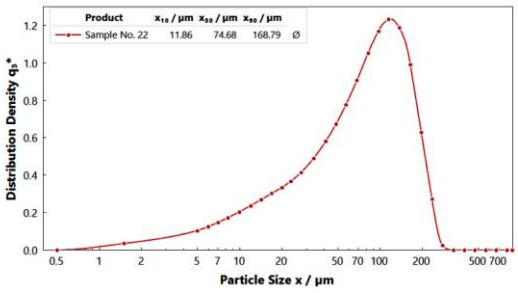

Figure 76. Density distribution q_3 of sample No. 22

The carbon combined content of the sintered part is 0.62±0.03% - for powder 22, steamed with density 6.3 g/cm^3 with a porosity range of 5-10%.

3.7.1. The Tensile Strength test results

Tensile tests were performed at temperatures of 23°C and 120°C. Figure 77-79 and Table 11. Data available for different sintering methods, test temperature and compact density. Young's Modulus results are presented in Figure 80-82 and Table 12.

The samples were produced by the conventional sintering method, and they were divided into two types of samples:

- Sintering/no steaming (1) - those without an additional steaming process
- Sintering/steaming (2) - those with an additional steaming process

No one sample showed yield the strength Rp0.2 [MPa] during the tensile test.

Table 11. The tensile strength test results for the compact made of FC-0208 (22) powder material.

Sintering method	**Test Temperature [°C]**	**Density [g/cm^3]**	**Tensile strength Rm [MPa]**
sintered/no steaming process.	23	5.9	91.9
	23	6.3	165
	23	6.9	201
sintered/no steaming process	120	5.9	113
	120	6.3	163
	120	6.9	223
sintered/steaming process.	23	5.9	132
	23	5.9	145
	23	6.3	131
	23	6.9	28.6
	23	6.9	151
sintered/steaming process.	120	5.9	105
	120	6.3	131
	120	6.9	191

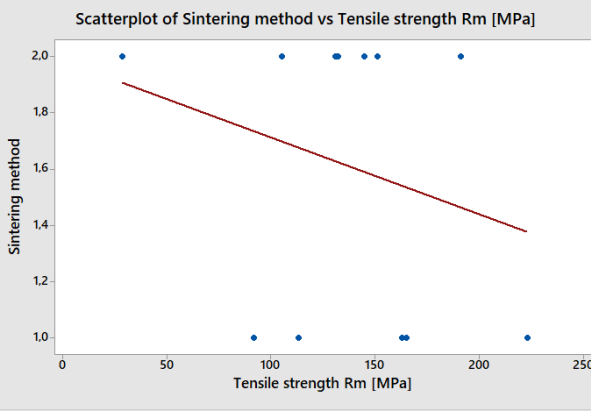

Figure 77. Scatterplot of the sintering method vs Tensile strength Rm [MPa]

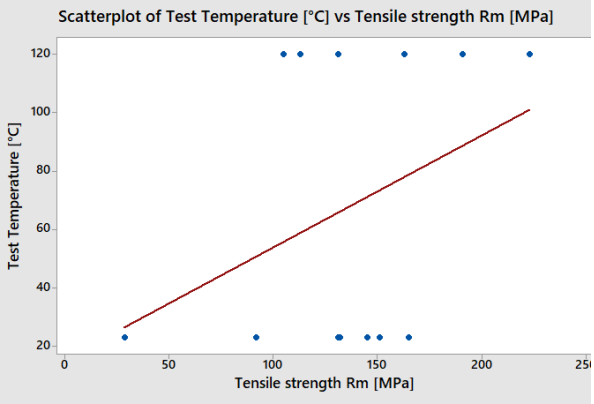

Figure 78. Scatterplot of Test Temperature vs Tensile strength Rm [MPa]

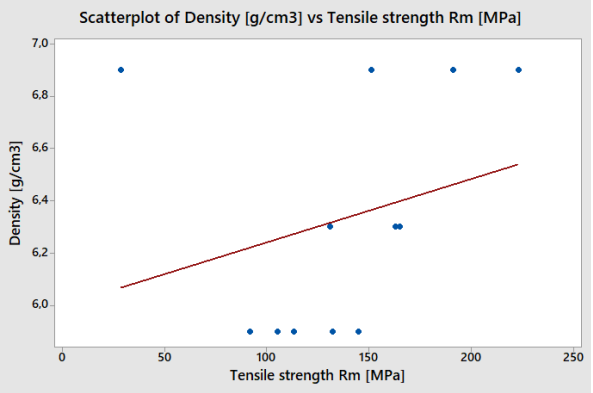

Figure 79. Scatterplot of Density vs Tensile strength Rm [MPa]

The tensile strength of the compact ranged from approximately 90 MPa to over 200 MPa. The result of 28 MPa has been omitted from the analysis.

Table 12. Young's Modulus results after tensile strength test for compact made of FC-0208 (22) powder material.

Sintering method	Test Temperature [°C]	Density [g/cm^3]	Young's Modulus [GPa]
sintered/no steaming process	23	5.9	37.9
	23	6.3	42
	23	6.9	95.8
	23	6.9	273
sintered/no steaming process	120	5.9	50.2
	120	6.3	49.9
	120	6.9	87.7
sintered/steaming process	23	6.9	18.8
	23	5.9	120
	23	5.9	138
	23	6.3	85.5
	23	6.9	85
sintered/steaming process	120	5.9	91
	120	6.3	75
	120	6.9	109
	120	6.9	309

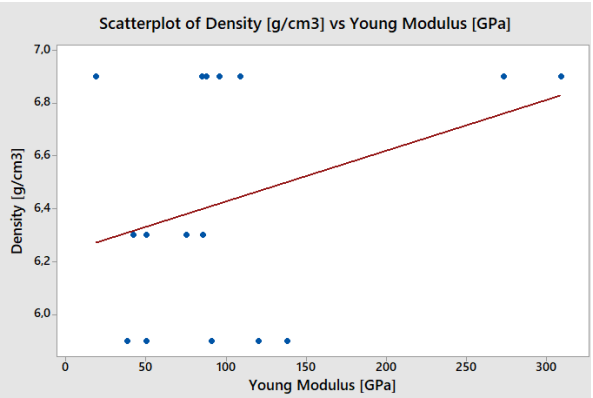

Figure 80. Scatterplot of Density [g/cm^3] vs Young's Modulus [GPa]

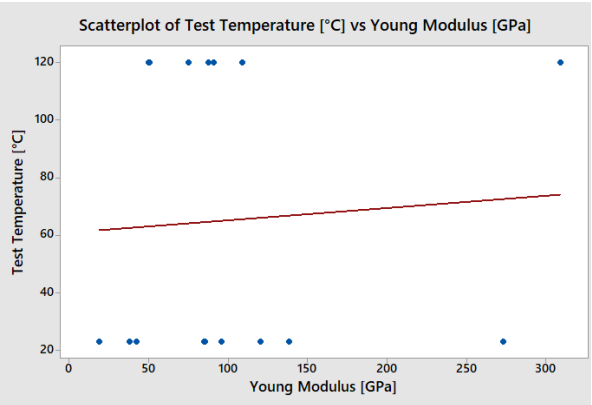

Figure 81. Scatterplot of Test temperature [°C] vs Young's Modulus [GPa]

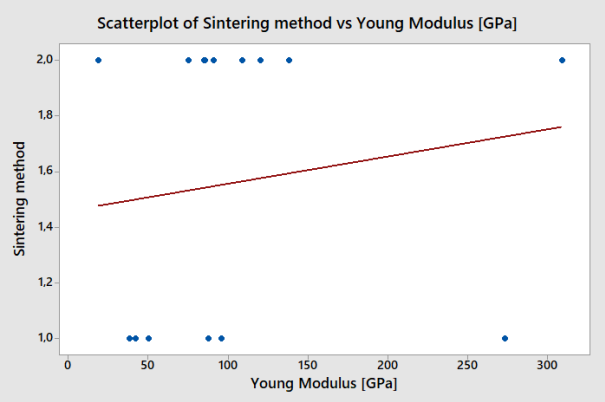

Figure 82. Scatterplot of the sintering method vs Young's Modulus [GPa]

Young's Modulus of the compact ranged from approximately 50 GPa to over 300 GPa. Regression analysis was used to determine the correlations of the density of the compact, temperature of the test, the type of sintering method and Young's Modulus values of these powder metal compacts. It was found that when the density increased the Young's Modulus increased. The test temperature has no impact. The test shows the same values for temperatures 23°C and 120°C. The sintering method with additional steaming shows higher versions of Young's Modulus.

3.7.2. Compression test results

The compression tests were performed at temperatures 23°C and 120°C. Data available for different sintering methods, test temperature and compact density in Figure 83-85 and Table 13.

Table 13. The compression strength test results for compact made of FC-0208 (22) powder material, cubes.

Sintering method	**Test Temperature [°C]**	**Density [g/cm^3]**	**Ed [GPa]**	**σd0.2 [MPa]**	**σdM [MPa]**	**ℰdB [%]**	**ℰdtM [%]**
sintered/no	23	5.9	5.49	252	540	13	21
steaming	23	6.3	5.69	268	614	16	25
process.	23	6.9	5.99	402	758	20	25
sintered/no	120	5.9	4.44	273	533	12	22
steaming	120	6.3	5.27	307	593	12	21
process.	120	6.9	6.07	397	744	14	22
sintered/	23	5.9	6.84	416	667	10	16
steaming	23	6.3	7.44	467	788	8	16
process.	23	6.9	7.59	446	761	10	17
sintered/	120	5.9	7.58	390	630	5	13
steaming	120	6.3	6.61	694	766	2	14
process.	120	6.9	7.66	467	766	14	18

a)

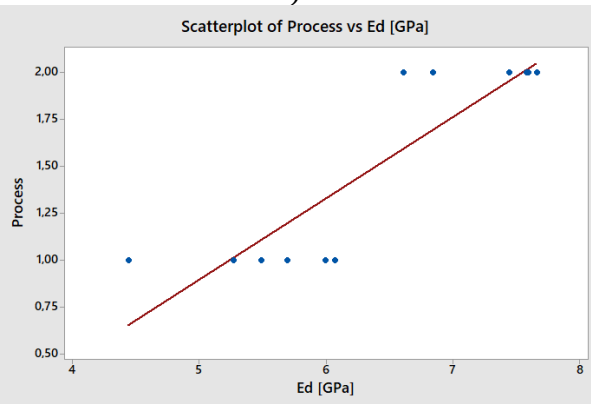

b)

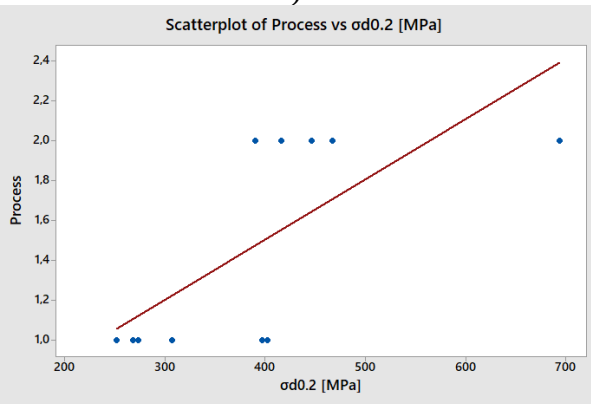

c)

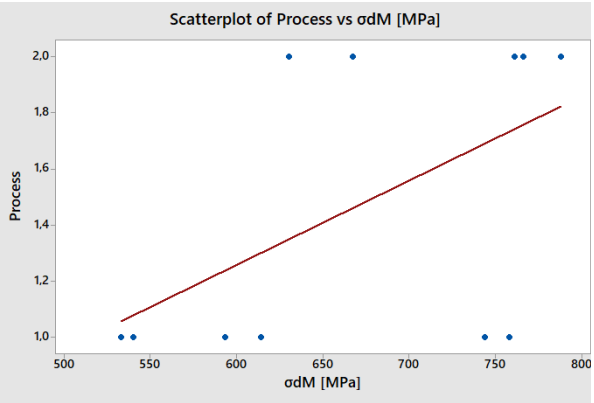

d)

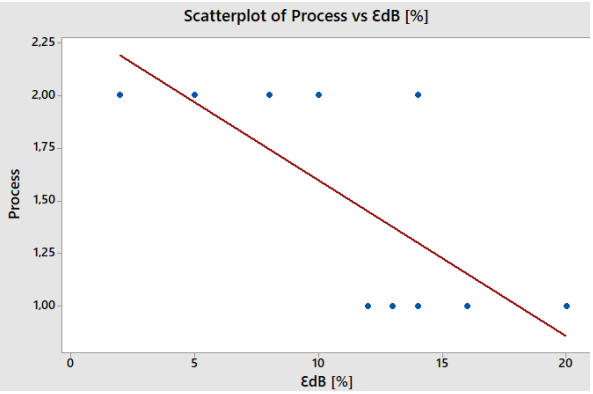

e)

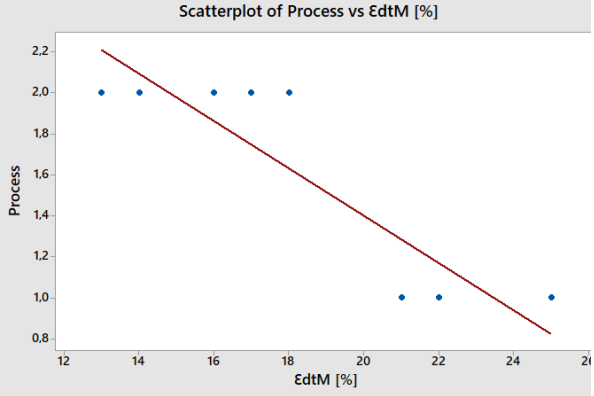

Figure 83. Scatterplot of Process vs a) Ed [GPa]; b) σd0.2 [MPa] ; c) σdM [MPa]; d) ƐdB [%]; e) ƐdtM [%].

a)

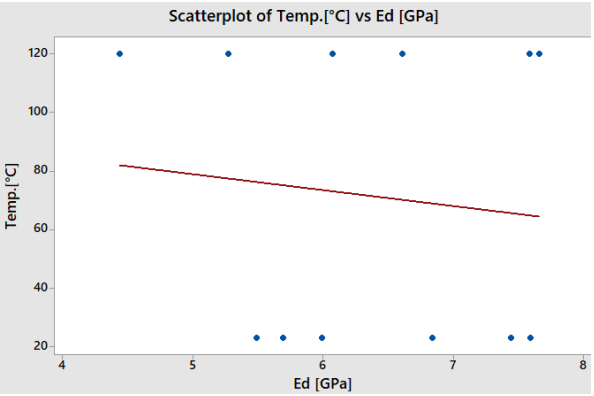

b)

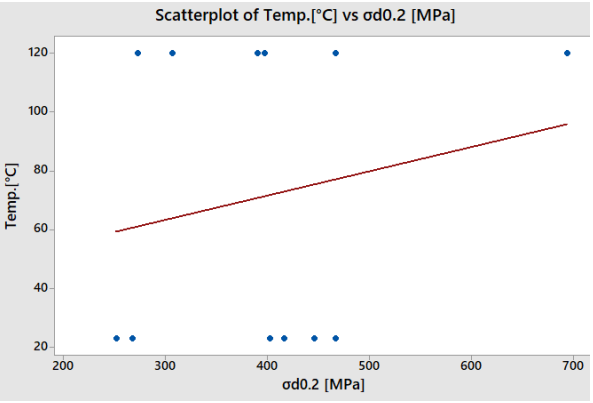

c) d)

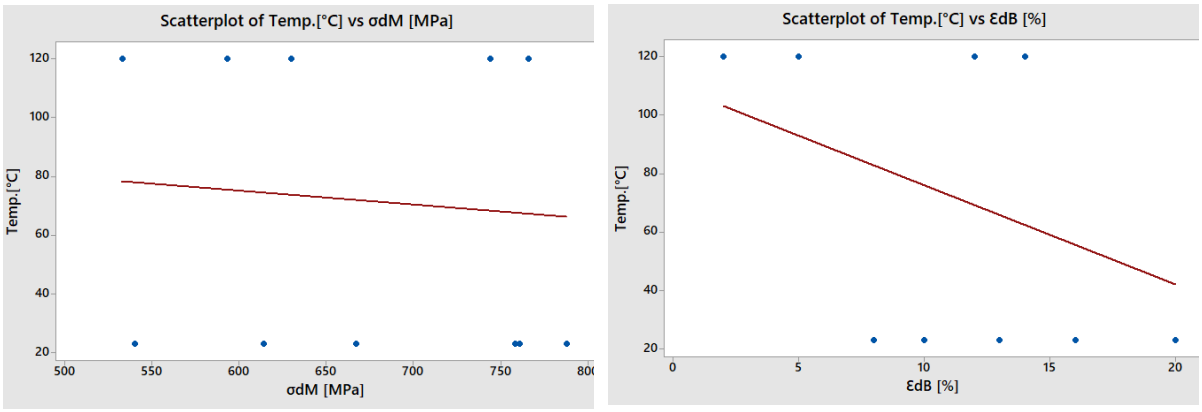

e)

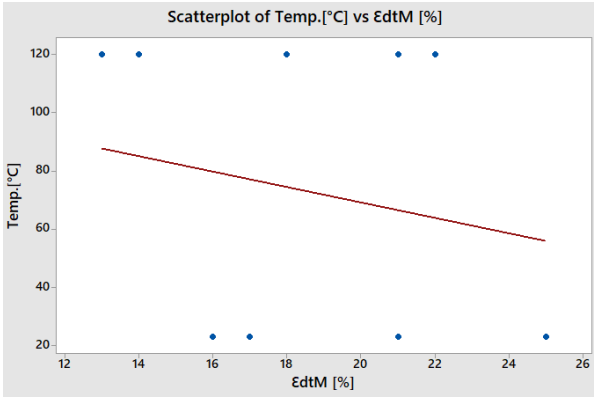

Figure 84. Scatterplot of Temperature [°C] vs a) Ed [GPa]; b) σd0.2 [MPa]; c) σdM [MPa]; d) ƐdB [%]; e) ƐdtM [%].

a) b)

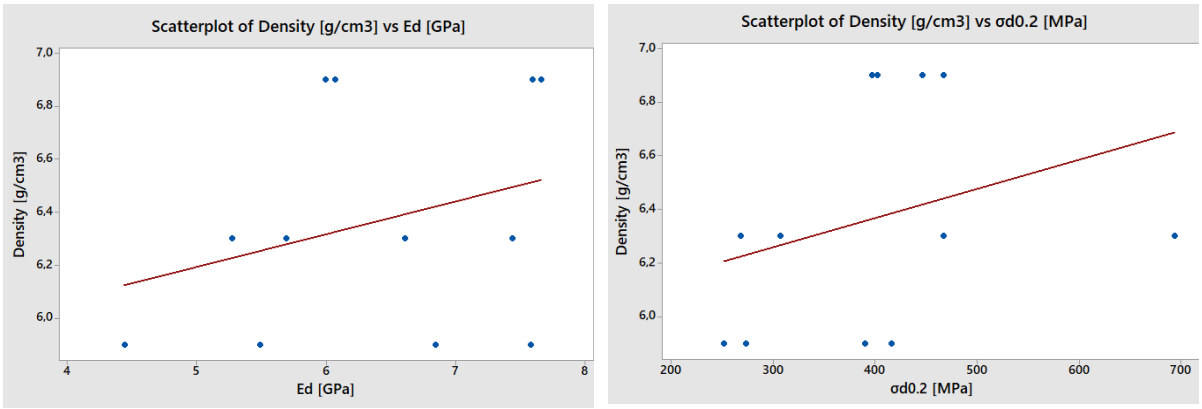

c)

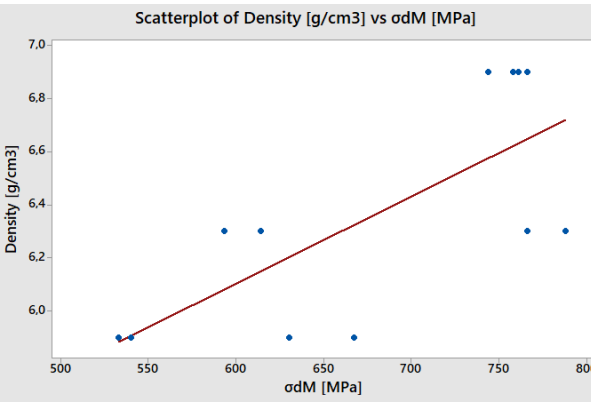

d)

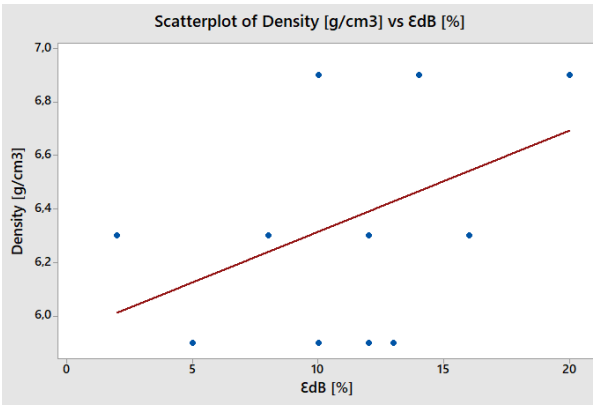

e)

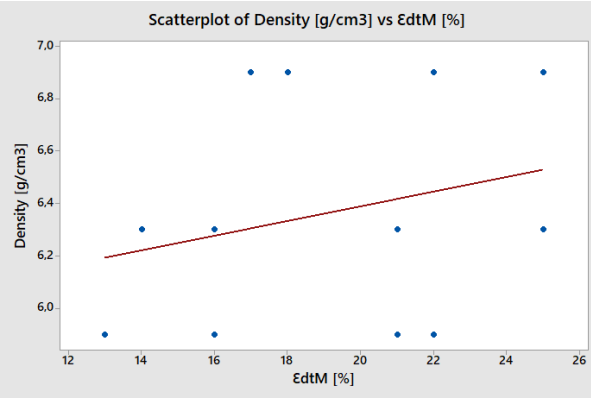

Figure 85. Scatterplot of Density [g/cm^3] vs a) Ed [GPa]; b) σd0.2 [MPa]; c) σdM [MPa]; d) ƐdB [%]; e) ƐdtM [%].

Young's Modulus of the compact ranged from approximately 4 GPa to over 8 GPa.

The yield strength of the compact ranged from approximately 150 MPa to over 600 MPs. The compression strength varied over the range of 520 - 800 MPa.

Regression analysis was used to determine the correlations of the density of the compact, temperature of the test, the type of sintering method and compression test results. It was found that when the density increased the compression test results increased. The test temperature has no impact. The test shows the same values for temperature 23°C and 120°C. The sintering method with additional steaming shows higher versions of Young's Modulus, yield strength and compression strength.

The repeated compression test results for compacts made of FC-0208 (22) powder material, with the sintering process, performed at temperature 23°C with hardness measurements are presented in Table 14 and Figure 86-92.

Table 14. The compression test results for compacts made of FC-0208 (22) powder material, with the sintering process, test performed at a temperature of 23°C.

Compact	**Density [g/cm^3]**	**Young's Modulus [MPa]**	**YIELD STRENGTH [MPa]**	**TENSILE STRENGTH Rs [MPa]**	**HARDNESS [HRB]**
F-0208 material sintered/no steaming process at a temperature of 23°C	5.9	7,332	359	705	51
	5.9	8,818	318	702	49
	5.9	8,150	334	691	50
	6.1	8,566	349	733	48
	6.1	8,561	340	734	52
	6.1	9,116	347	747	51
	6.3	8,996	360	833	50
	6.3	9,299	359	815	50
	6.3	8,736	352	789	50
	6.5	10,127	342	864	64
	6.5	9,663	364	831	61
	6.5	9,654	372	841	60
	6.7	9,876	463	850	72
	6.7	11,690	406	847	70
	6.7	11,520	399	901	71
	6.9	10,176	453	803	78
	6.9	10,754	433	852	78
	6.9	11,775	414	847	77

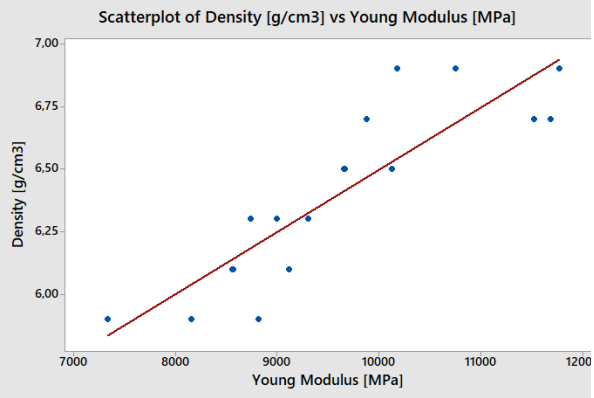

Figure 86. Scatterplot of Density [g/cm^3] vs Young's Modulus [MPa]

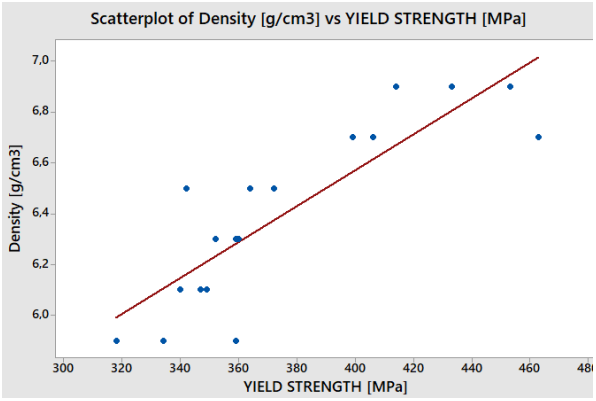

Figure 87. Scatterplot of Density [g/cm^3] vs Yield Strength [MPa]

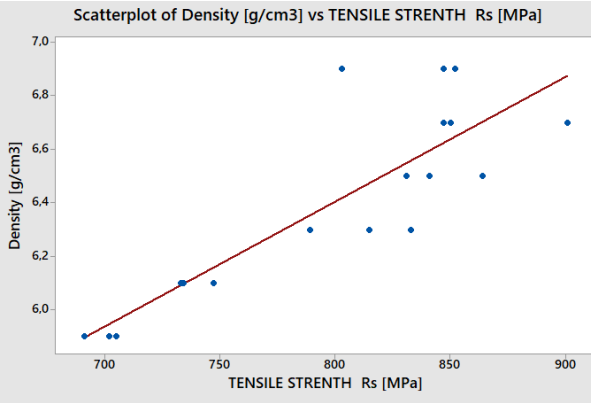

Figure 88. Scatterplot of Density [g/cm^3] vs Tensile Strength [MPa]

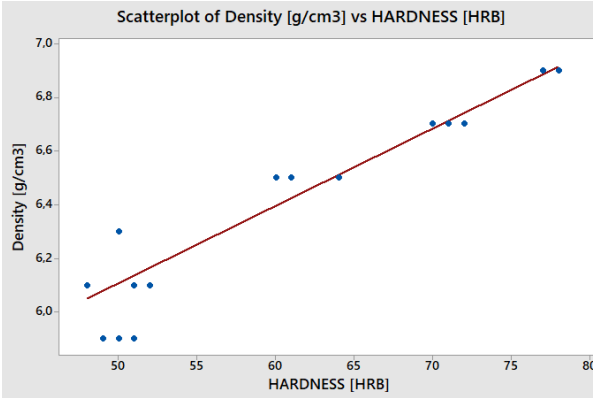

Figure 89. Scatterplot of Density [g/cm^3] vs Hardness [HRB]

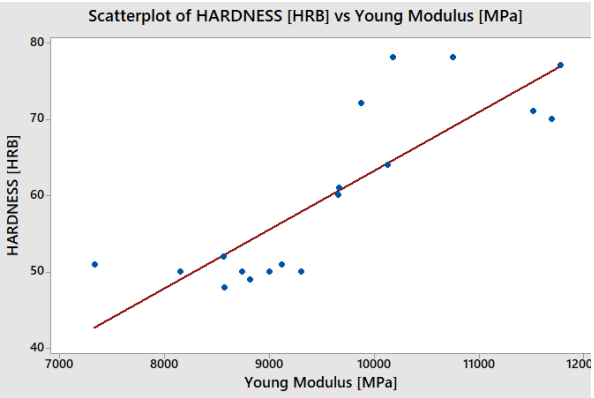

Figure 90. Scatterplot of Hardness [HRB] vs Young's Modulus [MPa]

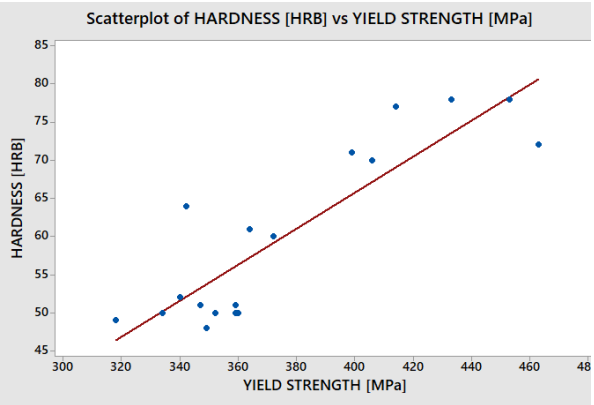

Figure 91. Scatterplot of Hardness [HRB] vs Yield Strength [MPa]

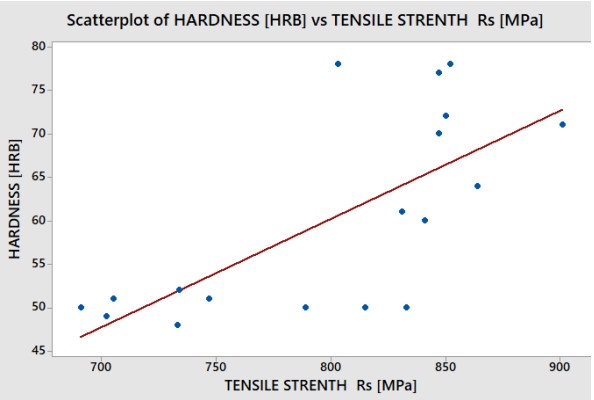

Figure 92. Scatterplot of Hardness [HRB] vs Tensile Strength [MPa]

The repeated compression test for compacts with the sintering process without additional steaming. It showed the Young's Modulus of the compact ranged from approximately 7 GPa to over 12 GPa. The yield strength of the compacts ranged from approximately 320 MPa to over 450 MPs.

The compression tensile strength varied over the range of 700 - 900 MPa. Regression analysis was used to determine the correlations of the density, hardness of the compact, and compression test results. It was found that when the density increased the compression test results increased. The same happened for hardness when the hardness increased the compression test results increased.

The repeated compression test results for compacts made of FC-0208 (22) powder material, with the sintering process and additional steaming process, performed at temperature 23°C with hardness measurements are presented in Table 15 and Figure 93-99.

Table 15. The compression test results for compact made of FC-0208 (22) powder material, with the sintering process and additional steaming process, test performed at temperature 23°C.

Compact	**Density [g/cm^3]**	**Young's Modulus [MPa]**	**YIELD STRENGTH [MPa]**	**TENSILE STRENGTH Rs [MPa]**	**Hardness [HRB]**
FC-0208 material sintered/ steaming process at 23°C temperature	5.9	11,176	465	683	87
	5.9	10,544	557	689	87
	5.9	10,068	536	703	87
	6.1	11,960	686	737	94
	6.1	11,290	680	740	95
	6.1	13,069	715	792	94
	6.3	12,350	649	778	90
	6.3	12,239	669	785	89
	6.3	10,067	724	782	90
	6.5	11,420	656	816	91
	6.5	12,074	593	769	91
	6.5	13,109	579	758	90
	6.7	11,969	550	743	89
	6.7	13,199	541	743	88
	6.7	11,107	654	794	88
	6.9	10,232	573	768	87
	6.9	12,575	493	807	88
	6.9	11,211	577	796	87

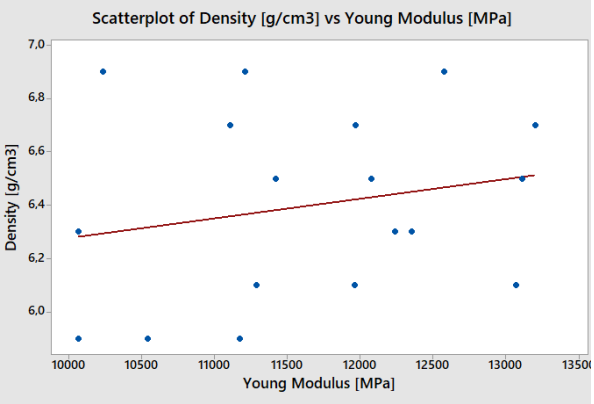

Figure 93. Scatterplot of Density [g/cm^3] vs Young's Modulus [MPa]

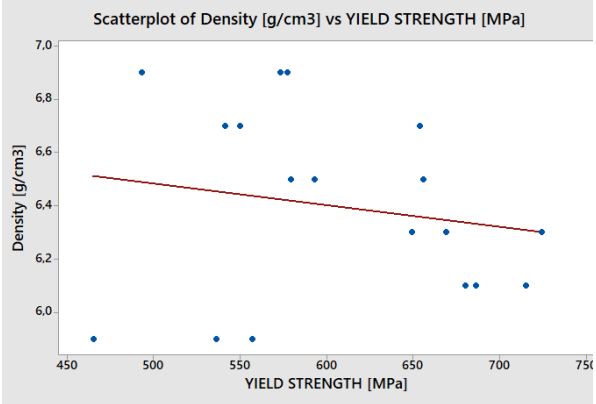

Figure 94. Scatterplot of Density [g/cm^3] vs Yield Strength [MPa]

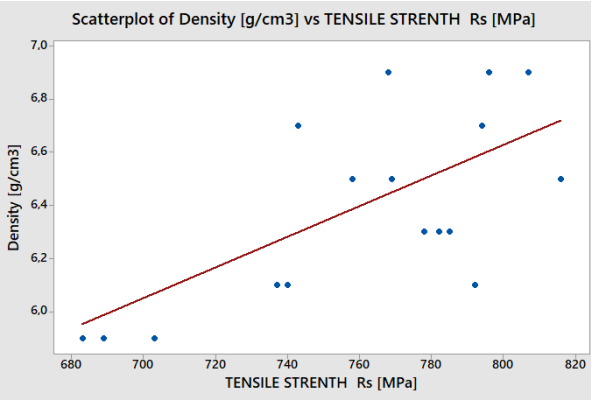

Figure 95. Scatterplot of Density [g/cm^3] vs Tensile Strength [MPa]

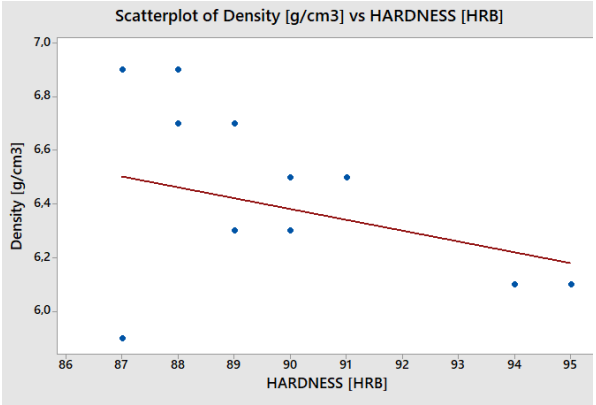

Figure 96. Scatterplot of Density [g/cm^3] vs Hardness [HRB]

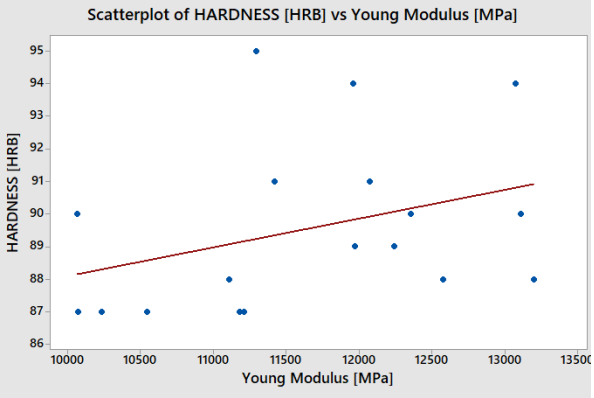

Figure 97. Scatterplot of Hardness [HRB] vs Young's Modulus [MPa]

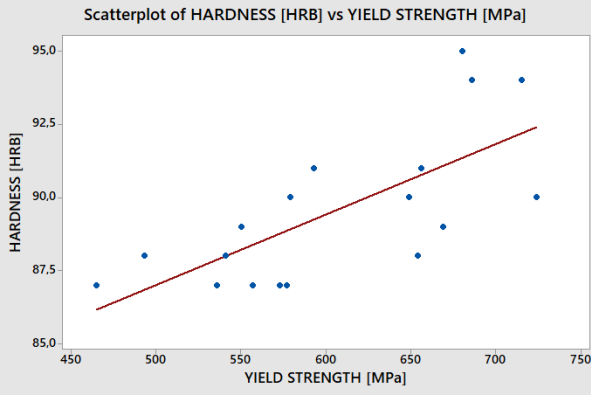

Figure 98. Scatterplot of Hardness [HRB] vs Yield Strength [MPa]

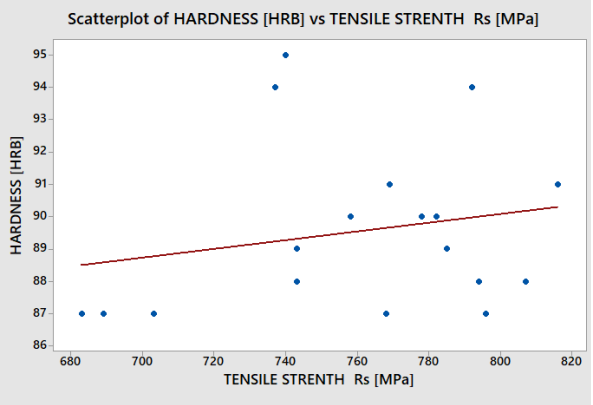

Figure 99. Scatterplot of Hardness [HRB] vs Tensile Strength [MPa]

The repeated compression test for compacts with the sintering process with additional steaming. It showed the Young's Modulus of the compact ranged from approximately 10 GPa to over 13 GPa. The yield strength of the compact ranged from approximately 450 MPa to over 720 MPa. The compression strength varied over the range of 650 - 820 MPa.

Regression analysis was used to determine the correlations of the density, hardness of the compact, and compression test results. It was found that when the density increased the compression test results increased. The same happened for hardness when the hardness

increased the compression test results increased. There was a slight inconsistency in showing the relationship between density and hardness, but it was considered as a measurement error.

3.7.3. Microstructure analysis for material FC-0208 (22) using Scanning Electron Microscope

In order to check the structure, a microscopic observation of the fractured samples. Figure 100 – 103 show the microstructure of the cross section of the compact, the microstructure of iron powders used.

a) b)

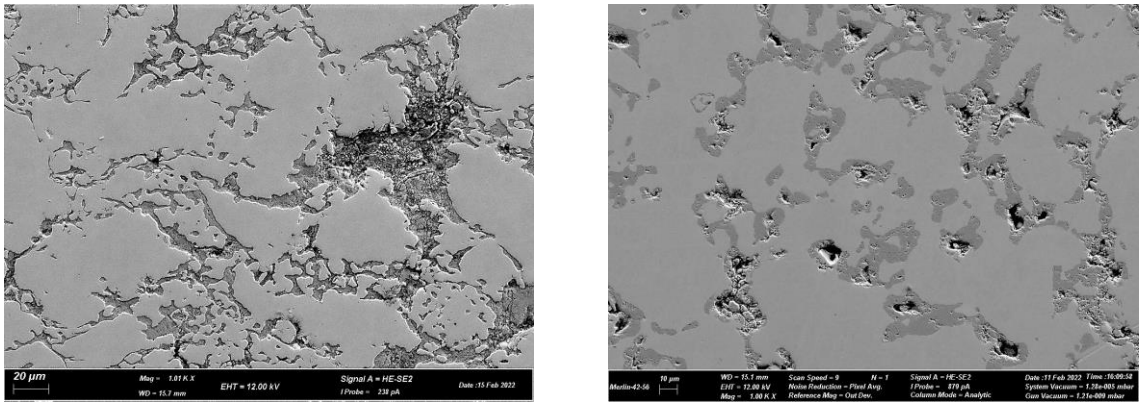

Figure 100. Compact with density 5.9 g/cm^3, a) after the sintering process, b) after sintering with the additional steaming process, Magnification 1000X

a) b)

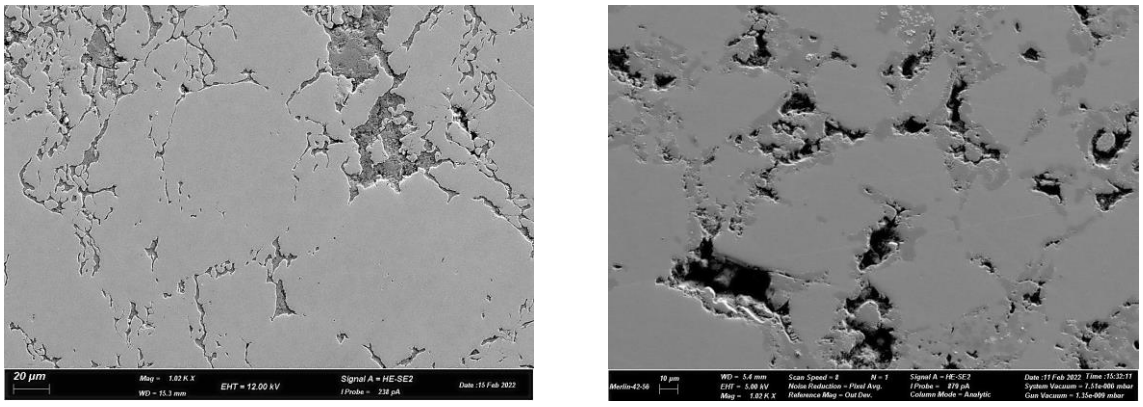

Figure 101. Compact with density 6.1 g/cm^3, a) after the sintering process, b) after sintering with the additional steaming process, Magnification 1000X

a) b)

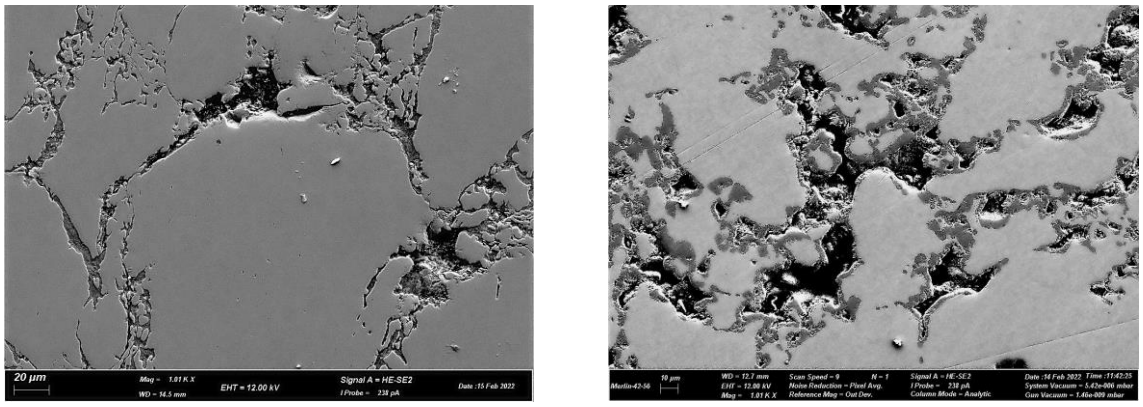

Figure 102. Compact with density 6.3 g/cm^3, a) after the sintering process, b) after sintering with the additional steaming process, Magnification 1000X

a) b)

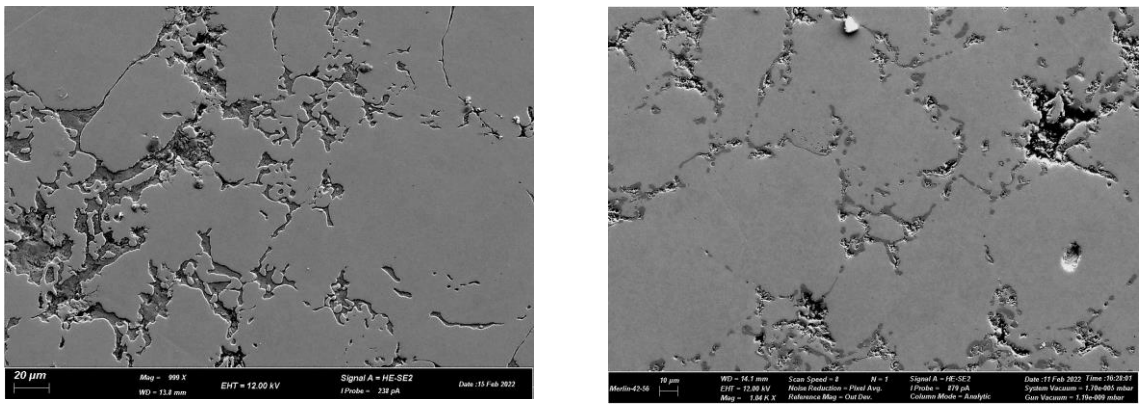

Figure 103. Compact with density 6.5 g/cm^3, a) after the sintering process, b) after sintering with the additional steaming process, Magnification 1000X

The EDS for sintered and not steaming sample were checked (Figure 104-107). The chemical composition is presented within Table 16 and Table 17.

SINTERED

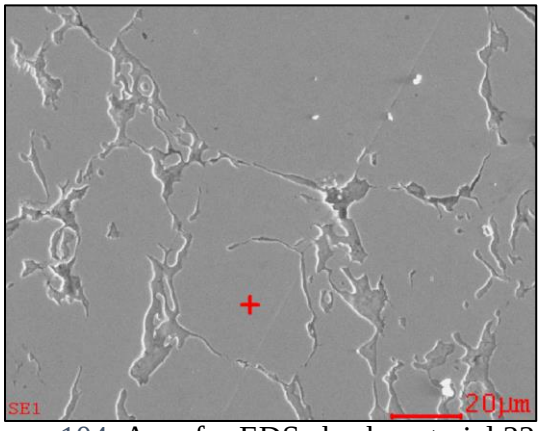

Figure 104. Area for EDS check material 22 FC-0208 sintered

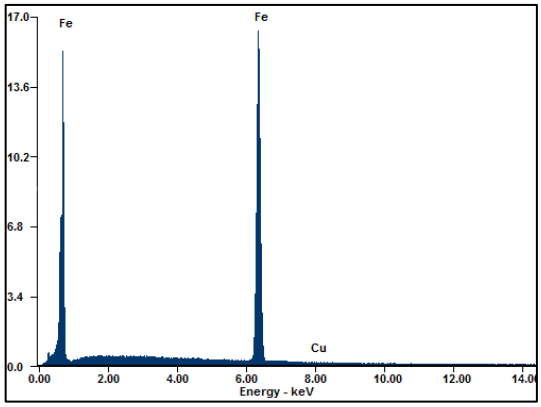

Figure 105. EDS chemical composition data FC-0208 sintered

Table 16. Chemical Composition 22 FC-0208 sintered

Element	Wt%	At%
FeK	99.68	99.72
CuK	00.32	00.28

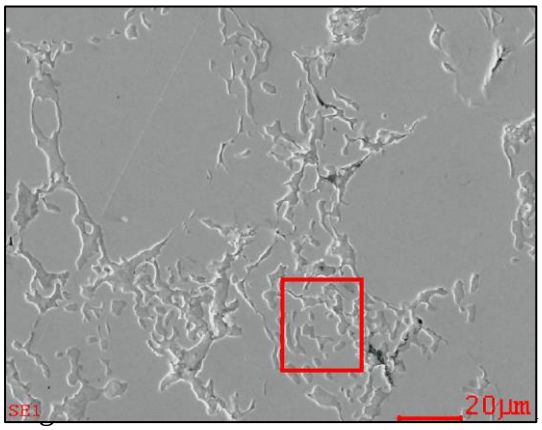

Figure 106. EDS chemical composition data 22 FC-0208 sintered

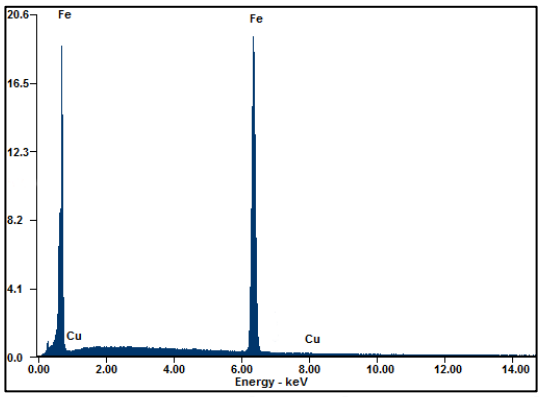

Figure 107. EDS chemical composition data FC-0208 sintered

Table 17. The chemical composition data FC-0208 sintered

Element	Wt%	At%
OK	10.04	28.14
FeK	86.28	69.26
CuK	03.68	02.59

The analysis showed that there is an increased amount of oxides in the crack area. It is common when the furnace and sintering atmosphere is not ideal, and it has errors. In most of these areas the parts have cracks.

The EDS for sintered and steaming sample were checked (Figure 108-111). The chemical composition is presented within Table 18 and Table 19.

STEAMED

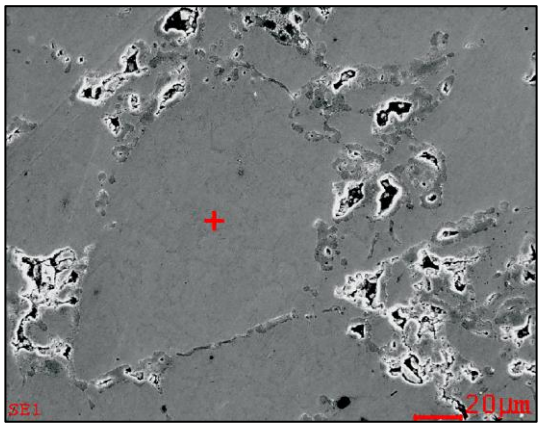

Figure 108. Area for EDS check material 22 FC-0208 steamed

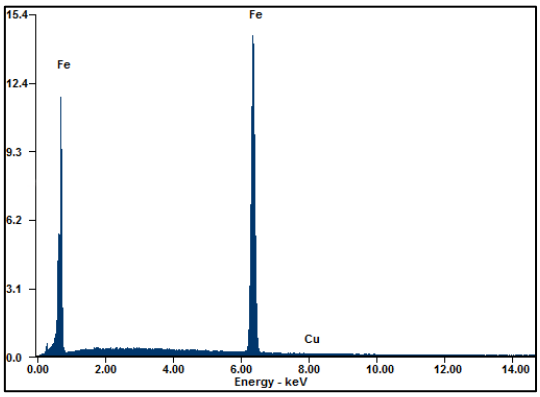

Figure 109. EDS chemical composition data FC-0208 steamed

Table 18. The chemical composition data FC-0208 steamed

Element	Wt%	At%
FeK	99.62	99.66
CuK	00.38	00.34

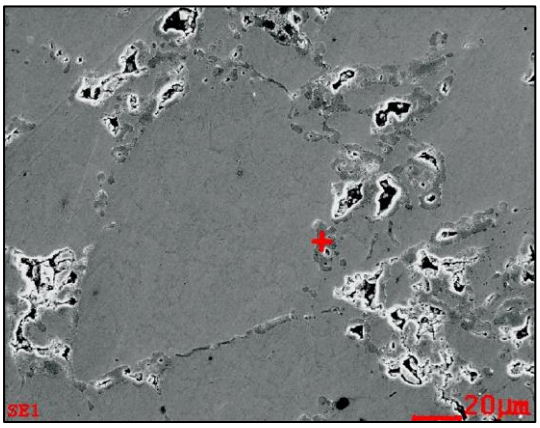

Figure 110. Area for EDS check material 22 FC-0208 steamed

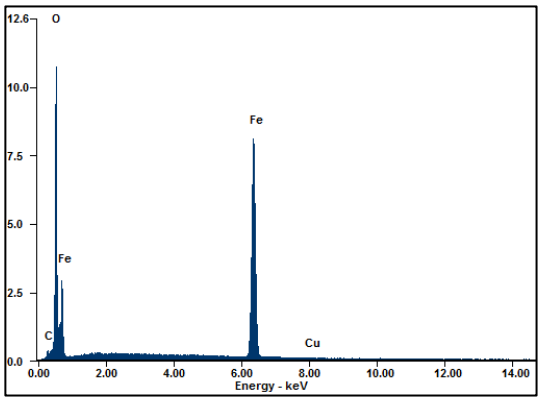

Figure 111. EDS chemical composition data FC-0208 steamed

Table 19. The chemical composition data FC-0208 steamed

Element	Wt%	At%
CK	03.31	08.73
OK	25.92	51.23
FeK	70.13	39.72
CuK	00.64	00.32

It can be seen that pores occur in places where oxides are present. There is also a higher copper content in the location of the cracks. The samples show a lot of oxide surfaces. The porosity is visible. In some places, impurities appear, which is related to the purity of the sintering process.

3.7.4. Transmission electron microscopy

TEM was undertaken to obtain more detailed information on the microstructure of Sample 22 FC-0208 after sintering/no steaming process; Material Fe-C-Cu compact as typical examples (selected area electron diffraction (SAED) patterns are also given in Figure 112.

a) b)

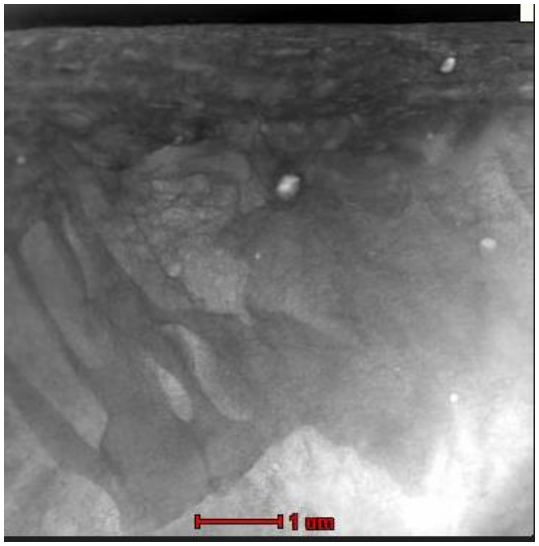

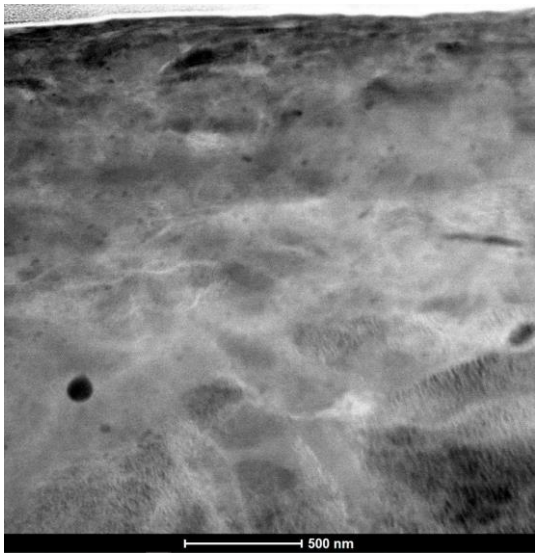

c) d)

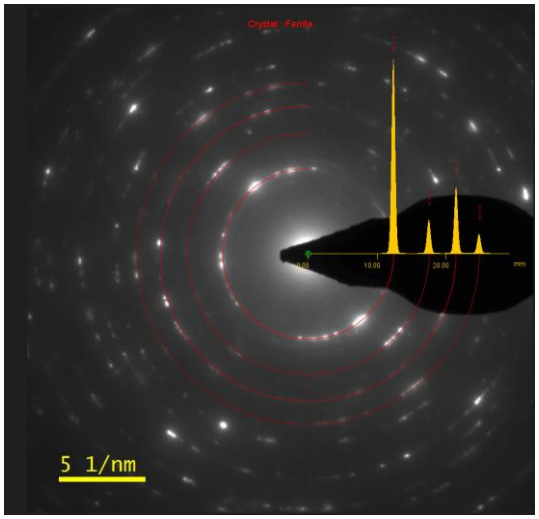

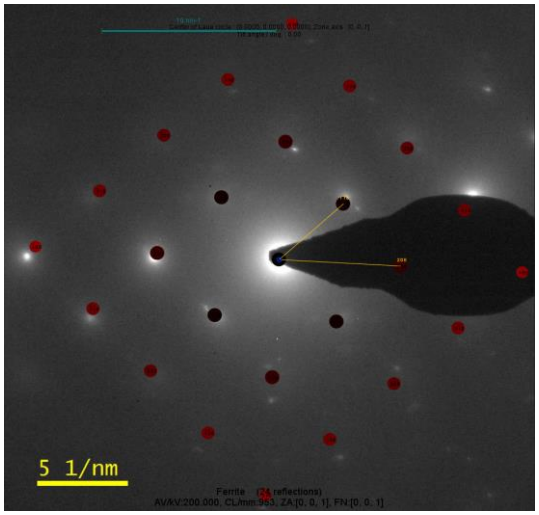

e)

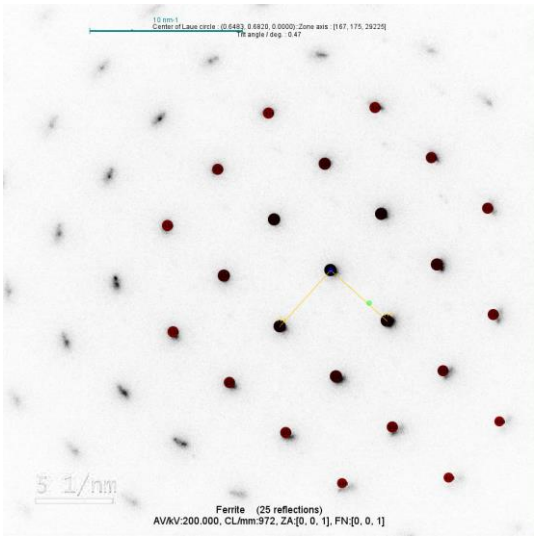

Figure 112. a), b) Bright field TEM images and c), d), e) corresponded SAEDs (Selected area electron diffraction) for Sample 22 Fc-0208 after sintering/no steaming process; Material Fe-C-Cu.

The TEM results are shown in above in Figure 112 shows a bright field TEM image and the corresponding diffraction pattern. The structure conforms to the ferrite phase. For powder metallurgy the Transmission Electron Microscopy has not shown anything more. Etched metallographic samples with nital should show ferrite, pearlite, and possibly free copper.

3.7.5. Finite Element Analysis, Drucker–Prager model

The objective of this part was to calibrate the material model for sinter material. A classical approach using elasticplastic material definition seems not to be effective. Results show a lack of stiffness and a wrong crack initiation location. This study was to compare three material models with the classic approach:

1. Cast Iron
2. Drucker Prager

3. Concrete damage plasticity

The analysis includes a simple tensile test (Figure 113) MPIF 10 [81, 97] and a compression test (Figure 114) (ISO 4506:2018).[51].

Both the tensile strength test and compression strength tests encountered problems during the laboratory execution. The tensile samples had broken outside of the gauge length. The compression sample buckled during the test. The tension test was simulated in terms of load deflection. The simulation of the compression test was only at the linear part of the load deflection curve. It was hard to estimate if the stiffness degradation is a result of buckling or plastic deformation. Therefore only using the linear behaviour should be the correct approach.

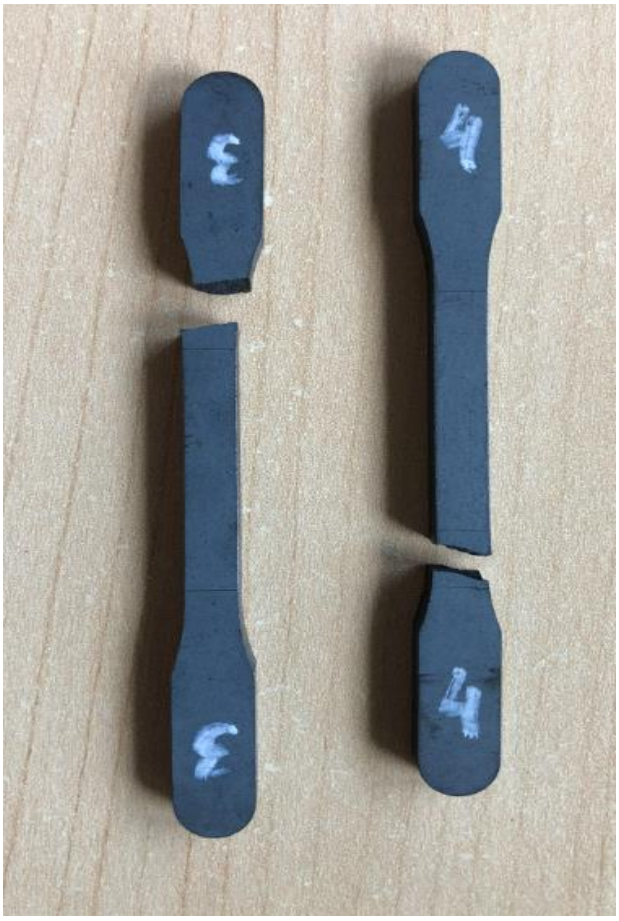

Figure 113. The sample after tensile strength test.

Figure 114. The sample after compression strength test.

Samples were measured in gauge length to confirm if the dimensions were maintained. The simulation used the dimensions from the measurements. The density of the prepared samples was equal to those proposed in MPIF STD 35 [11] and equal to 6.3 g/cm^3. The circular runout was not measured.

Load-deflection results were collected in the figures below (Figure 115, 116). The simulation was aimed at the lowest test results (Tension - sample 2, Compression - 3). It can be seen that compression test results were not reproduced in the simulation. The main roadblock is the buckling of specimens, which is difficult to reproduce without the correct material data.

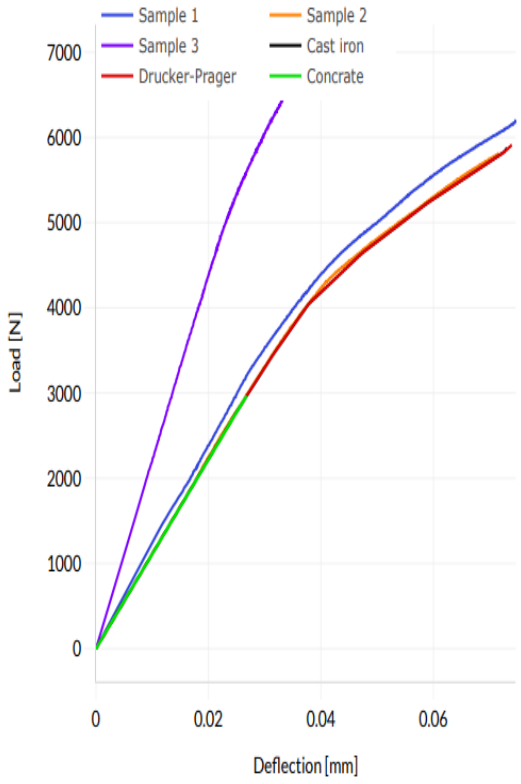

Figure 115. Tension test summary

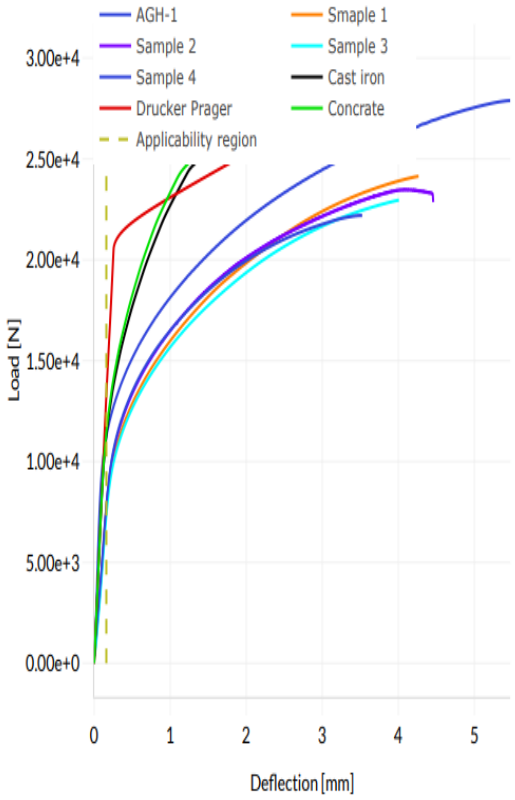

Figure 116. Compression test summary

The cast iron model gave an easy definition and good correlation. For the Drucker Prager model an optimization was required to achieve the tensile results. The compression test behaved linearity up to the cut off. Within the Concrete damage plasticity model it was difficult to achieve a convergence. The tensile test strength did not reach the full test. The compression test behaviour was correlated using an optimization approach.

Following contour plots the results from the end of the simulation can be presented. The corresponding load can be found in Table 20 and triaxiality results comparison on samples the results from the end of the simulation (Figure 117-122).

Table 20. Reaction force measured at the end of simulation

Material model	Tensile test [kN]	Compression test [kN]
Cast iron	5.9	29
Concrete damage plasticity	2.9	29
Drucker Prager	5.9	28

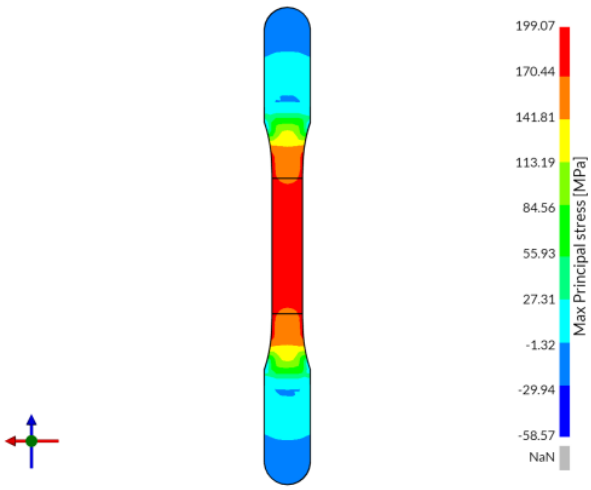

Figure 117. Tension test – Cast iron under 5.9N load

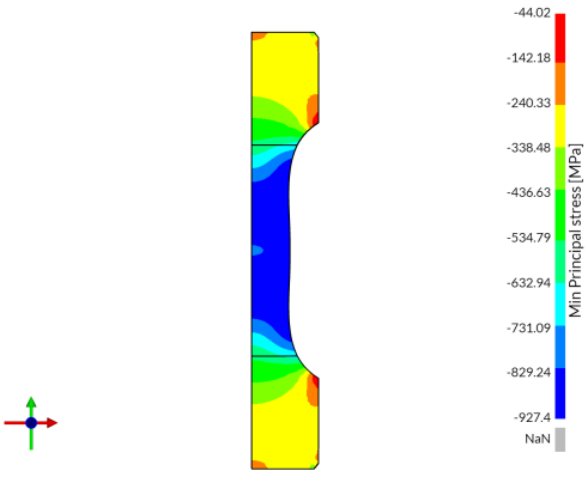

Figure 118. Compression test – Cast iron under 29 kN load

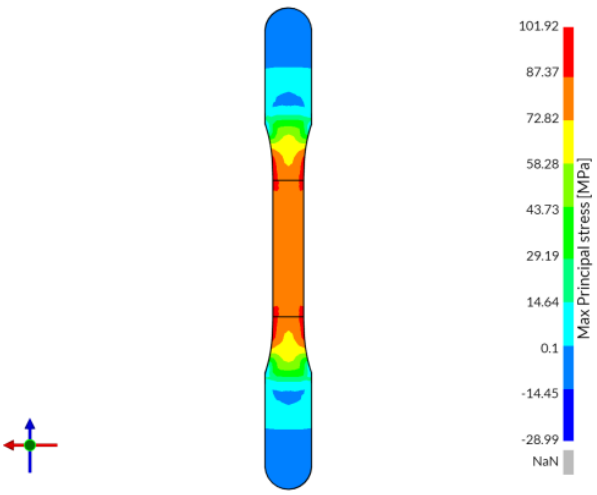

Figure 119. Tension test – Concrete damage plasticity under 2.9 kN load

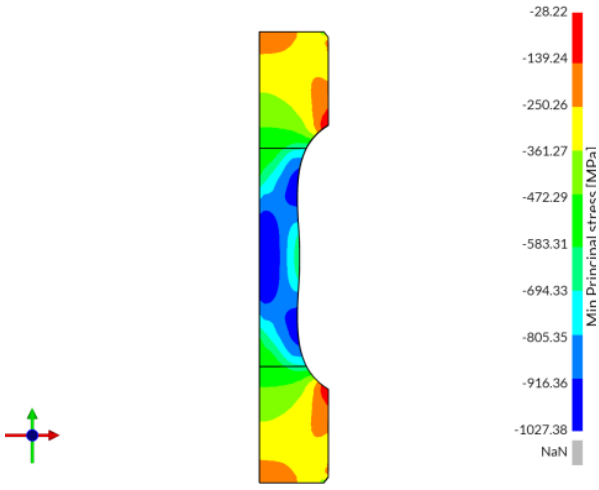

Figure 120. Compression test - Concrete damage plasticity under 29 kN load

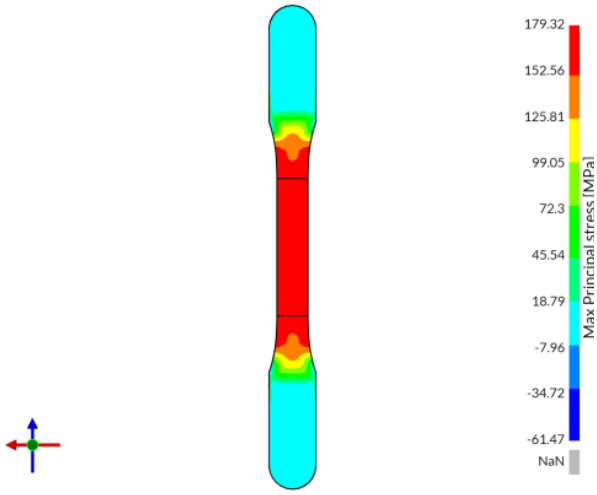

Figure 121. Tension test – Drucker Prager under 5.9 kN load

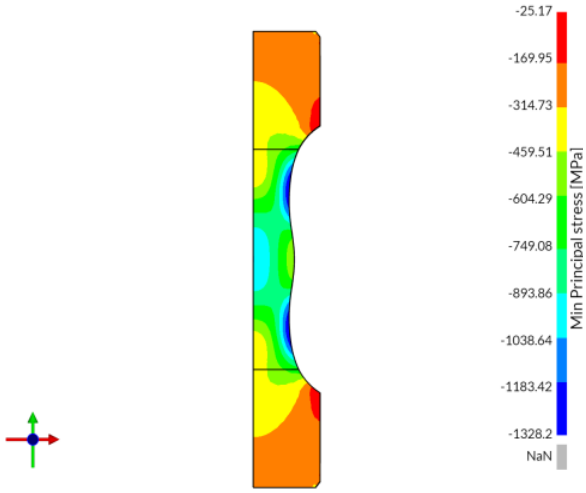

Figure 122. Compression test – Drucker Prager under 28kN load

The material definition was obtained based on the stress-strain relationship from the test samples, and for the Drucker-Prager and Concrete damage plasticity material definition optimization was performed to find the best fitting parameters. Assuming a yield point at 0.2% of total strain seems to be incorrect for material where the maximum measured strain in the tension test is 0.3%. In this case, the yield point should be established where linear behaviour ends. The measured Young's modulus was 81 GPa.

In addition it was found that the simulation of the crack propagation process showed that the shear crack starts in the area with the highest shear stress and the lowest relative density distribution. The behaviour of the compact and cracking should start from the simulation of the compacting process to prevent the further propagation of the crack. [98]

The main aim of this part of the research was to determine the identification and presentation of different results of the compression tests for iron-based sinter components, and calibrate the material model for this test. The research procedure included interdisciplinary research: Characteristics of the sintered element (microscopic examination, chemical composition), Finite Element Analysis of elements from the selected material, and compression test results. This experiment showed a proper compression test performance for sinter elements. During compressive testing a material experiences opposing uniaxial forces that push inward upon the specimen from opposite sides.

The goal of compression tests was to detect the behaviour or response of the materials and obtain the corresponding compressive properties when it experiences compressive loads. Finite element analysis (FEA) is a numerical modelling method that splits a problem into finite parts and solves them computationally using the modern-day computer processor. The choice of model to be used depends largely on the analysis type, the kind of material, the experimental data available for calibration of the model parameters, and the range of pressure stress values that the material is likely to experience. The Drucker–Prager yield criterion is a pressure-dependent model for determining whether a material has failed or undergone plastic yielding.
The tested material was FC-0208 (22). This material consists of iron, copper (1.5-3.9 wt%) and carbon (0.6-0.9 wt%). Iron-based samples were tested according to tensile test requirements (MPIF 10) and compression test requirements (ISO 4506:2018). Scanning Electron Microscopy (SEM) was used for microstructure and fractography observations. For simulation purposes, the Drucker Prager model was used.

After the tensile test, the sample broke outside the gauge length. The compression sample had a buckle during the test. Due to the porous material the resultant yield strength differs for tension and compression significantly. The tests were repeated, and the average of the results was used to create the simulation model for powder metal compacts.

3.8. Description of the results of the testing of sintered elements from material Fe-C-Cu with discussion

The compact made of Fe-C-Cu, powder material 4, were produced from the material with a particle size of 27-236 μm.

The compact made of Fe-C-Cu, powder material 18, were produced from the material with a particle size of 10-224 μm.

The compact made of Fe-C-Cu, powder material 26, were produced from the material with a particle size of 16-223 μm.

The carbon combined content of the sintered part is 0.90±0.03% - for powder 4, steamed with a density of 6.3 g/cm^3 where it was expected to be in accordance with MPIF 35 norm (0.6-0.9)%.

The carbon combined content of the sintered part is 0.5±0.03% - for powder 18, steamed with a density of 6.3 g/cm^3 where it was expected to be in accordance with MPIF 35 norm (0.3-0.6)%.

The carbon combined content of the sintered part is 0.64±0.03% - for powder 26, steamed with a density of 6.3 g/cm^3 where it was expected to be in accordance with MPIF 35 norm (0.6 - 0.9)%.

The provided data confirmed that the delivered material is within the required range of carbon, and there is no carbon lost after the sintering and steaming process.

3.8.1. The tensile test results

The tensile tests for compacts made of Fe-C-Cu powder material were performed at temperatures of 23°C and 120°C. Data available for different sintering methods, test temperatures and compact density. The results are presented in Figure 123-126 and Table 21 and 22.

Young's Modulus results after tensile strengths test for compact made of Fe-C-Cu powder material are presented in Figure 127 – 130, and Table 23 and 24.

Table 21. The tensile test results for compacts made of Fe-C-Cu powder material.

Process	Test Temperature [°C]	Material Part Number (PN)	Material Type	Density [g/cm^3]	Yield strength Rp0.2 [MPa]	Tensile strength Rm [MPa]
sintered/no steaming process.	23	18	FC-0205	5.9	/	232
	23	18	FC-0205	6.9	/	379
sintered/no steaming process.	120	18	FC-0205	5.9	/	220
	120	18	FC-0205	6.9	442	444
sintered/ steaming process.	23	18	FC-0205	5.9	/	138
	23	18	FC-0205	6.9	/	435
sintered/ steaming process.	120	18	FC-0205	5.9	/	147
	120	18	FC-0205	6.9	/	377
sintered/no steaming process	23	4	Fc-0208	5.9	/	195
	23	4	Fc-0208	6.9	405	464
	23	26	Fc-0208	5.9	/	188
	23	26	Fc-0208	6.9	/	350
	23	26	Fc-0208	6.9	/	N/A

Table 22. The tensile test results for compacts made of Fe-C-Cu powder material (continuation).

Process	Test Temperature [°C]	Material Part Number (PN)	Material Type	Density [g/cm^3]	Yield strength Rp0.2 [MPa]	Tensile strength Rm [MPa]
sintered/ steaming process	23	4	Fc-0208	5.9	172	174
	23	4	Fc-0208	6.9	/	382
	23	26	Fc-0208	5.9	/	173
	23	26	Fc-0208	6.9	/	350
	23	26	Fc-0208	6.9	/	361
sintered/ steaming process.	120	4	Fc-0208	5.9	/	154
	120	4	Fc-0208	6.9	/	330
	120	26	Fc-0208	5.9	/	147
	120	26	Fc-0208	6.9	/	324
	120	26	Fc-0208	6.9	/	348

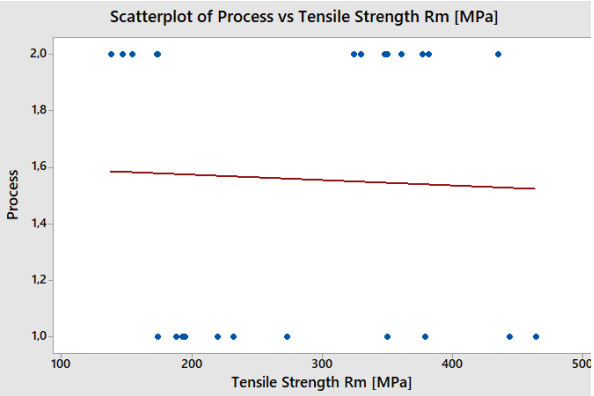

Figure 123. Scatterplot of Process vs Tensile Strength Rm [MPa]

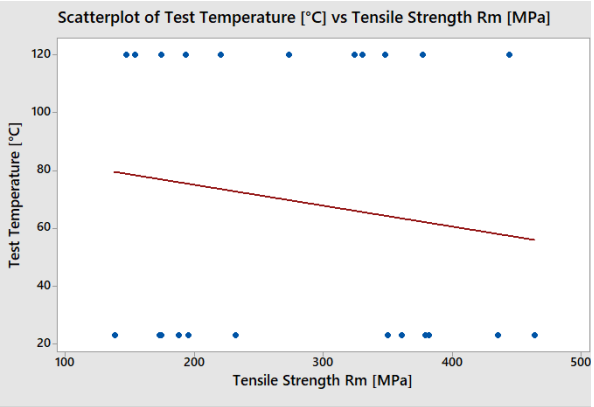

Figure 124. Scatterplot of Temperature [°C] vs Tensile Strength Rm [MPa]

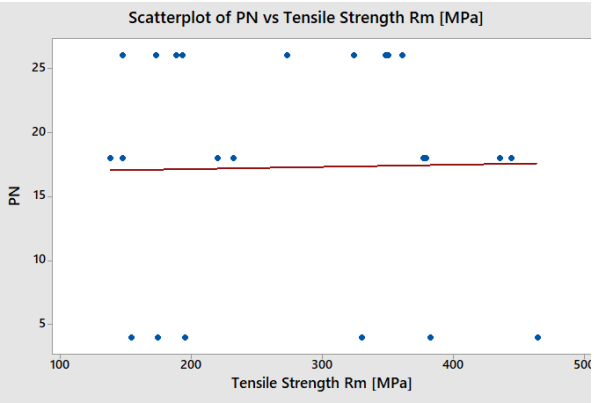

Figure 125. Scatterplot of PN vs Tensile Strength Rm [MPa]

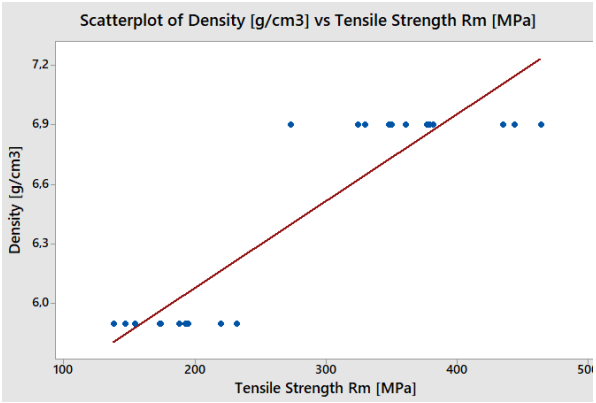

Figure 126. Scatterplot of Density [g/cm^3] vs Tensile Strength Rm [MPa]

The tensile strength varied over the range of 100 - 460 MPa. Regression analysis was used to determine the correlations of the density, hardness of the compact, sintering method and powder material type, and tensile strength results.

The process and test temperature have a slight influence on the tensile strength Rm [MPa] parameters. The samples sintered/not steamed show lower ultimate tensile strength Rm [MPa] data. Higher density higher tensile strength Rm [MPa] for all samples.

Table 23. Young's Modulus results after tensile strength test for compact made of Fc-C-Cu powder material, oars.

Process	**Test Temperature [°C]**	**Material Part Number (PN)**	**Material Type**	**Density [g/cm^3]**	**Young's Modulus [GPa]**
sintered/no steaming process.	23	18	FC-0205	5.9	83.7
	23	18	FC-0205	6.9	83.7
sintered/no steaming process.	120	18	FC-0205	5.9	45.5
	120	18	FC-0205	6.9	135
sintered/ steaming process.	23	18	FC-0205	5.9	99
	23	18	FC-0205	6.9	283
sintered/ steaming process.	120	18	FC-0205	5.9	94.9
	120	18	FC-0205	6.9	183

Table 24. Young's Modulus results after tensile strength test for compact made of Fc-C-Cu powder material. oars. (continuation).

Process	Test Temperature [°C]	Material Part Number (PN)	Material Type	Density [g/cm^3]	Young's Modulus [GPa]
sintered/no steaming process.	23	4	Fc-0208	5.9	46.9
	23	4	Fc-0208	6.9	188
	23	26	Fc-0208	5.9	73.1
	23	26	Fc-0208	6.9	107
sintered/no steaming process.	120	4	Fc-0208	5.9	43.2
	120	4	Fc-0208	6.9	N/A
	120	26	Fc-0208	5.9	61
	120	26	Fc-0208	6.9	147
sintered/ steaming process.	23	4	Fc-0208	5.9	149
	23	4	Fc-0208	6.9	102
	23	26	Fc-0208	5.9	90.7
	23	26	Fc-0208	6.9	107
	23	26	Fc-0208	6.9	103
sintered/ steaming process.	120	4	Fc-0208	5.9	191
	120	4	Fc-0208	6.9	100
	120	26	Fc-0208	5.9	83.5
	120	26	Fc-0208	6.9	88.2
	120	26	Fc-0208	6.9	98.2

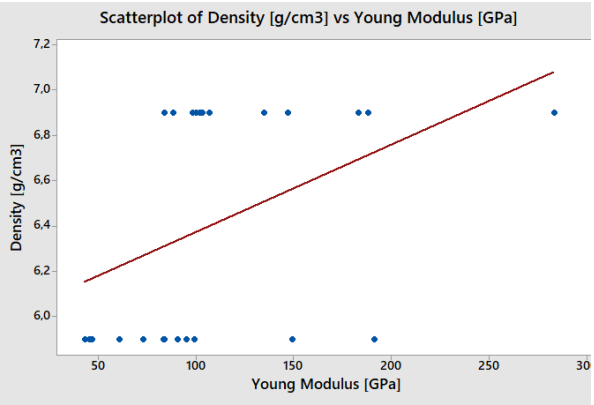

Figure 127. Scatterplot of Density [g/cm^3] vs Young's Modulus [GPa]

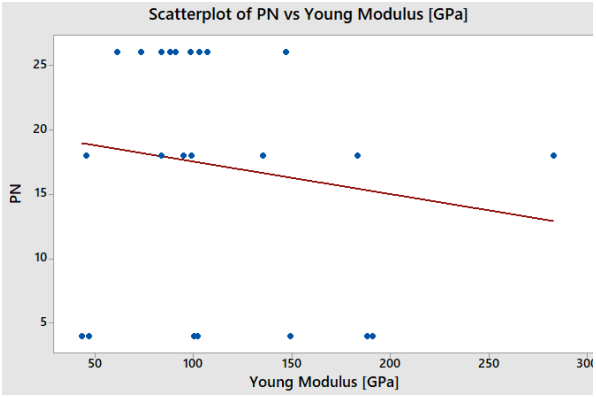

Figure 128. Scatterplot of PN vs Young's Modulus [GPa]

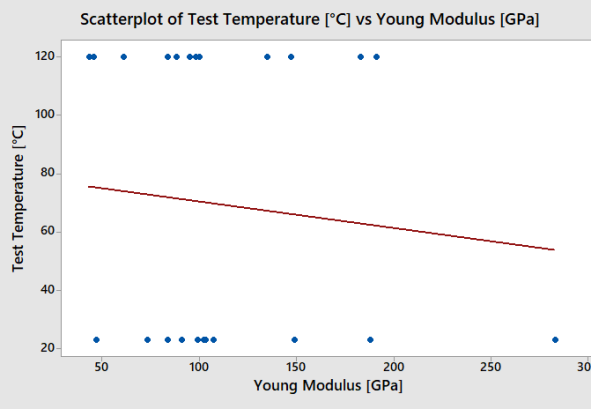

Figure 129. Scatterplot of Temperature [°C] vs Young's Modulus [GPa]

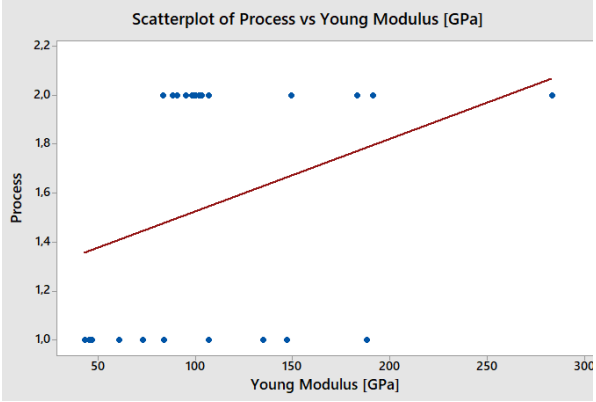

Figure 130. Scatterplot of Process vs Young's Modulus [GPa]

Young's Modulus of the compact ranged from approximately 50 GPa to over 300 GPa. Regression analysis was used to determine the correlations of the density of the compact, temperature of the test, the type of sintering method, powder material type and Young's Modulus values of these powder metal compacts. It was found that when the density increased Young's Modulus increased. The test temperature has no impact. The test shows the same values for temperatures 23°C and 120°C. The sintering method with additional steaming shows higher versions of Young's Modulus.

3.8.2. The compression test results

The compression tests were performed at temperatures of 23°C and 120°C. Data available for different sintering methods, test temperature and compact density in Figure 131 – 134 and Table 25.

Table 25. The compression strength test results for compacts made of Fe-C-Cu powder material, cubes.

Process	Test Temperature [°C]	Material Part Number (PN)	Material Type	Density [g/cm^3]	Ed [GPa]	σd0.2 [MPa]	σdM [MPa]	ℰdB [%]	ℰdtM [%]
sintered/no steaming process	23	18	FC-0205	5.9	6.58	284	845	24	36
	23	18	FC-0205	6.9	6.9	566	1,087	23	38
sintered/no steaming process	120	18	FC-0205	5.9	6.6	285	791	21	33
	120	18	FC-0205	6.9	6.63	518	1,070	23	37
sintered/steaming process	23	18	FC-0205	5.9	6.77	752	790	6	16
	23	18	FC-0205	6.9	8.2	560	1,102	24	36
sintered/steaming process	120	18	FC-0205	5.9	7.53	554	768	5	15
	120	18	FC-0205	6.9	8.11	571	1,054	18	31
	120	18	FC-0205	6.9	7.53	554	768	5	15
sintered/no steaming process	23	4	Fc-0208	5.9	6.07	289	593	14	23
	23	4	Fc-0208	6.9	7.66	431	1,057	23	36
	23	26	Fc-0208	5.9	5.18	293	617	26	36
	23	26	Fc-0208	6.9	6.31	386	872	31	42
sintered/no steaming process	120	4	Fc-0208	5.9	5.92	271	571	16	24
	120	4	Fc-0208	6.9	7.04	478	926	21	33
	120	26	Fc-0208	5.9	4.68	274	560	23	31
	120	26	Fc-0208	6.9	7.32	344	837	26	34
sintered/ steaming process	23	4	Fc-0208	5.9	7.67	678	880	5	15
	23	4	Fc-0208	6.9	7.67	771	1,128	17	31
	23	26	Fc-0208	5.9	7.31	511	734	7	16
	23	26	Fc-0208	6.9	4.64	429	899	25	36
sintered/ steaming process	120	4	Fc-0208	5.9	7.23	763	847	6	16
	120	4	Fc-0208	6.9	7.98	640	1,110	18	31
	120	26	Fc-0208	5.9	7.93	559	695	6	13
	120	26	Fc-0208	6.9	8.05	472	855	21	29

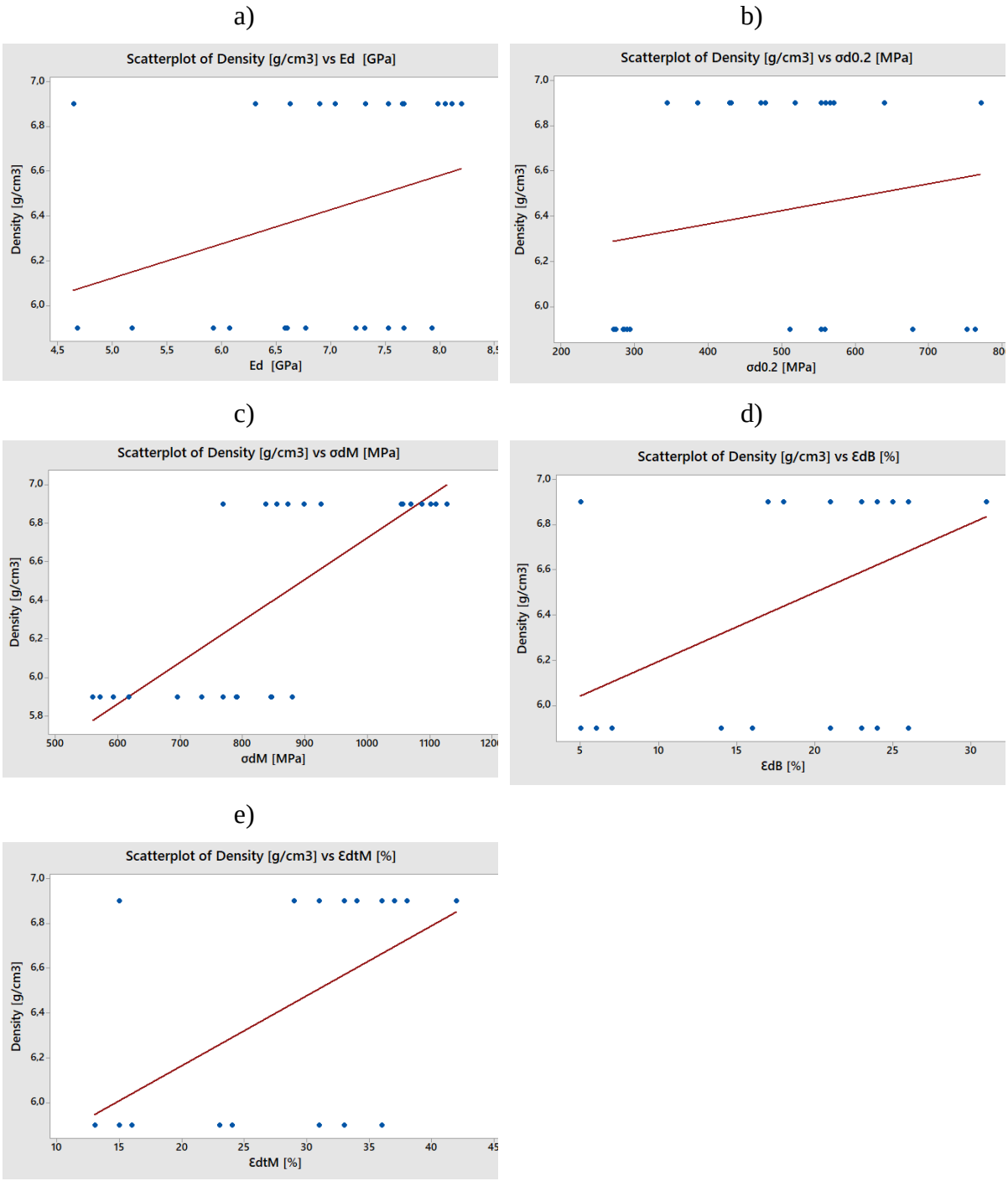

Figure 131. Scatterplot of Density [g/cm^3] vs a) Ed [GPa]; b) σd0.2 [MPa]; c) σdM [MPa]; d) ƐdB [%]; e) ƐdtM [%].

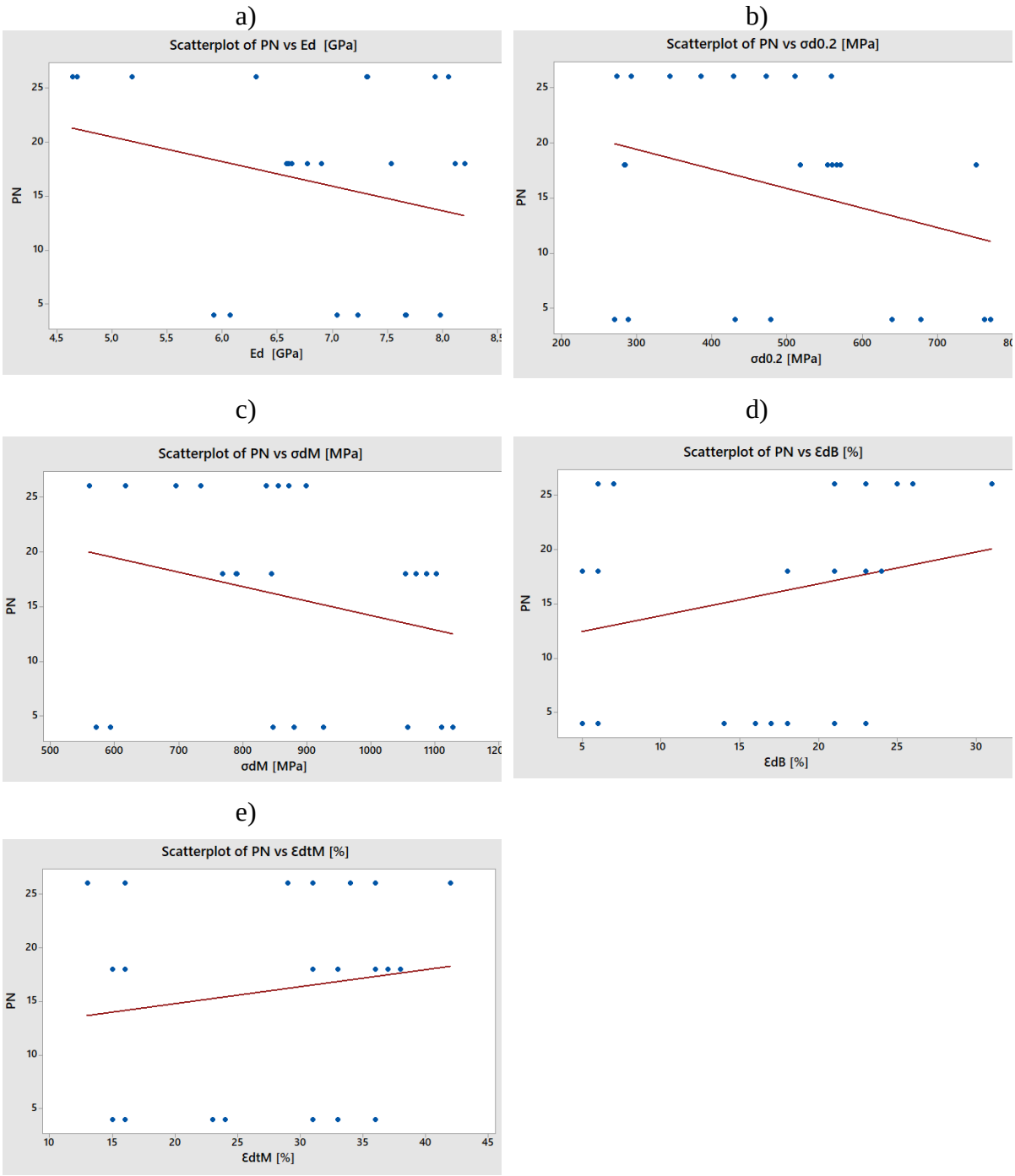

Figure 132. Scatterplot of PN vs a) Ed [GPa]; b) σd0.2 [MPa]; c) σdM [MPa]; d) ƐdB [%]; e) ƐdtM [%].

a)

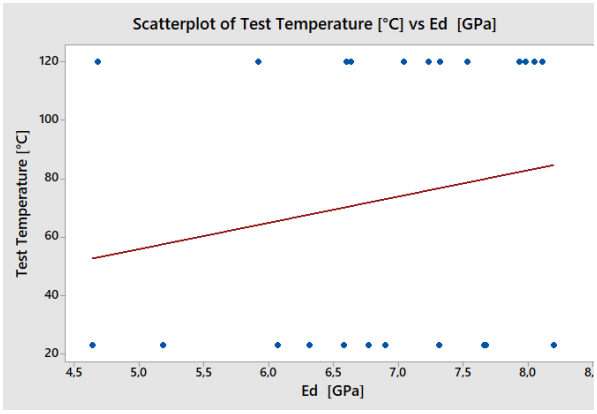

b)

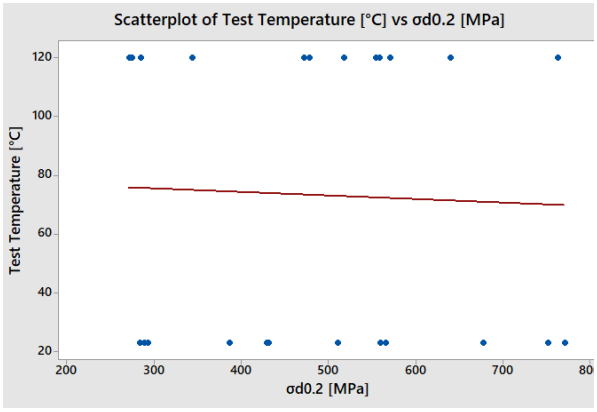

c)

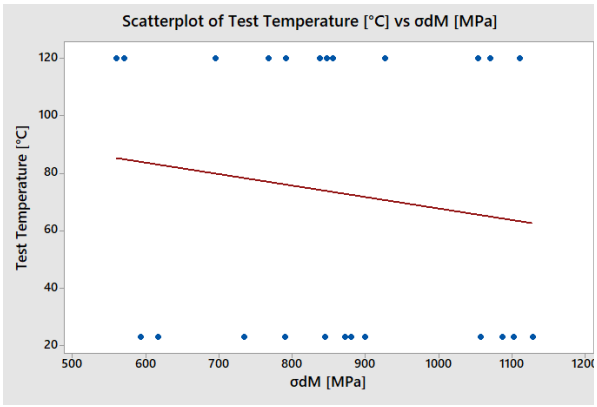

d)

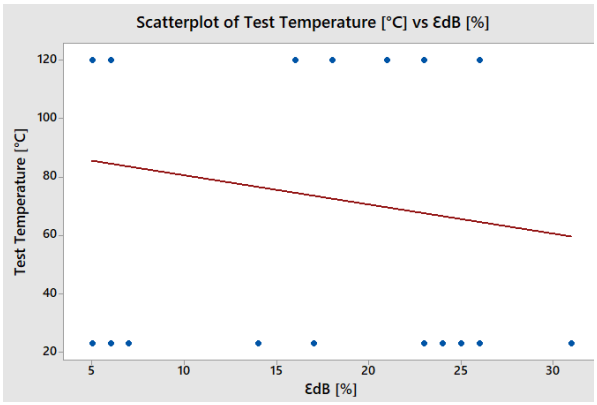

e)

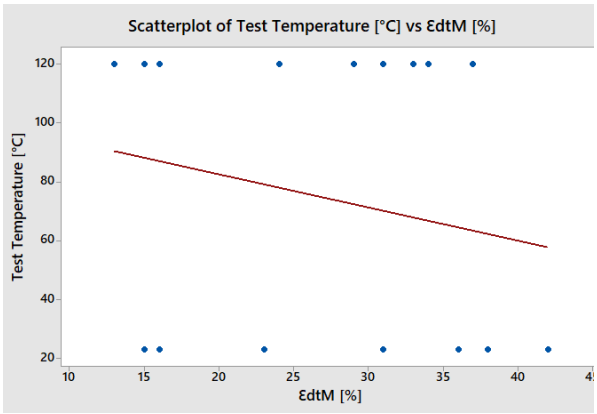

Figure 133. Scatterplot of Test Temperature [°C] vs a) Ed [GPa]; b) σd0.2 [MPa]; c) σdM [MPa]; d) ƐdB [%]; e) ƐdtM [%].

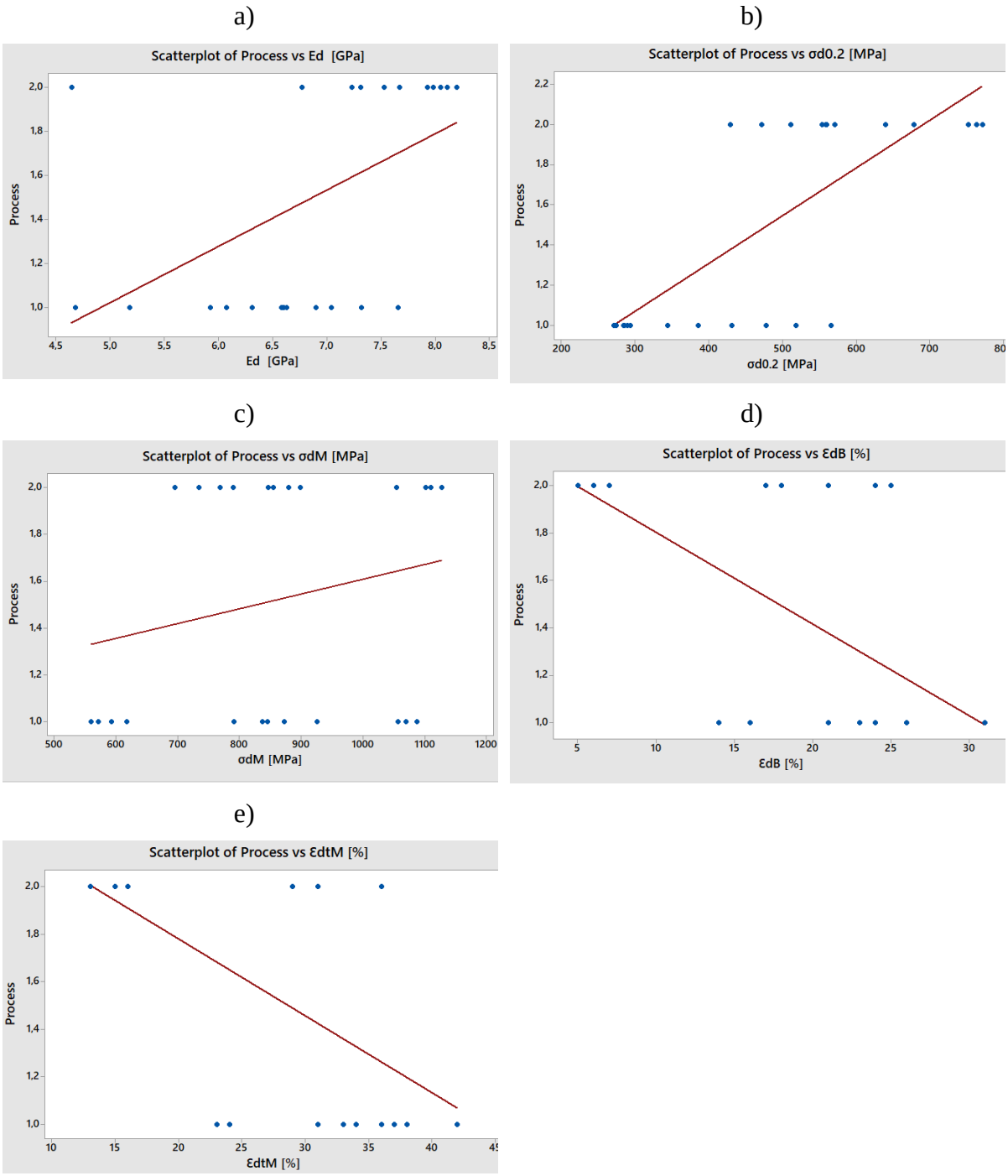

Figure 134. Scatterplot of Process vs a) Ed [GPa]; b) σd0.2 [MPa]; c) σdM [MPa]; d) ƐdB [%]; e) ƐdtM [%].

Young's Modulus of the compact ranged from approximately 4 GPa to over 8 GPa.

The yield strength of the compact ranged from approximately 250 MPa to over 700 MPa. The compression strength varied over the range of 550 - 1100 MPa.

Regression analysis was used to determine the correlations of the density of the compact, temperature of the test, the type of sintering method and compression test results. It was found that when the density increased the compression test results increased. The test temperature has no impact. The test shows the same values for temperatures 23°C and 120°C. The sintering method with additional steaming shows higher versions of Young's Modulus, yield strength and compression strength.

3.8.3. Microstructure analysis for material Fe-C-Cu using scanning microscopy

SEM was performed on the microstructure of parts made of Fe-C-Cu powder material. The results are presented in Figure 135 - 164 below, for different densities and magnification.

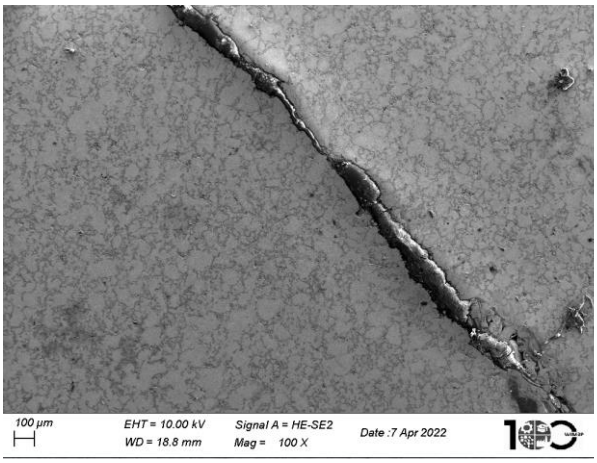

Figure 135. SEM observation for compacts from powder metal 4, steamed, density 5.9 [g/cm^3], Magnification 100X, after compression test

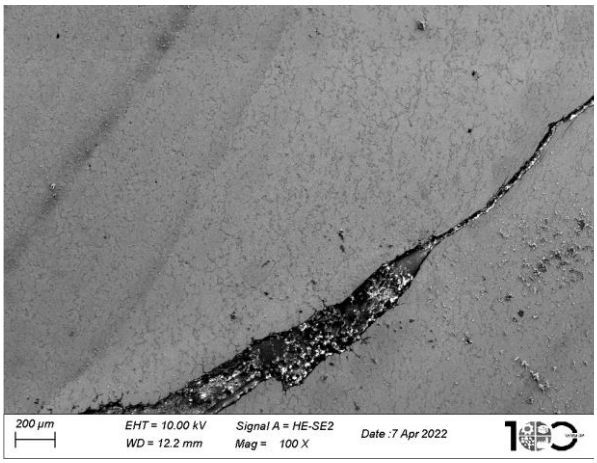

Figure 136. SEM observation for compacts from powder metal 4, steamed, density 6.9 [g/cm^3], Magnification 100X, after compression test

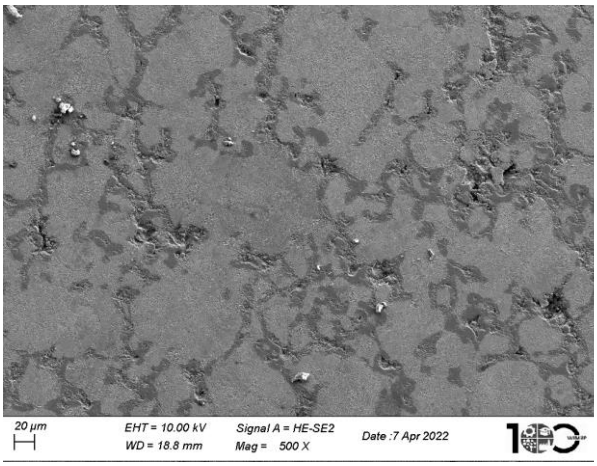

Figure 137. SEM observation for compact from powder metal 4, steamed, density 5.9 [g/cm^3], Magnification 500X, after compression test

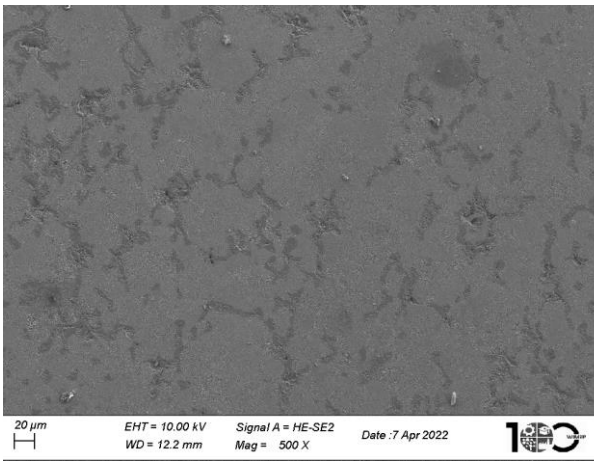

Figure 138. SEM observation for compact from powder metal 4, steamed, density 6.9 [g/cm^3], Magnification 500X, after compression test

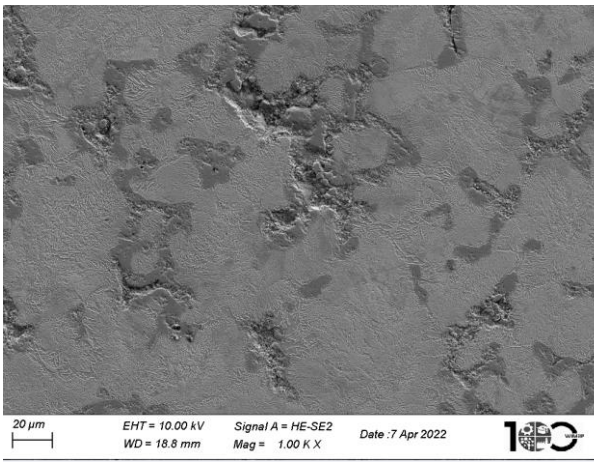

Figure 139. SEM observation for compact from powder metal 4, steamed, density 5.9 [g/cm^3], Magnification 1000X, after compression test

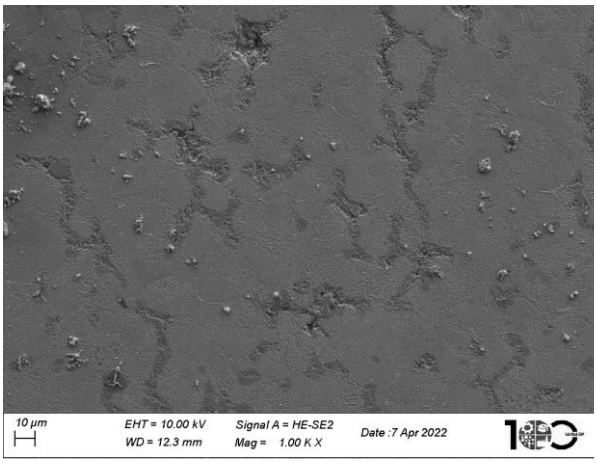

Figure 140. SEM observation for compact from powder metal 4, steamed, density 6.9 [g/cm^3], Magnification 1000X, after compression test

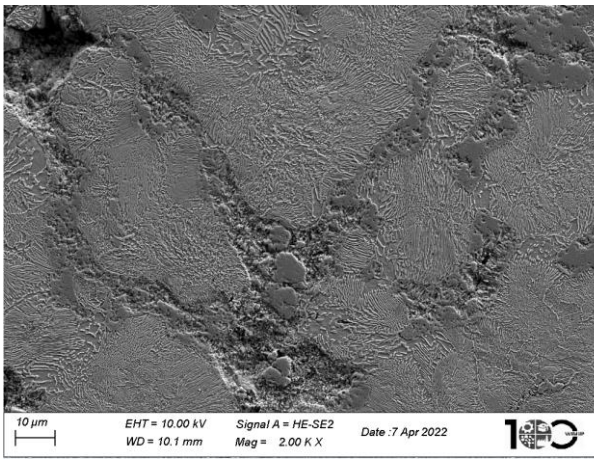

Figure 141 SEM observation for compact from powder metal 4, steamed, density 5.9 [g/cm^3], Magnification 2000X, after compression test

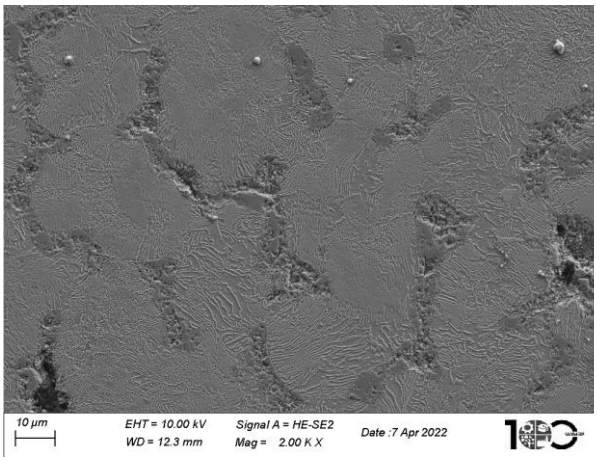

Figure 142 SEM observation for compact from powder metal 4, steamed, density 6.9 [g/cm^3], Magnification 2000X, after compression test

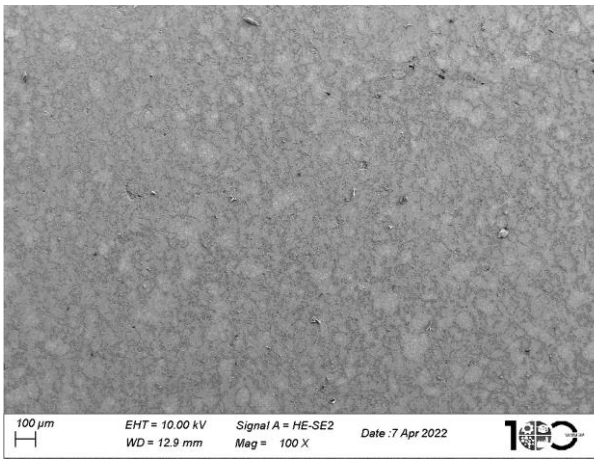

Figure 143. SEM observation for compact from powder metal 18, sintered/steamed, density 5.9 [g/cm^3], Magnification 100X, after compression test

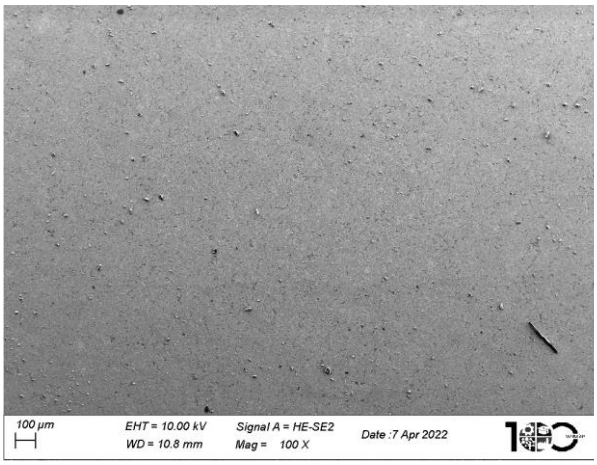

Figure 144. SEM observation for compact from powder metal 18, sintered/steamed, density 6.9 [g/cm^3], Magnification 100X, after compression test

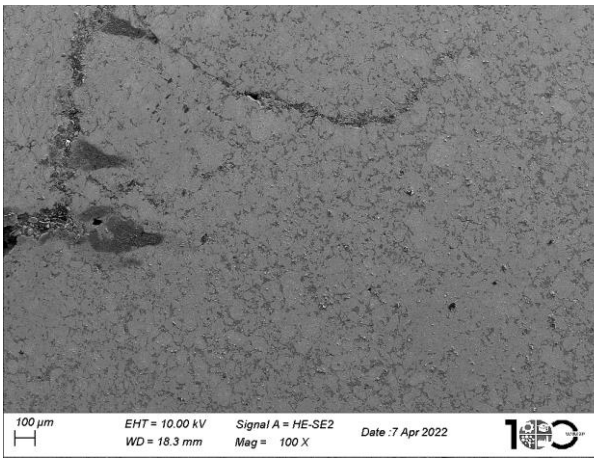

Figure 145. SEM observation for compact from powder metal 18, sintered/not steamed, density 5.9 [g/cm^3], Magnification 100X, after compression test

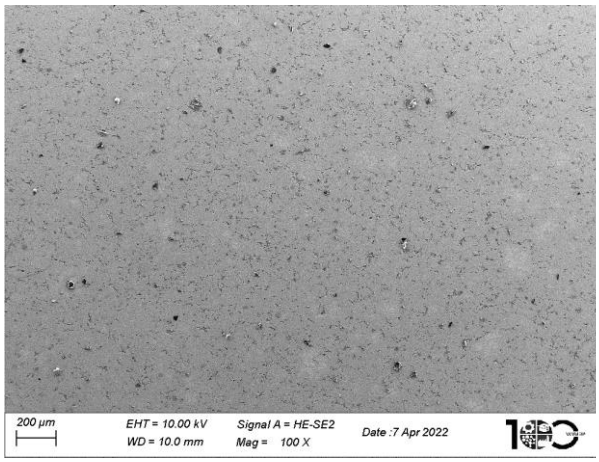

Figure 146. SEM observation for compact from powder metal 18, sintered/not steamed, density 6.9 [g/cm^3], Magnification 100X, after compression test

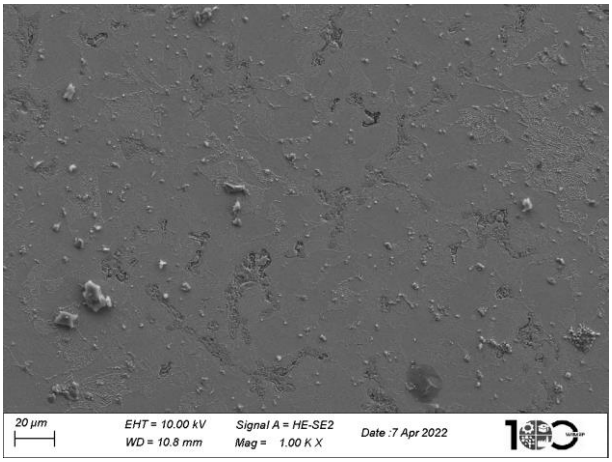

Figure 147. SEM observation for compact from powder metal 18, sintered/steamed, density 6.9 [g/cm^3], Magnification 1000X, after compression test

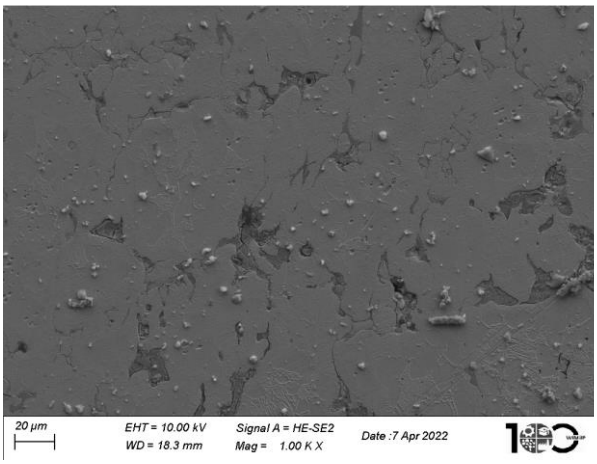

Figure 148. SEM observation for compact from powder metal 18, sintered/not steamed, density 5.9 [g/cm^3], Magnification 1000X, after compression test

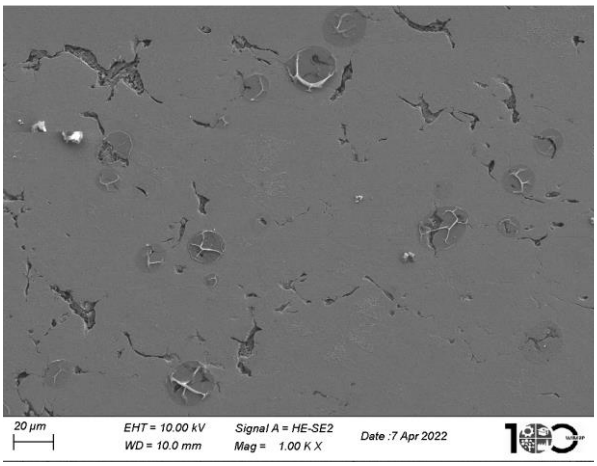

Figure 149. SEM observation for compact from powder metal 18, sintered/not steamed, density 6.9 [g/cm^3], Magnification 1000X, after compression test

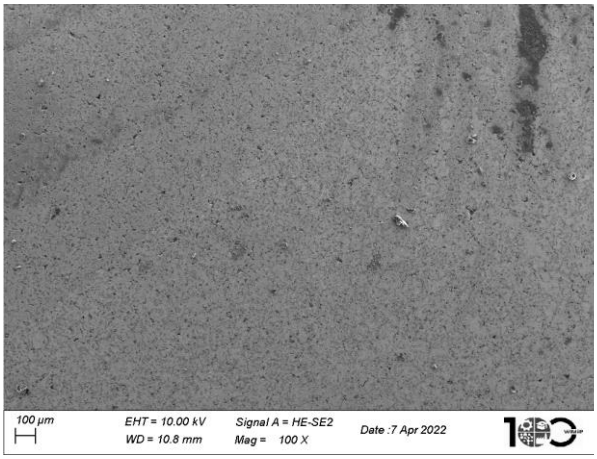

Figure 150. SEM observation for compact from powder metal 26, sintered/steamed, density 5.9 [g/cm^3], Magnification 100X, after compression test

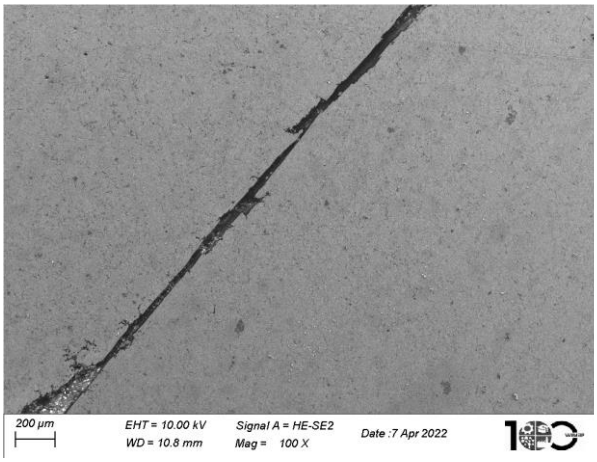

Figure 151. SEM observation for compact from powder metal 26, sintered/steamed, density 6.9 [g/cm^3], Magnification 100X, after compression test

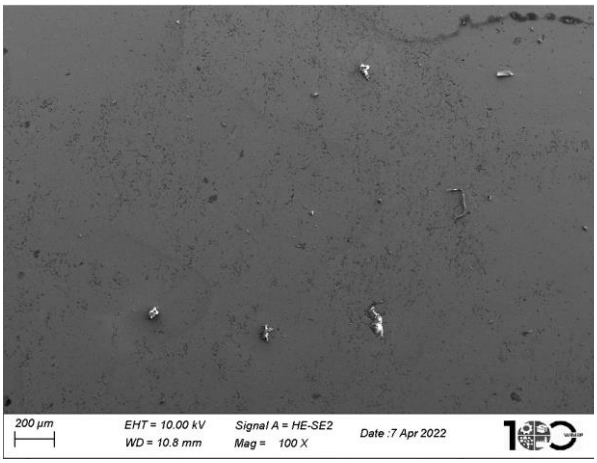

Figure 152. SEM observation for compact from powder metal 26, sintered/not steamed, density 5.9 [g/cm^3], Magnification 100X, after compression test

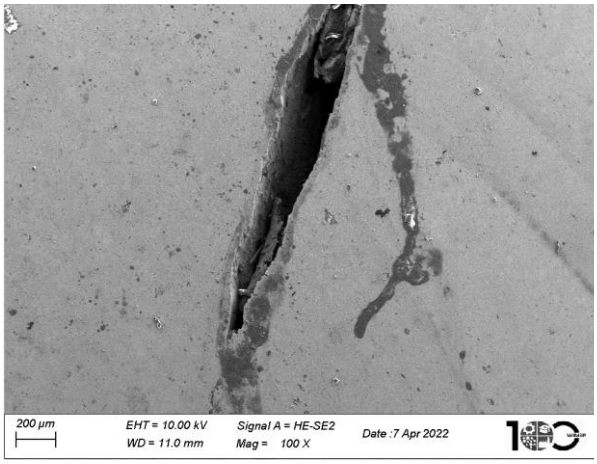

Figure 153. SEM observation for compact from powder metal 26, sintered/not steamed, density 6.9 [g/cm^3], Magnification 100X, after compression test

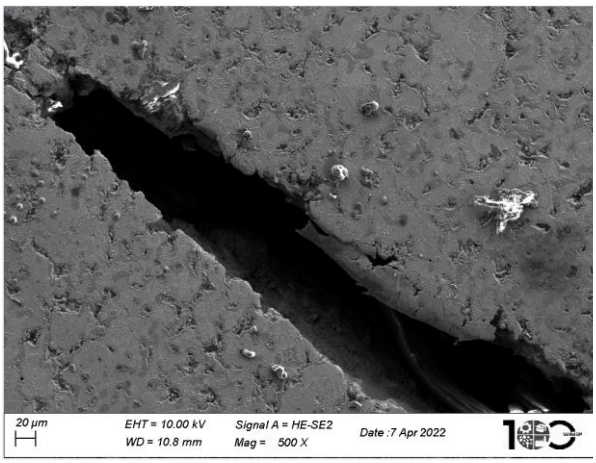

Figure 154. SEM observation for compact from powder metal 26, sintered/steamed, density 5.9 [g/cm^3], Magnification 500X, after compression test

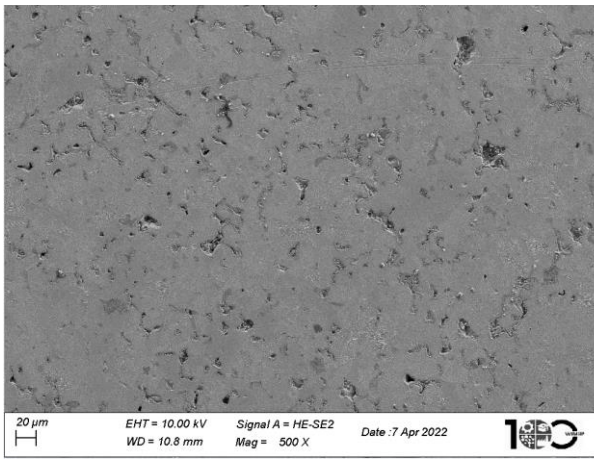

Figure 155. SEM observation for compact from powder metal 26, sintered/steamed, density 6.9 [g/cm^3], Magnification 500X, after compression test

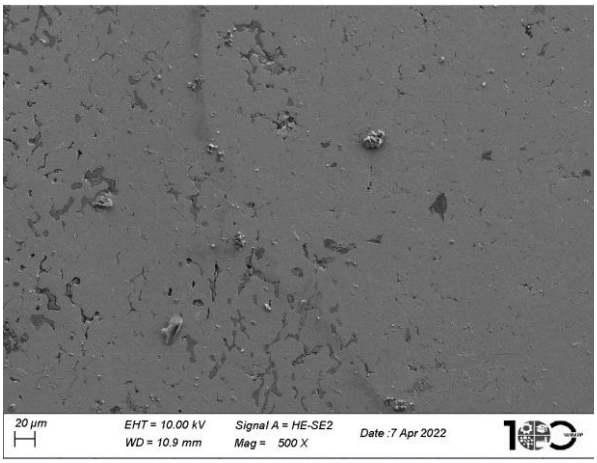

Figure 156. SEM observation for compact from powder metal 26, sintered/not steamed, density 5.9 [g/cm^3], Magnification 500X, after compression test

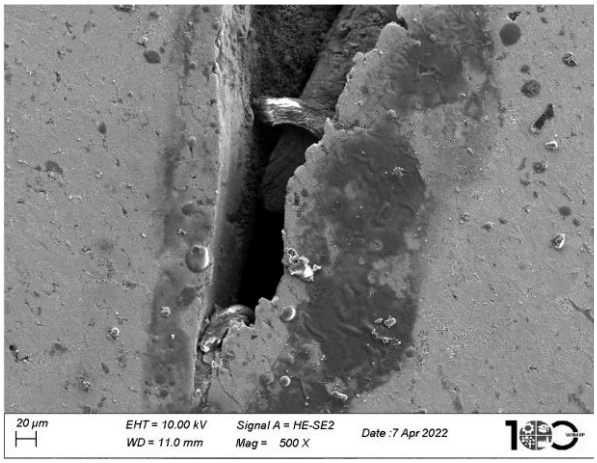

Figure 157. SEM observation for compact from powder metal 26, sintered/not steamed, density 6.9 [g/cm^3], Magnification 500X, after compression test

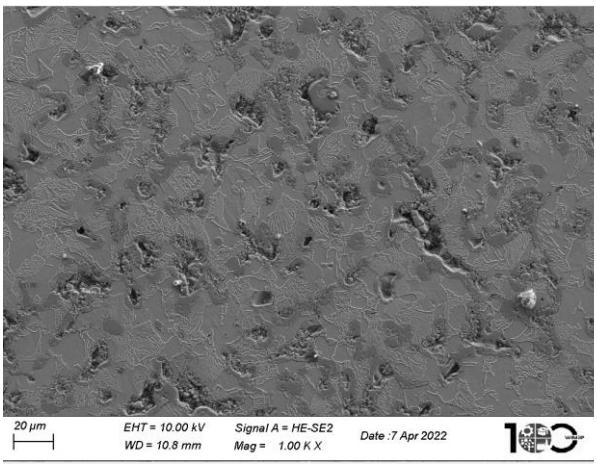

Figure 158. SEM observation for compact from powder metal 26, sintered/steamed, density 5.9 [g/cm^3], Magnification 1000X, after compression test

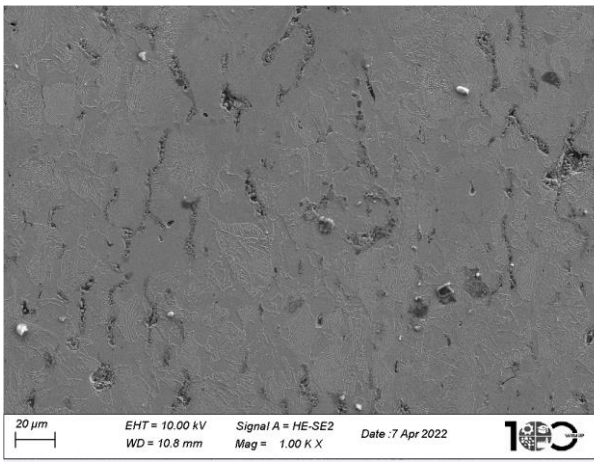

Figure 159. SEM observation for compact from powder metal 26, sintered/steamed, density 6.9 [g/cm^3], Magnification 1000X, after compression test

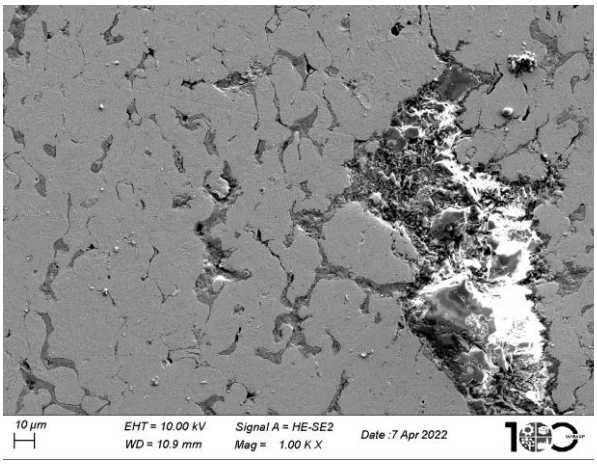

Figure 160. SEM observation for compact from powder metal 26, sintered/not steamed, density 5.9 [g/cm^3], Magnification 1000X, after compression test

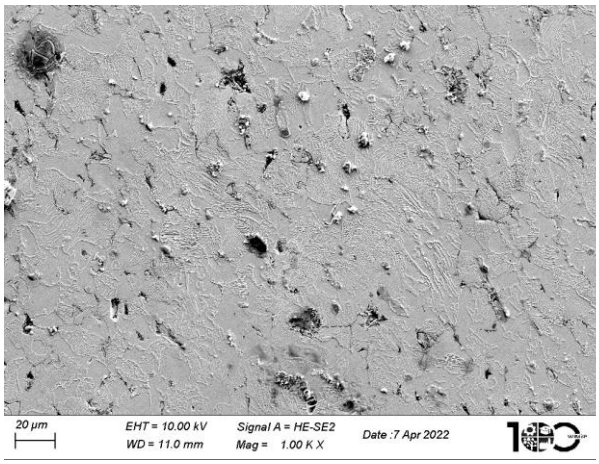

Figure 161. SEM observation for compact from powder metal 26, sintered/not steamed, density 6.9 [g/cm^3], Magnification 1000X, after compression test

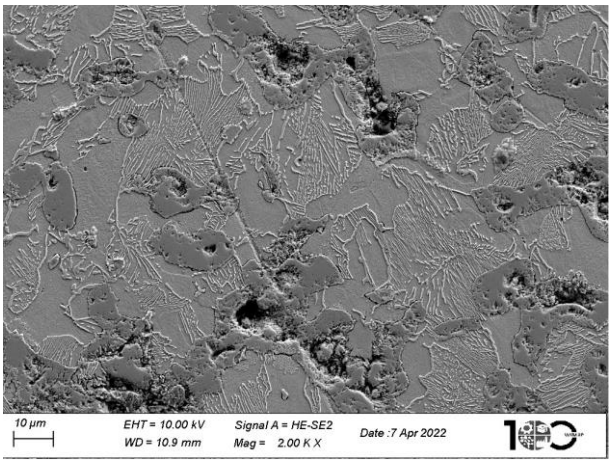

/

Figure 162. SEM observation for compact from powder metal 26, sintered/steamed, density 5.9 [g/cm^3], Magnification 2000X, after compression test

/

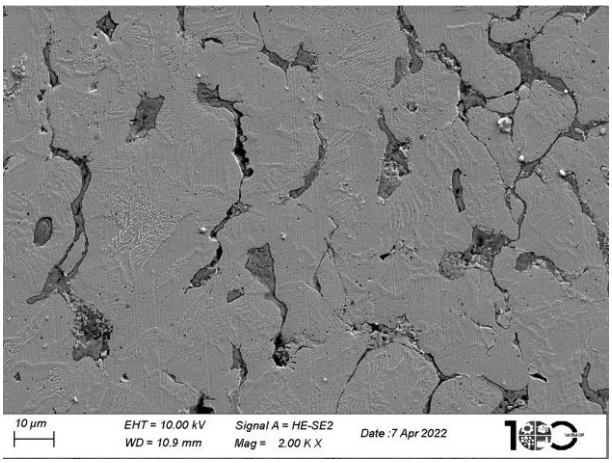

Figure 163. SEM observation for compact from powder metal 26, sintered/not steamed, density 5.9 [g/cm^3], Magnification 2000X, after compression test

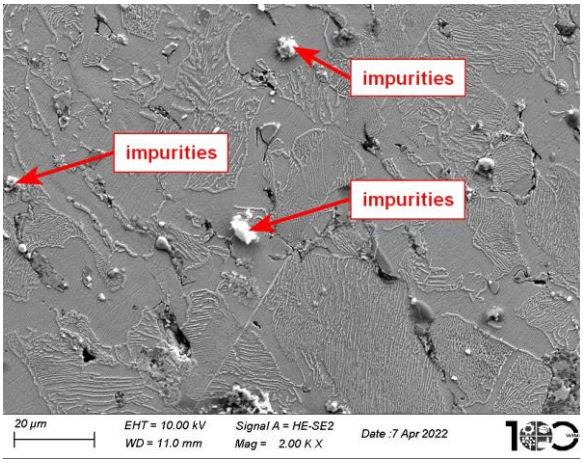

Figure 164. SEM observation for compact from powder metal 26, sintered/not steamed, density 6.9 [g/cm^3], Magnification 2000X, after compression test

There were visible pores. The impurities coming from quality of the sintering process. There is no significant difference in structure of these compacts. In some areas copper segregation appears.

3.9. Description of the results of testing of sintered element from material Fe-C with discussion

The compacts made of Fe-C, powder material 2 were produced from material with a particle size of 3 -141 µm.

The compacts made of Fe-C, powder material 17 were produced from material with a particle size of 20 - 240 µm.

The carbon combined content of the sintered part is 1.06±0.02% - for powder 2, steamed with a density of 6.3 g/cm^3 where it was expected to be in accordance with MPIF 35 norm (0.3-0.6)%.

The carbon combined content of the sintered part is 0.3±0.02% - for powder 18, steamed with a density of 6.3 g/cm^3 where it was expected to be in accordance with MPIF 35 norm (0.3-0.6)%.

The provided data confirmed that the delivered material is within the required range of carbon for PN 17.

The Material from powder 2 does not match the MPIF 35 requirement.

3.9.1.The tensile test results for material Fe-C

Tensile tests were performed at temperatures of 23°C and 120°C. Data available for different sintering methods, test temperature and compact density in Figure 165 - 172 and Table 26 and 27

Table 26. The tensile strength test results for compact made of F-0005 powder material.

Process	Test Temperature [°C]	Material Part Number (PN)	Material Type	Density [g/cm^3]	Yield strength Rp0.2 [MPa]	Tensile strength Rm [MPa]
sintered/no steaming process	23	2	F-0005	5.9	142	174
	23	2	F-0005	5.9	142	174
	23	2	F-0005	6.9	246	289
	23	17	F-0005	5.9	124	140
	23	17	F-0005	6.9	226	212
	23	17	F-0005	6.9	/	201
sintered/no steaming process	120	2	F-0005	5.9	130	146
	120	2	F-0005	5.9	/	128
	120	2	F-0005	6.9	239	274
	120	17	F-0005	5.9	129	143
	120	17	F-0005	6.9	229	297
sintered/steaming process	23	2	F-0005	5.9	/	132
	23	2	F-0005	6.9	287	296
	23	17	F-0005	5.9	/	132
	23	17	F-0005	6.9	/	259

Table 27. The tensile strength test results for compact made of F-0005 powder material. (continuation)

Process	Test Temperature [°C]	Material Part Number (PN)	Material Type	Density [g/cm^3]	Yield strength Rp0.2 [MPa]	Tensile strength Rm [MPa]
sintered/steaming process	120	2	F-0005	5.9	/	128
	120	2	F-0005	6.9	/	257
	120	17	F-0005	5.9	/	79.2
	120	17	F-0005	6.9	93.1	263
	120	17	F-0005	6.9	253	261

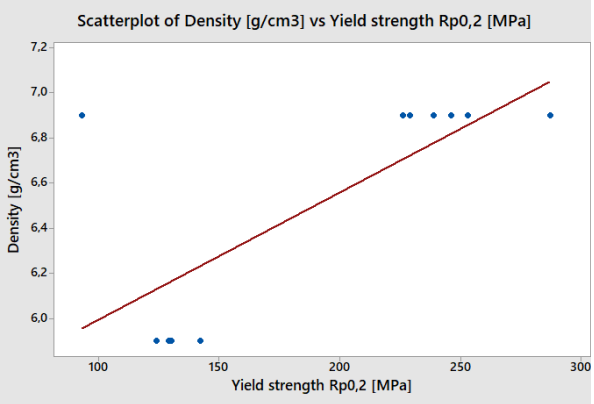

Figure 165. Scatterplot of Density [g/cm^3] vs yield strength Rp0.2 [MPa]

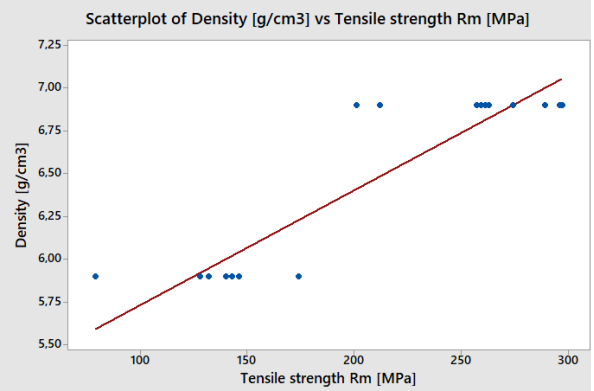

Figure 166. Scatterplot of Density [g/cm^3] vs tensile strength Rm [MPa]

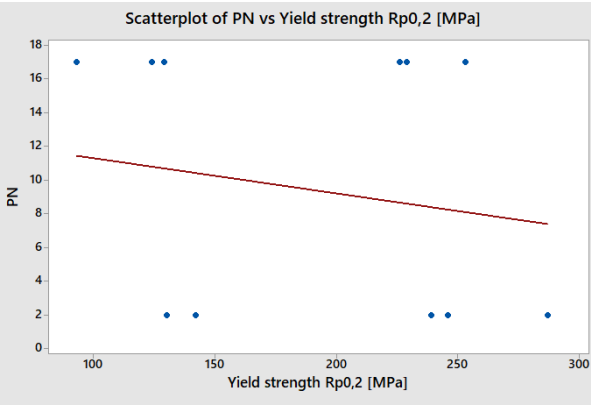

Figure 167. Scatterplot of PN vs yield strength Rp0.2 [MPa]

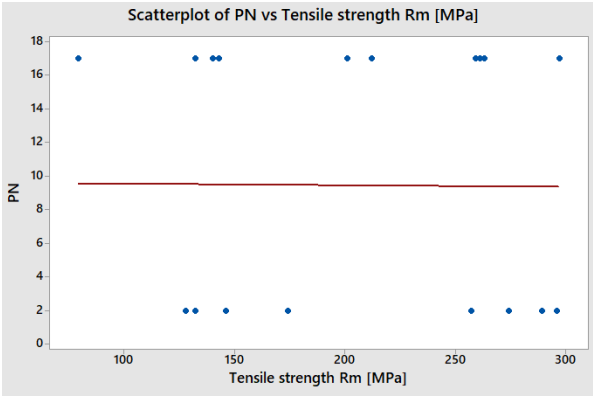

Figure 168. Scatterplot of PN vs tensile strength Rm [MPa]

The tensile strength of the compacts ranged from approximately 79 MPa to over 290 MPa. The yield strength of the compacts ranged from approximately 90 MPa to over 240 MPa.

Regression analysis was used to determine the correlations of the density of the compact, temperature of the test, the type of sintering method, powder material type and yield and tensile strength values of these powder metal compacts. It was found that when the density increased the yield and tensile strength increased. The test temperature has no impact. The test shows the same values for temperatures 23°C and 120°C. The sintering method with additional steaming shows higher versions of yield strength. The temperature and type of process does not have an impact on tensile strength values.

The Young's modulus data for tensile strength test is presented in Table 28 and 29, and Figure 173 - 176.

Table 28. Young's Modulus results after tensile strength test for compact made of F-0005, powder material.

Process	**Test Temperature [°C]**	**Material Part Number (PN)**	**Density [g/cm^3]**	**Young's Modulus [GPa]**
sintered/ no steaming process	23	2	5.9	34.5
	23	2	5.9	34.5
	23	2	6.9	62.2
	23	17	5.9	91.70
	23	17	6.9	99.3
	23	17	6.9	95.8

Table 29. Young's Modulus results after tensile strength test for compact made of F-0005, powder material. *(*continuation*)*

Process	Test Temperature [°C]	Material Part Number (PN)	Density [g/cm^3]	Young's Modulus [GPa]
sintered/ no steaming process	120	2	5.9	43.3
	120	2	5.9	74.4
	120	2	6.9	63.3
	120	17	5.9	137
	120	17	6.9	73.3
sintered/ steaming process	23	2	5.9	101
	23	2	6.9	105
	23	17	5.9	303
	23	17	6.9	88.8
sintered/ steaming process	120	2	5.9	101
	120	2	6.9	105
	120	17	5.9	303
	120	17	6.9	88.8

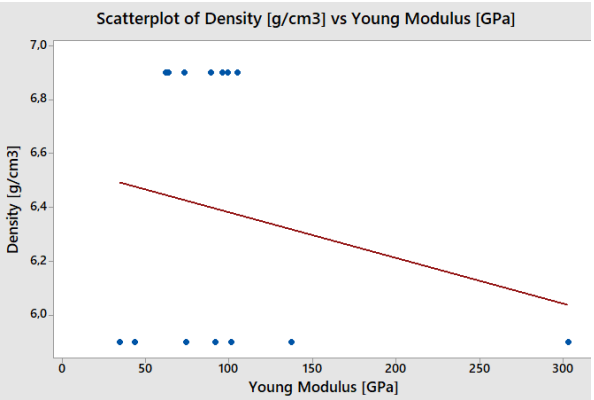

Figure 169. Scatterplot of Density [g/cm^3] vs Young's Modulus [GPa]

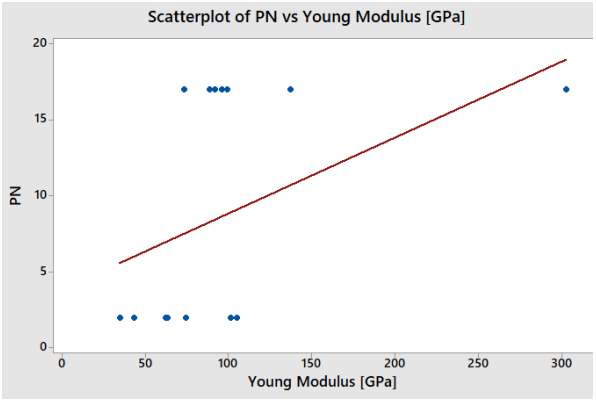

Figure 170. Scatterplot of PN vs Young's Modulus [GPa]

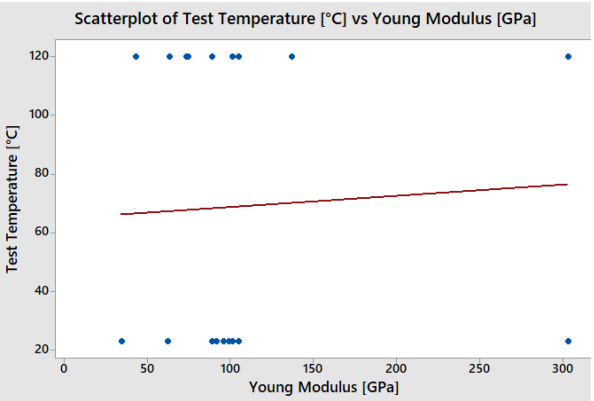

Figure 171. Scatterplot of Test Temperature [°C] vs Young's Modulus [GPa]

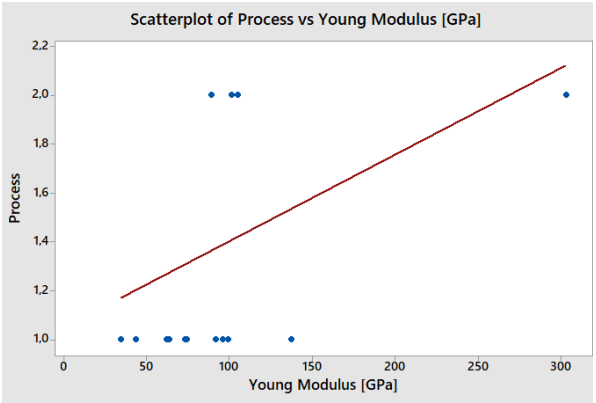

Figure 172. Scatterplot of Process vs Young's Modulus [GPa]

Young's Modulus of the compacts ranged from approximately 50 GPa to over 300 GPa. Regression analysis was used to determine the correlations of the density of the compact, temperature of the test, the type of sintering method and Young's Modulus values of these powder metal compacts. It was found that when the density increased the Young's Modulus decreased. The 303GPa at 5.9 g/cm^3 seems to be an outlier. The test temperature had no impact. The test shows the same values for temperatures 23°C and 120°C. The sintering method with additional steaming shows higher versions of Young's Modulus.

3.9.2. The compression test results for material Fe-C

The compression tests were performed at temperatures of 23°C and 120°C. Data available for different sintering methods, test temperature and compact density in Figure 177 - 180 and Table 30.

Table 30. The compression strength test results for compact made of F-0005 powder material. (cubes).

Process	**Test Temperature [°C]**	**Material Part Number (PN)**	**Density [g/cm^3]**	**Ed [GPa]**	**σd0.2 [MPa]**	**σdM [MPa]**	**Ɛ dB [%]**	**Ɛ dtM [%]**
sintered/no steaming process.	23	2	5.9	6.15	172	548	24	30
	23	2	6.9	7.43	279	646	11	18
	23	17	5.9	4.31	160	698	N/A	49
	23	17	6.9	6.79	257	1067	N/A	60
sintered/no steaming process.	120	2	5.9	4.32	194	447	21	27
	120	2	6.9	5.58	385	667	11	21
	120	17	5.9	4.45	166	770	N/A	51
	120	17	6.9	5.83	270	756	33	42
sintered/steaming process.	23	2	5.9	7.74	477	801	6	14
	23	2	6.9	8.04	407	764	8	15
	23	17	5.9	6.85	537	669	9	13
	23	17	6.9	7.18	387	813	30	37
sintered/steaming process	120	2	5.9	6.94	646	747	7	14
	120	2	6.9	6.75	491	686	6	15
	120	17	5.9	7.36	510	660	4	12
	120	17	6.9	6.22	444	762	21	30

a)

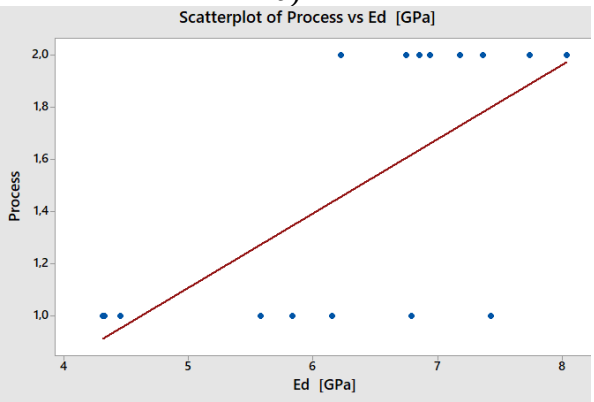

b)

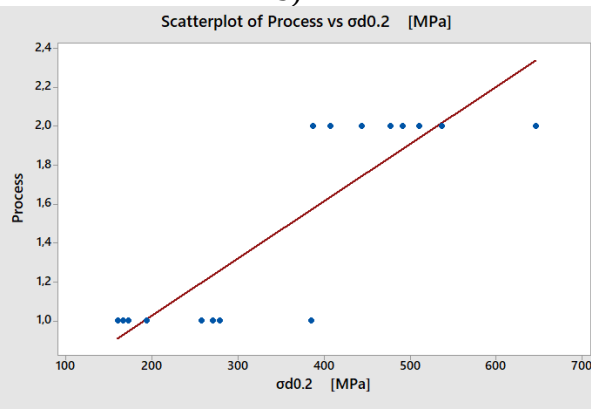

c) d)

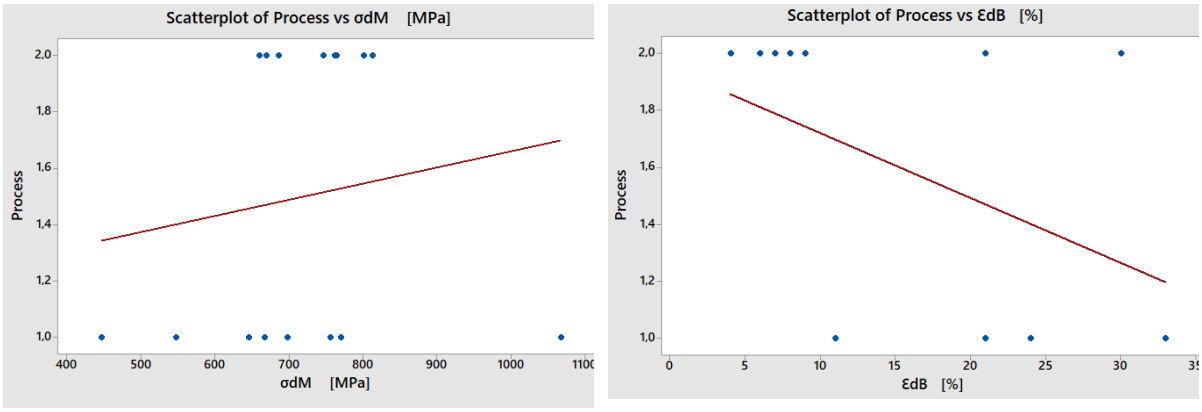

e)

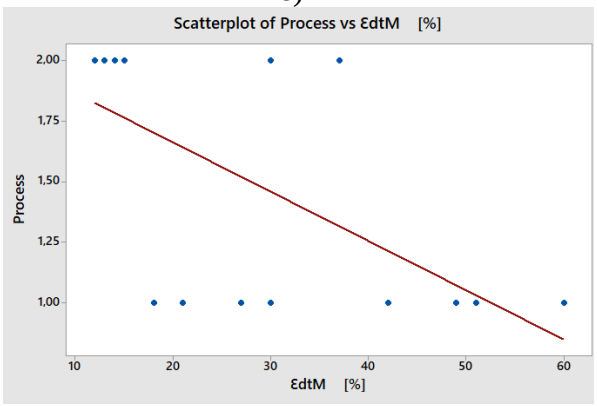

Figure 173. Scatterplot of Process vs a) Ed [GPa]; b) σd0.2 [MPa] ; c) σdM [MPa]; d) Ɛ dB [%]; e) ƐdtM [%].

a) b)

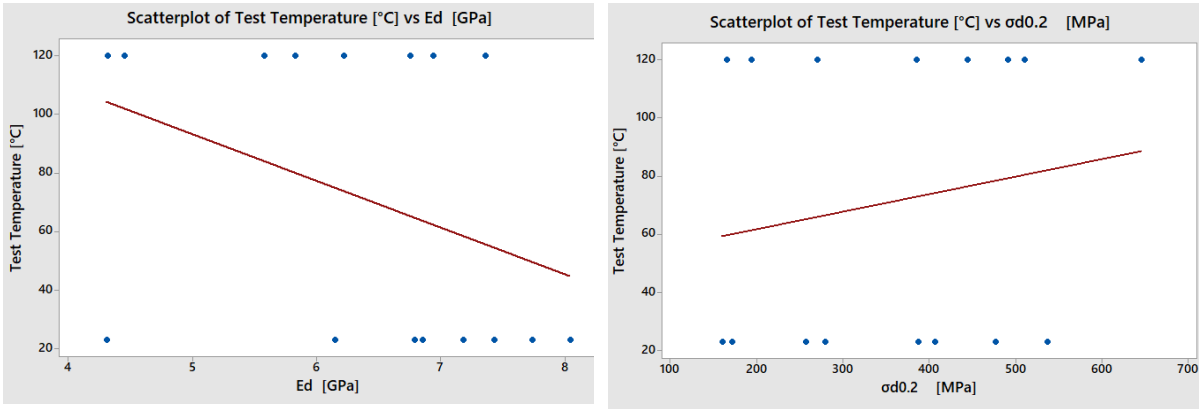

c) d)

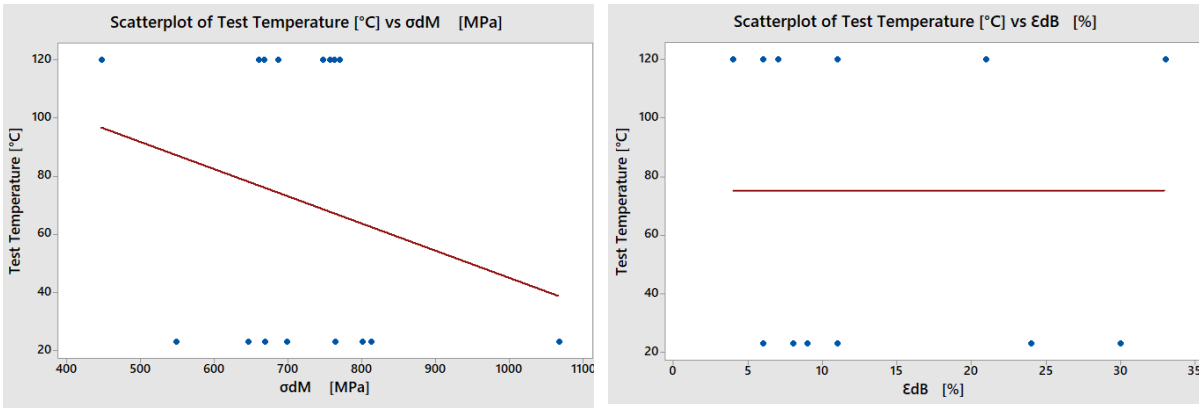

e)

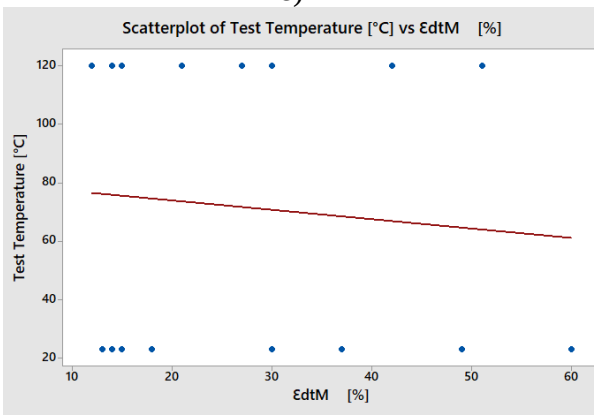

Figure 174. Scatterplot of Temperature [°C] vs a) Ed [GPa]; b) σd0.2 [MPa] ; c) σdM [MPa]; d) Ɛ dB [%]; e) ƐdtM [%].

a) b)

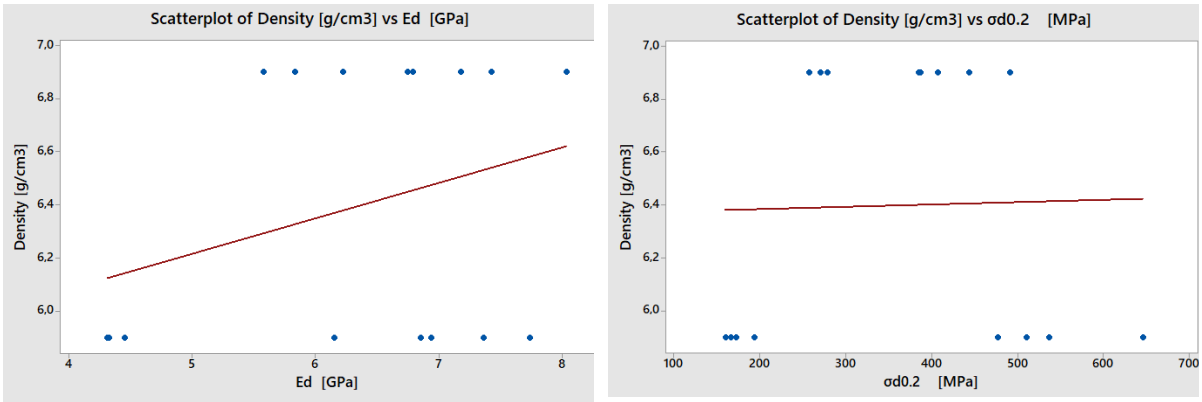

c) d)

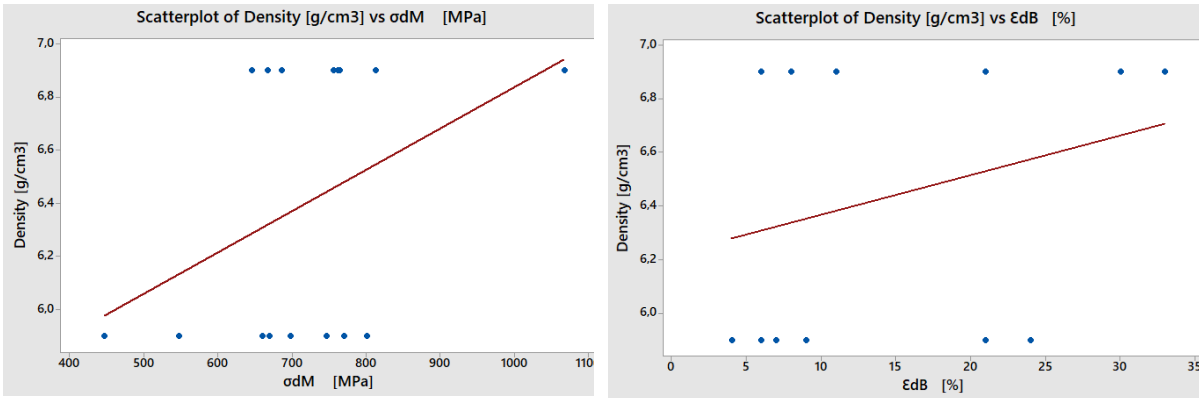

e)

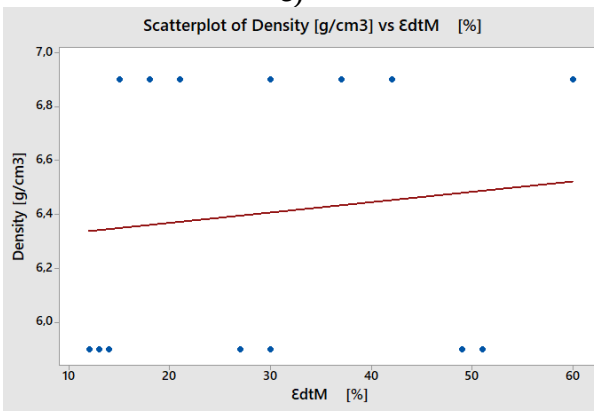

Figure 175. Figure X. Scatterplot of Density [g/cm^3] vs a) Ed [GPa]; b) σd0.2 [MPa] ; c) σdM [MPa]; d) ƐdB [%]; e) ƐdtM [%].

a) b)

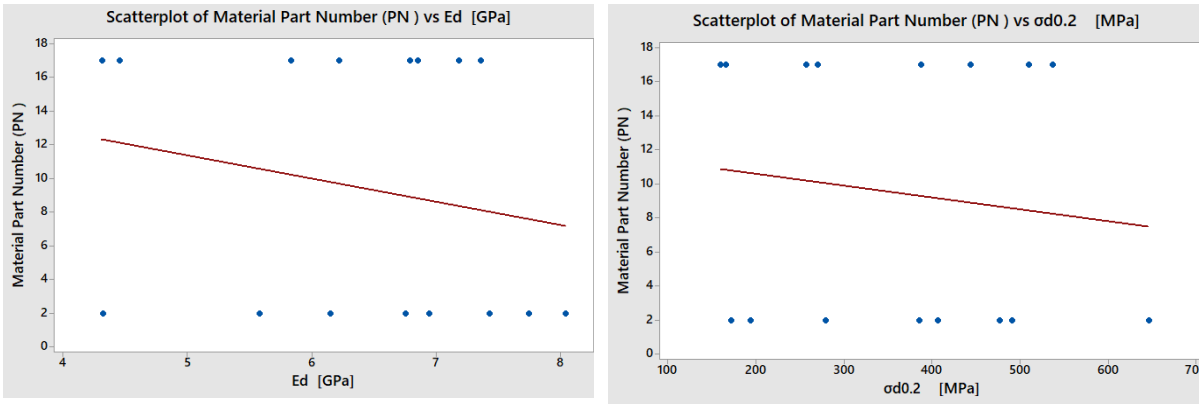

c) d)

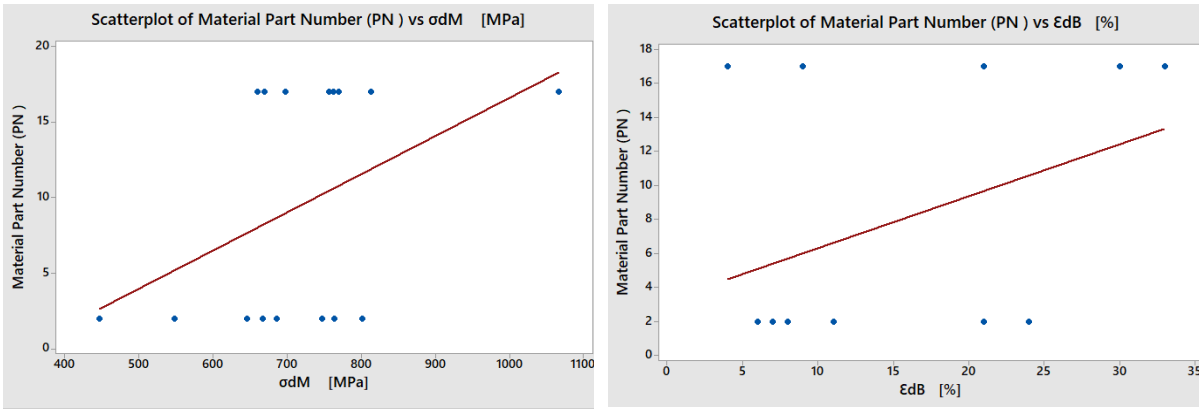

e)

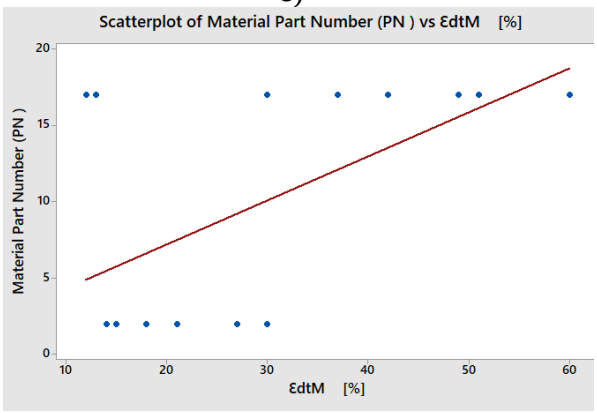

Figure 176. Scatterplot of PN vs a) Ed [GPa]; b) σd0.2 [MPa] ; c) σdM [MPa]; d) ƐdB [%]; e) ƐdtM [%].

The yield strength of the compacts ranged from approximately 150 MPa to over 650 MPa. The compression strength varied over the range of 450 - 1000 MPa.

Regression analysis was used to determine the correlations of the density of the compact, temperature of the test, the type of sintering method and compression test results. It was found that when the density increased the compression test results increased. The test temperature has no impact. The test shows the same values for temperatures 23°C and 120°C.The sintering method with additional steaming shows higher versions of Young's Modulus, yield strength and compression strength.

Repeated compression test were carried out on samples from powder material Fe-C (17) to see the relationship with hardness measurement. Data are presented in separate tables for samples made of powder material Fe-C (17) without steaming (Figure 181-187), (Table 31), and with an additional steaming process (Figure 188-194), (Table 32 and 33).

Table 31. The repeated test, the compression strength test results for compacts made of F-0005 powder material, cubes, material sintered/not steaming process

Material Type Part Number (PN)	**MPIF Material Type**	**Density [g/cm^3]**	**Young's Modulus [Mpa]**	**YIELD STRENGTH [Mpa]**	**TENSILE STRENGTH Rs [Mpa]**	**Hardness [HRB]**
17	F-0005	**5.9**	5,648	170	1,765	25
17	F-0005	**5.9**	5,083	173	1,834	24
17	F-0005	**5.9**	6,361	152	1,522	/
17	F-0005	**6.1**	7,203	185	1,213	35
17	F-0005	**6.1**	8,237	188	1,254	26
17	F-0005	**6.1**	10,137	178	1,191	/
17	F-0005	**6.3**	6,559	205	1,599	21
17	F-0005	**6.3**	5,452	220	1,662	26
17	F-0005	**6.3**	6,463	201	1,884	/
17	F-0005	**6.5**	9,791	229	1,649	32
17	F-0005	**6.5**	7,588	260	1,618	33
17	F-0005	**6.5**	10,082	221	1,416	/
17	F-0005	**6.7**	10,367	224	1,451	43
17	F-0005	**6.7**	6,691	304	1,392	40
17	F-0005	**6.7**	8,990	262	1,576	/
17	F-0005	**6.9**	11,649	280	1,462	53
17	F-0005	**6.9**	9,357	302	1,628	51
17	F-0005	**6.9**	11,875	279	1,455	/

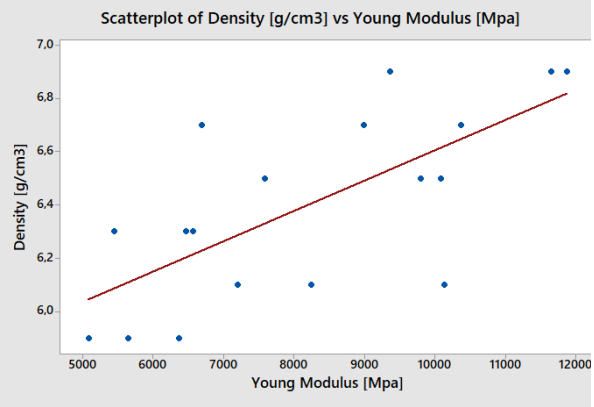

Figure 177. Scatterplot of Density [g/cm^3] vs Young's Modulus [MPa]

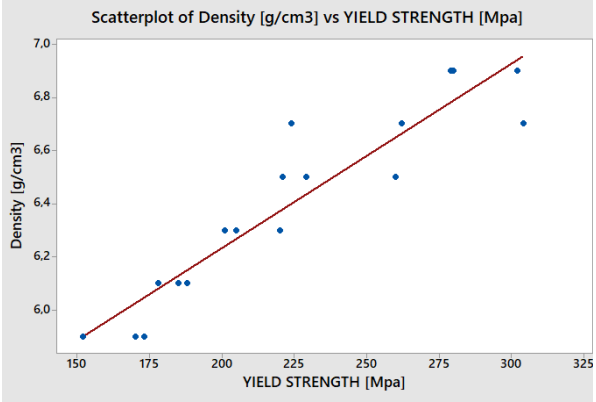

Figure 178. Scatterplot of Density [g/cm^3] vs Yield Strength [MPa]

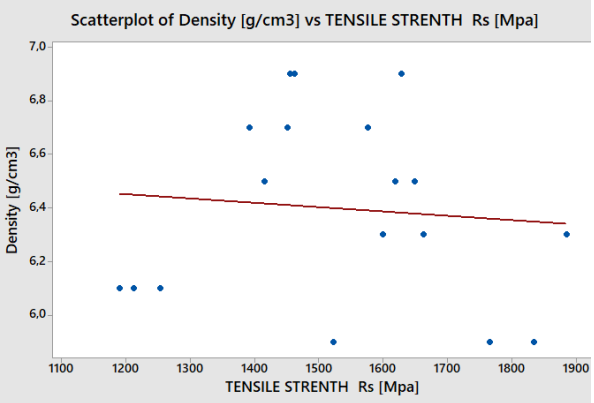

Figure 179. Scatterplot of Density [g/cm^3] vs Tensile Strength [MPa]

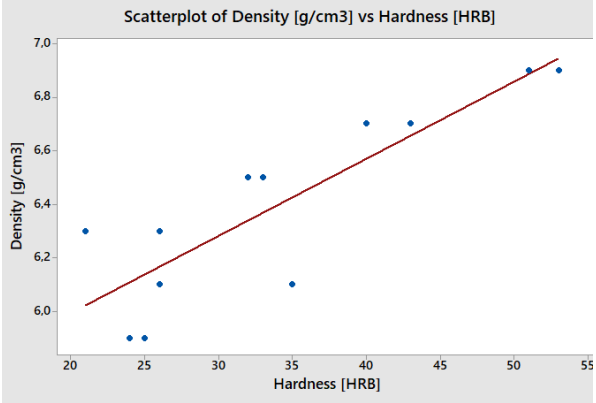

Figure 180. Scatterplot of Density [g/cm^3] vs Hardness [HRB]

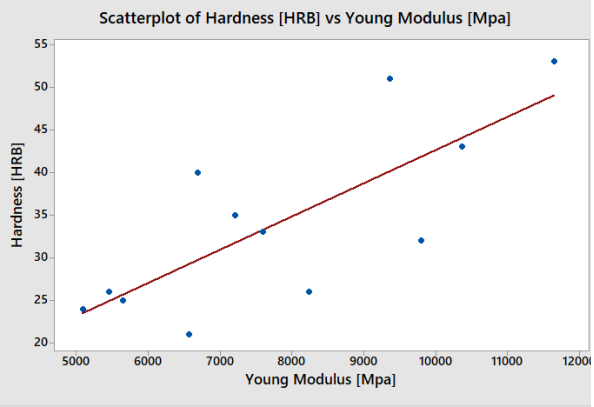

Figure 181. Scatterplot of Hardness [HRB] vs Young's Modulus [MPa]

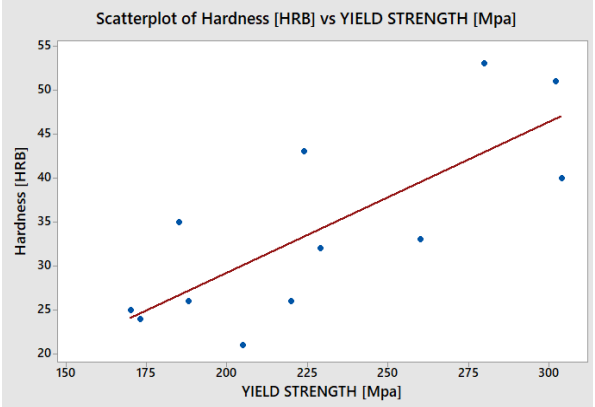

Figure 182. Scatterplot of Hardness [HRB] vs Yield Strength [MPa]

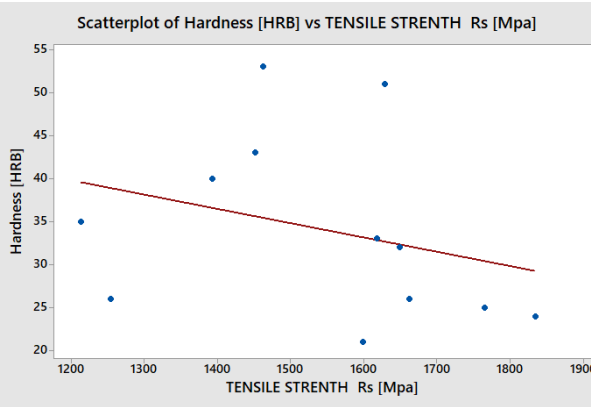

Figure 183. Scatterplot of Hardness [HRB] vs Tensile Strength [MPa]

The repeated compression test for compacts with the sintering process without additional steaming. It showed Young's Modulus of the compact ranged from approximately 5,000 MPa to 12,000 MPa. The yield strength of the compacts ranged from approximately 160 MPa to over 300 MPa. The compression strength of the compacts ranged from approximately 1,200 MPa to over 1,800 MPa. Regression analysis was used to determine the correlations of the density, hardness, and compression test results. It was found that when the density increased the compression test results increased. The same happened for hardness when the hardness increased the compression test results increased.

Table 32. The repeated test, the compression strength test results for compact made of F-0005 powder material, cubes. material sintered/ steaming process

Material Type Part Number (PN)	**MPIF Material Type**	**Density** [g/cm^3]	**Young's Modulus [Mpa]**	**YIELD STRENGTH [Mpa]**	**TENSILE STRENGTH Rs [Mpa]**	**Hardness [HRB]**
17	F-0005	**5.9**	9,083	508	658	88
17	F-0005	**5.9**	9,775	525	666	88
17	F-0005	**5.9**	9,526	519	667	/
17	F-0005	**6.1**	10,486	671	768	98
17	F-0005	**6.1**	10,818	698	775	96
17	F-0005	**6.1**	11,602	776	860	N/A
17	F-0005	**6.3**	10,964	655	919	88
17	F-0005	**6.3**	12,505	532	1,028	87
17	F-0005	**6.3**	10,812	633	864	/

Table 33. The repeated test, the compression strength test results for compact made of F-0005 powder material, cubes, material sintered/ steaming process (continuation).

17	F-0005	**6.5**	8,977	461	1,541	82
17	F-0005	**6.5**	9,128	472	1,059	85
17	F-0005	**6.5**	5,310	539	1,481	N/A
17	F-0005	**6.7**	8,510	464	1,681	78
17	F-0005	**6.7**	7,564	502	864	80
17	F-0005	**6.7**	8,257	475	815	/
17	F-0005	**6.9**	8,032	457	965	80
17	F-0005	**6.9**	7,903	466	1,259	70
17	F-0005	**6.9**	6,991	478	2,060	/

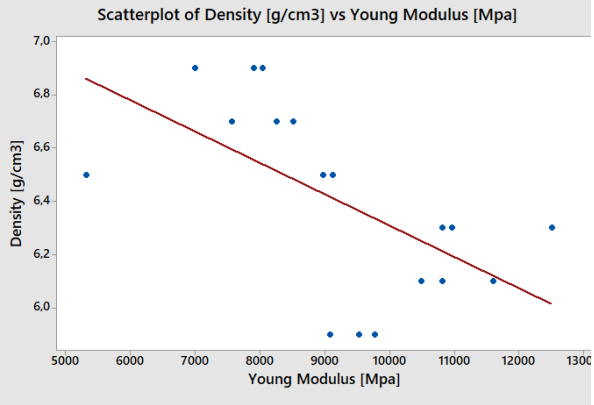

Figure 184. Scatterplot of Density [g/cm^3] vs Young's Modulus [MPa]

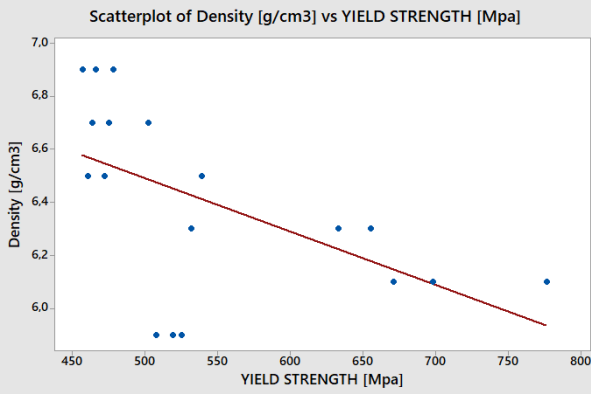

Figure 185. Scatterplot of Density [g/cm^3] vs Yield Strength [MPa]

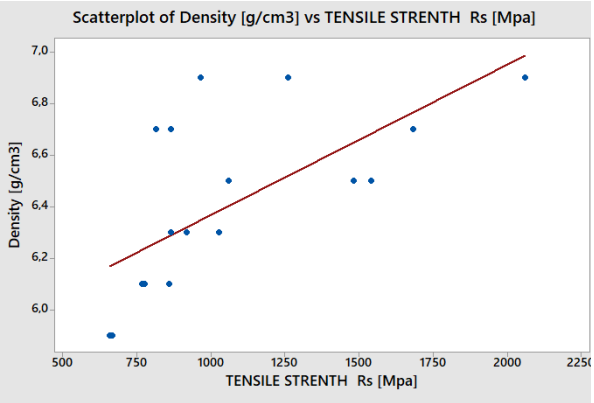

Figure 186. Scatterplot of Density [g/cm^3] vs Tensile Strength [MPa]

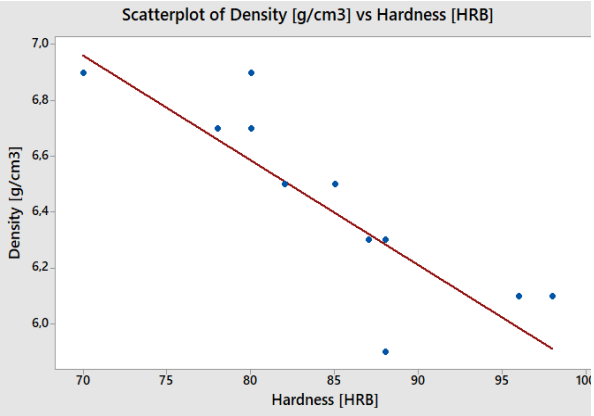

Figure 187. Scatterplot of Density [g/cm^3] vs Hardness [HRB]

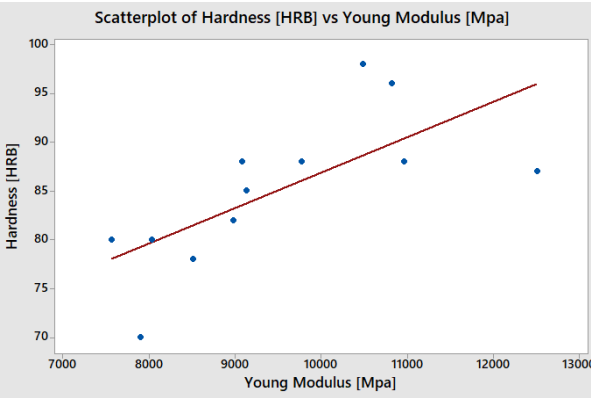

Figure 188. Scatterplot of Hardness [HRB] vs Young's Modulus [MPa]

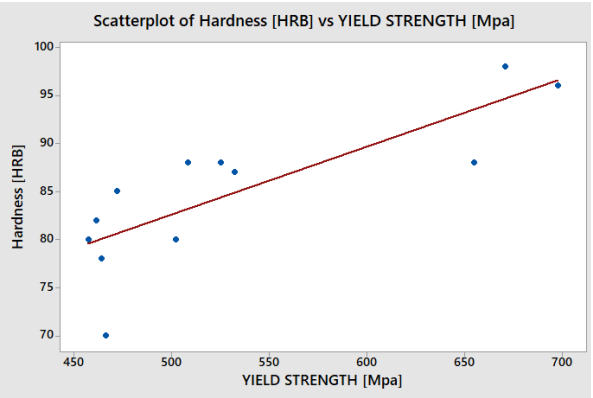

Figure 189. Scatterplot of Hardness [HRB] vs Yield Strength [MPa]

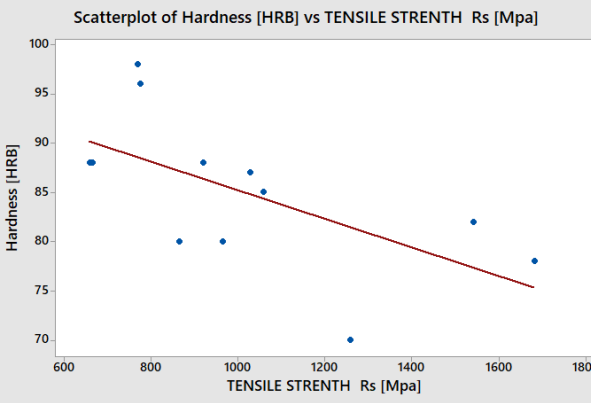

Figure 190. Scatterplot of Hardness [HRB] vs Tensile Strength [MPa]

The repeated compression test for compacts with the sintering process with additional steaming. It showed Young's Modulus of the compacts ranged from approximately 6000 MPa to over 12500 GPa. The yield strength of the compacts ranged from approximately 450 MPa to over 700 MPa. The compression strength varied over the range of 650 - 1600 MPa.

Regression analysis was used to determine the correlations of the density, hardness, and compression test results. It was found that when the density increased Young's Modulus and Yield strength decreased, and Compression strength increased. When the hardness increased Young's Modulus and Yield strength increased, and tensile strength decreased. When density increased the hardness decreased.

3.9.3. Microstructure analysis for material Fe-C using scanning microscopy

SEM was performed on the microstructure of parts made of Fe-C powder material. The results are presented in Figure 195, 196 below, for different densities and magnification.

a) a)

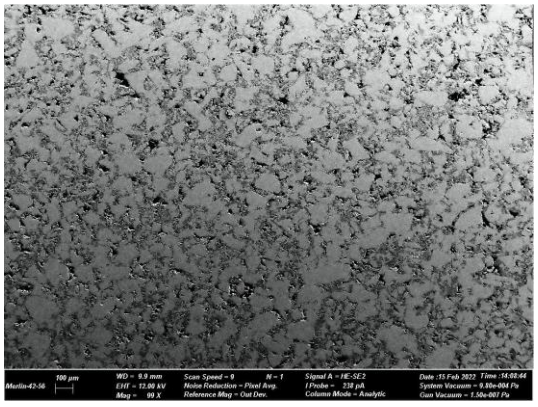

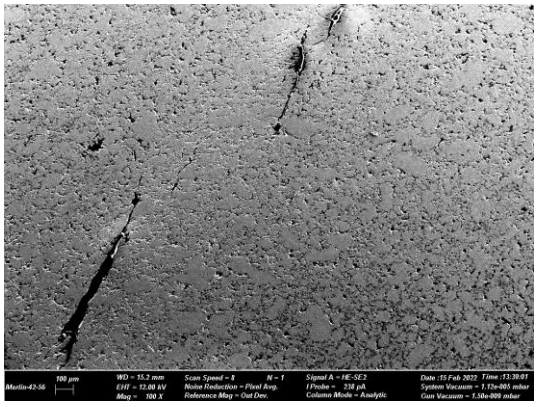

b)

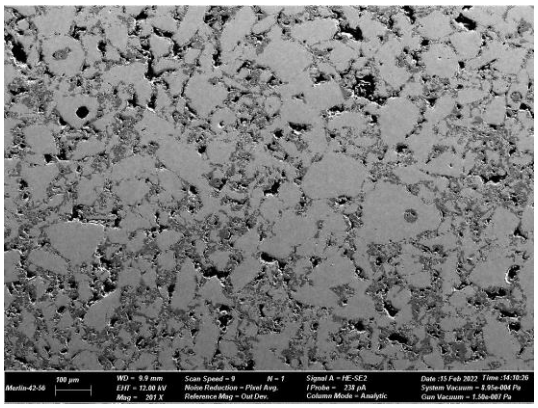

b)

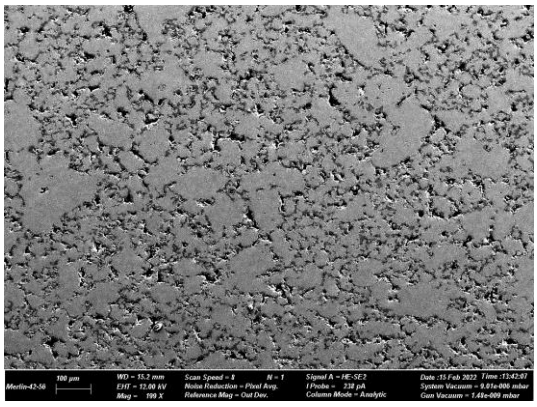

c)

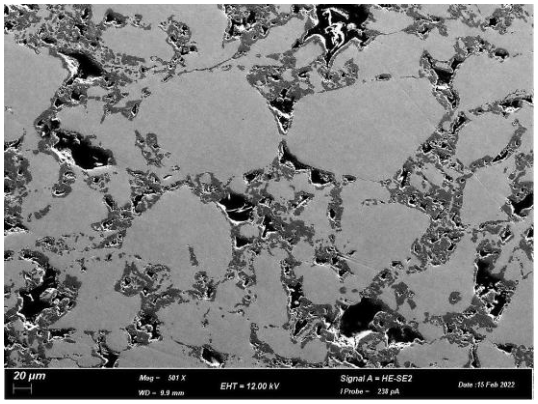

c)

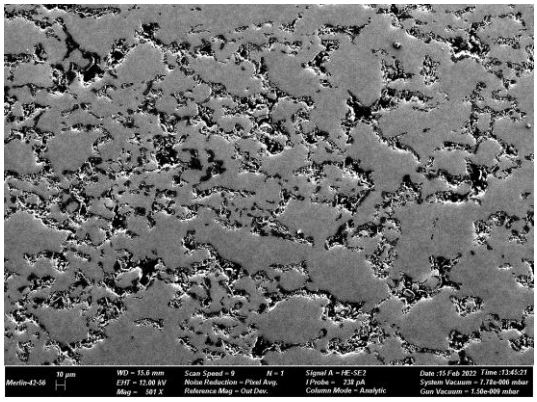

d)

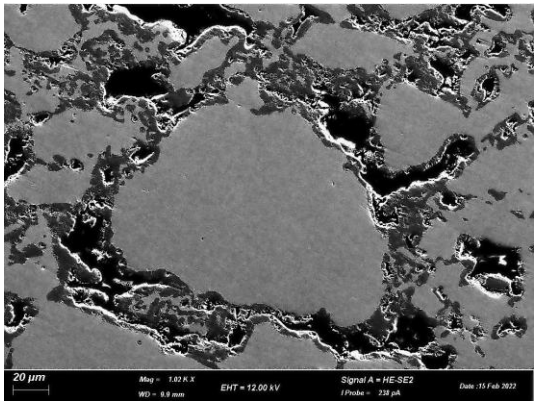

d)

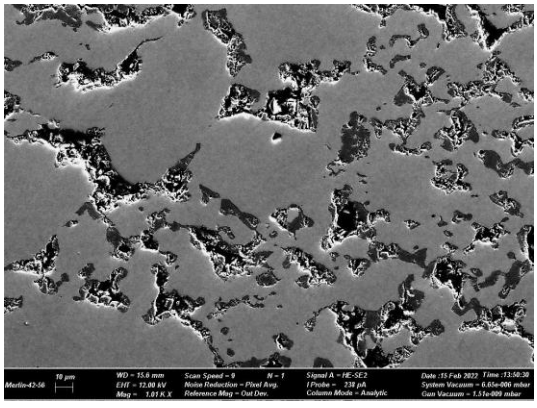

e)

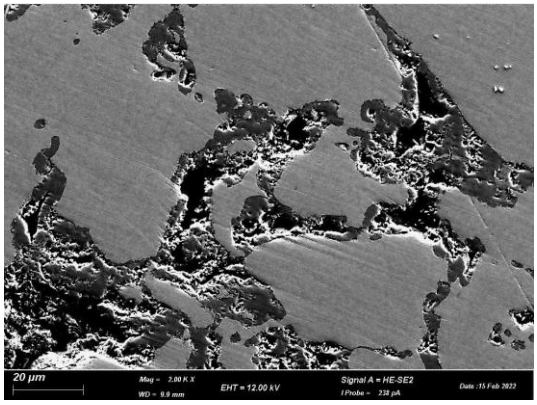

Figure 191. SEM microstructure of compact made of powder material 17, after sintering with additional steaming process, with density 6.1 [g/cm^3], a) Magnification 100X, b) Magnification 200X, c) Magnification 500X, d) Magnification 1000X, e) Magnification 2000X

e)

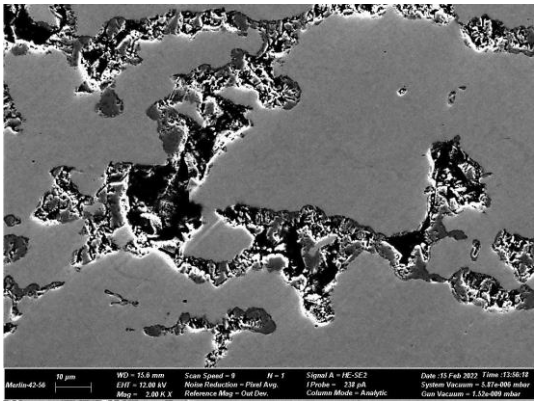

Figure 192. SEM microstructure of compact made of powder material 17, after sintering with additional steaming process, with density 6.3 [g/cm^3], a a) Magnification 100X, b) Magnification 200X, c) Magnification 500X, d) Magnification 1000X, e) Magnification 2000X

There were visible pores. The impurities coming from the quality of the sintering process. There is no significant difference in the structure of these compacts.

The word “ferrite” can be traced back to lodestone, a mineral based on magnetite, Fe3O4, which was used in navigation for many centuries, and studied for its physical and magnetic properties since the 1930s. These materials are under development due to their magnetic, optical and conductive properties. [99]. The growth of ferrous powder metallurgy is outstanding. This technology is used as a cheaper alternative process to machining, casting, stamp forging and other similar metal working technologies. It has becoming more interesting not only for the automotive industry but also for lawns, garden mowers, tractors and locks. [63].

The examples of the structure of the ferrite and pearlite of the compacts is presented in the Figure 197 and Figure 198.

In Figure 197 ferrite and black spots (which are the pores) are visible.

In Figure 198 ferrite and perlite, and black spots (which are the pores) are visible.

The sintering process of iron based powder materials led to a microstructure of ferrite grains and rows of pores. The microstructure of sintered Fe–C–Cu alloys is heterogeneous and consists of fine pearlite and islands of ferrite. [35]

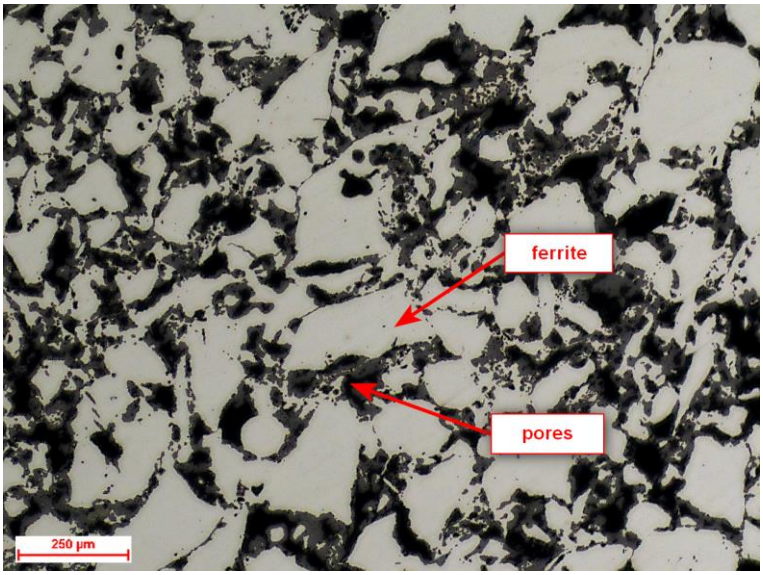

Figure 193. Sinter element 17 sintered/steamed with density 6.1 g/cm^3, Magnification 100X

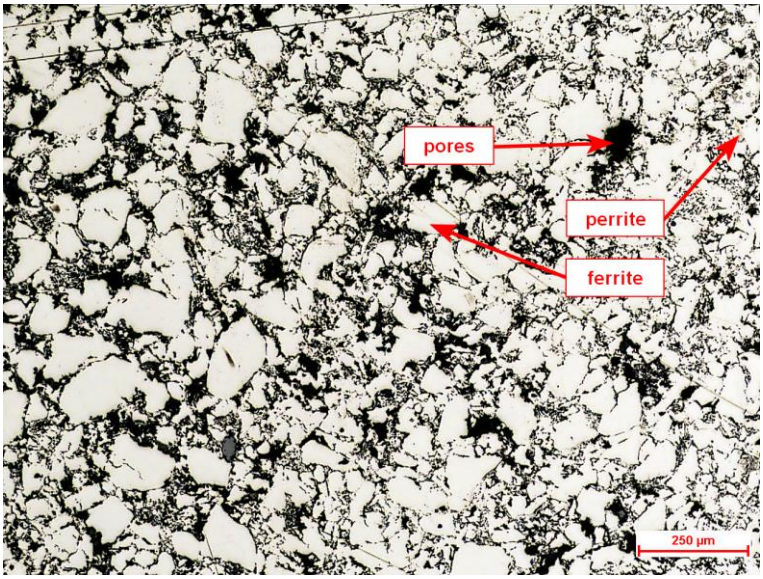

Figure 194. Sinter element 22 sintered/not steamed with density 6,1 g/cm^3, Magnification 100X

High density means the high strength of compacted parts, and it is a desirable feature with powder metallurgy. [33] The literature data shows the influence of the used iron powders as the metal matrix base on the quality of sintered material. [100]

Part density or controlled porosity is unique to powder metallurgy, and it allows the possibility of self lubrication, reduced mass, and the ability to select the density of critical sections of the part to meet specific part performance requirements.

Density significantly influences the overall part performance as measured by the yield and tensile strength, ductility, impact toughness and fatigue resistance. [95]

4. Conclusions

1.

The tests in the study were carried out on six different types of powder materials. Each material demonstrated a specific chemical composition, derived directly from the powder supplier. Those materials were subjected to a conventional sintering method. Half of the mouldings were additionally treated with oxidation. The aim of the study was to check the influence of the chemical composition on the mechanical properties of the moulded parts produced. Due to the large number of samples to be tested, it was assumed that the strength tests could be affected by:

- the type of sintered powder,

- the segregation of copper, which was a component of the powder mixture,

- powder storage time period before it was used in the densification/sintering processes,

- the quality of production process,

- the grain size of powder material,

- porosity,

- ferrite/perlite microstructure.

The results of the compression and tensile tests were scattered due to material porosity. In order to determine the relationship of data and results, the tests were separated into the

analysis of sintered components from powder material 22 (FC – 0208) and the analysis of sintered components from the other powder materials, i.e. Fe-C-Cu and Fe-C.

2.

Comprehensive tests were carried out on FC-0208 (Fe-C-Cu), as this was a new material used in that particular conventional manufacturing process. It was also noted that many mouldings, produced from this material, had cracking in their application use. The sintered components were subjected to compression and tensile strength tests. It was noted that the samples had been cracking around the jaws during the tensile tests, rather than in the middle of the sample length, beyond the gauge length. The repeated tests - using the same sample but a different apparatus - confirmed that the tests had been carried out correctly.

Sample buckling occurred during the compression test, which is a normal occurrence during compression strength tests. Due to the porosity of the test sample, it was noted that the yield strength had differed in compression and tensile tests.

A tensile test of the powder 22 moulding showed that temperature had no effect on the tensile strength parameters of the tensile strength, i.e. the ability of the test sample to resist fracture when a pulling force is applied in the direction parallel to its longitudinal axis. Neither did temperature have any effects on the value of Young's Modulus, a parameter that determines the material elasticity level during tensile tests. Differences in results were not apparent for the samples either with or without additional oxidation A relationship was observed, namely that tensile strength and Young's modulus values had both increased together with density.

The compression test also demonstrated that temperature differences, either 23°C or 120°C, had no effect on differences in test results. As density increased, hardness of the sintered components increased as well. Density and hardness increase were also associated with increased compression strength, yield strength and Young's modulus values.

The Drucker Prager model was used to model the behaviour of a sintered component in the study. The results differed among literature data, standards and the results from real tests. It was also found that there was no information in the standards about the type of powder material, i.e. by which manufacturing process the material had been produced.

A prototype model of a sintered component was developed, based on the finite element analysis in the Abaqus program. The model indicated further research directions regarding the properties of sintered components.

Strength test simulations and a wide range of tests made it possible to establish a material base. The knowledge gained from the research will facilitate the standardization of the materials used to produce sintered components.

The porosity of the sintered components tested was in the range of 0.02-25%. For the same material type porosity varied by approximately 10 per cent.

Fractography of fractures after the test showed that copper segregation and an exaggerated amount of oxides had appeared in those areas. Purity of the tested components did not show the required quality, either; many impurities were observed on the structure surface.

3.

Sintered components, manufactured from Fe-C-Cu material (FC-0205 and Fc-0208) of 18.4.26 sample and Fe-C (F-0005) of 2.17 sample, were also subjected to strength tests. However, no such comprehensive tests (as for sample 22) were carried out on those materials.

Observations with an optical microscope revealed ferrite and pearlite structures. It was a typical phase component for the components under study. Those structures did not depend on the density of the compact under study.

The tensile test for the Fe-C-Cu samples showed no yield strength. However, as density increased, tensile strength increased as well. For a density of 5.9 g/cm^3 tensile strength is in the range of 150-250 MPa, with a density of 6.9 g/cm^3 in the range of 260-480 MPa.

For samples 4 and 18, the tensile strength was within the range of 150-500 MPa, while for sample 26, it was within the range of 150-350 MPa (the results occur in a smaller range). Neither room temperature nor an elevated temperature changed the material properties. It did not affect the test results, either. The data of tests of the samples with an additional coating were more cumulative, occurring over a narrower range of values.

The compression strength test for the Fe-C-Cu samples showed that, as the density increased, the parameters of compression strength increased as well. The range for PN 26 was the narrowest, with the compression strength within the range of 580-910 MPa, while the other PN samples demonstrated results within the range of 270-780 MPa.

Compression strength was higher for the samples without additional heat treatment. By contrast, Young's modulus was higher for the samples with additional heat treatment.

For the samples, produced from Fe-C powder material (F-0005), similarly as for the Fe-C-Cu samples, the tensile test did not show any yield strength. The test, carried out at an elevated temperature of 120°C, did not induce any difference in the results. In contrast, together with an increase in density, the tensile strength increased by up to twofold. The oxidation-treated samples generated results with a narrower range.

A compression test of the samples, produced from Fe-C powder material (F-0005), also showed an increase, both in Young's Modulus and in the compression strength with additional heat treatment. The process with additional heat treatment demonstrated significantly higher values than the process without such treatment. The samples, produced from material 17, provided more consistent results within a series of repetitions (trial) than the samples produced from powder material 2.

It was noted in the course of the study that the type of powder material (sponge or atomised) had demonstrated the highest influence on the results of the strength tests carried out. This fact is confirmed by a number of literature sources, as well as by the behaviour of sintered components produced from sponge powder 2 and 26. Those samples did not break before the end of the test and were able to retain most of the parameters from the compression and tensile tests.

4.

As part of the implementation works, a workstation was set up to determine density and porosity by means of the Archimedes method. These tests are performed when approving a sintered component for mass production. Microscopic studies enabled a data base to be created with the knowledge on the structure of sintered components, produced from various powder materials. An analysis of carbon loss during the production process was also implemented. The studies showed carbon loss in the tested conventional process at the level of 0.1%, which was in compliance with the ASTM E1019 test. The percentage of carbon supplied in the powder material should be equal to the percentage of carbon in the sintered part produced. Lost carbon is converted into costs and losses in the production process.

As part of the implementation works, a model was designed and developed to simulate sintered components. An initial study, carried out by the finite element method, illustrated the status quo and revealed further possible research directions. They should focus on creating the FEA (Finite Element Method) models of densification and of moulded part formation processes.

A prior analysis of the manufacturing stage enables the potential areas of later cracking to be revealed much earlier than any analysis of the finished sintered parts.

The study showed that the most suitable type of material for the conventional sintering process studied had, in that case been the sponge material. The chemical composition and density of the sintered component had less influence and importance with regards to the properties of sintered components.

Literature

1. DIN 31692, Gleitlager 2. Werkstoffe, Prüfung, Berechnung, Begriffe, 1980
2. Herbert W. Cremer, Trefor Davies; *Chemical engineering practice: in twelve volumes. Vol. 2, Solid state*; London : Butterworths Scientific Publications, 1956.
3. Anish Upadhyaya; G S Upadhyaya Powder Metallurgy, Science, Technology and Materials; ISBN 978 1 4398 5746 5
4. Stanula Agnieszka, Pilarczyk Wirginia; *Combined carbon content assessment method for powder metallurgy*, Journal of Achievements of Materials and Manufacturing Engineering, International OCSCO World Press, vol. 114, nr 1, 2022, s. 15-21, DOI:10.5604/01.3001.0016.1479
5. MPIF STANDARAD TEST, MPIF 03, 2019 Edition, 2019
6. ISO 13517:2013: Metallic powders — *Determination of flowrate by means of a calibrated funnel (Gustavsson flowmeter*); Publication date: 2013-05
7. ISO 4490:2018; Metallic powders — *Determination of flow rate by means of a calibrated funnel (Hall flowmeter)*; Publication date : 2018-04
8. Mats Larsson, Erich Brandner and Stefan Gustavsson, *Introduction to a new standardized test method for powder mixes, the Gustavsson flowmeter funnel*. Presented at Euro PM 2013 in Gothenburg on September, 2013.
9. Oleg D. Neikov, Nikolay A. Yefimov; *Chapter 1 - Powder Characterization and Testing; Handbook of Non-Ferrous Metal Powders (Second Edition) Technologies and Applications 2019*, Pages 3-62; https://doi.org/10.1016/B978-0-08-100543-9.00001-4
10. PN-EN ISO 3252:2019-12 - wersja angielska; *Metalurgia proszków - Terminologia*; Data publikacji 19-12-2019
11. MPIF 35 P/M STRUCTURAL, *Materials Standards for PM Structural Parts*; 2020 Edition
12. North America Hoganas, *Production of Sintering Components*, Copyright Hoganas AB, 2004

13. Rahul Unnikrishnan, Jabbar Gardy, Ben F. Spencer, Robin Kurinjimala, Avishek Dey, Vahid Nekouie, Sandeep Irukuvarghula, Ali Hassanpour, Christoph Eisenmenger-Sittner John A. Francis, Michael Preuss; *Functionalization of metallic powder for performance enhancement;* Materials & Design Volume 221, September 2022, 110900; https://doi.org/10.1016/j.matdes.2022.110900 0264-1275/ 2022 The Authors. Published by Elsevier Ltd
14. Bo Hu; *Roles of Iron Metal Powders in Semi-Metallic Friction Materials*; The 7th International Technical Exchange & Product Exhibition on Friction Materials (June 16-18, 2005, Wuhan, China).
15. C.S. Kang, S.C. Lee, K.T. Kima, O. Rozenberg; *Densification behavior of iron powder during cold stepped compaction;* Materials Science and Engineering A 452–453 (2007) 359–366; doi:10.1016/j.msea.2006.10.113
16. Hamid Salehi, John Cummins, Enrico Gallino, Neil Harrison, Ali Hassanpour, Mike Bradley; A new approach to quantify powder's bed surface roughness in additive manufacturing; Powder Technology 407 (2022) 117614; https://doi.org/10.1016/j.powtec.2022.117614
17. Danni Chena, Kaili Lia, Hongya Yua, Jianliang Zuoa, Xi Chenb, Baochun Guoa, Guangze Hanb, Zhongwu Liua; Effects of secondary particle size distribution on the magnetic properties of carbonyl iron powder cores; Journal of Magnetism and Magnetic Materials Volume 497, 1 March 2020, 166062; https://doi.org/10.1016/j.jmmm.2019.166062
18. L. Grosseau-Poussarda, X. Milhet, C. Huvier, J. F. Dinhut; *Consolidation of iron powders through the influence of phosphate thin films*; journal of materials processing technology 205 (2008) 151–159; doi:10.1016/j.jmatprotec.2007.11.123
19. Jan Leżański; *Proszki metali i wysokotopliwych faz: metody wytwarzania;* Kraków: Wydawnictwa AGH, 1994
20. *PRODUCTION OF IRON AND STEEL POWDER;* Höganäs PM-school, 2004
21. Ilaria Baesso, David Karl, Andrea Spitzer, Aleksander Gurlo, Jens Günster, Andrea Zocca; *Characterization of powder flow behavior for additive manufacturing*; Additive Manufacturing 47 (2021) 102250; https://doi.org/10.1016/j.addma.2021.102250

22. Harish Singh Dhami, Priti Ranjan Panda, Koushik Viswanathan; Production of powders for metal additive manufacturing applications using surface grinding; Manufacturing Letters Volume 32, April 2022, Pages 54-58; https://doi.org/10.1016/j.mfglet.2022.02.004
23. Stanula Agnieszka, Pilarczyk Wirginia: *Konwencjonalna metoda spiekania materiału FC-0208,* W: TalentDetector2022_Winter: Międzynarodowa Studencka Konferencja Naukowa, Gliwice, styczeń, 2022. T. 2 / Bonek Mirosław (red.), Prace Katedry Materiałów Inżynierskich i Biomedycznych, 2022, Politechnika Śląska, ISBN 978-83-65138-31-6, s. 711-723
24. M.M. Rahman, S.S.M. Nor; *An experimental investigation of metal powder compaction at elevated temperature*; Mechanics of Materials 41 (2009) 553–560; doi:10.1016/j.mechmat.2008.12.003
25. K. Yamaguchi, N. Takakura and S. Imatani; *Compaction and Sintering Characteristics of Composite Metal Powders;* Journal of Materials Processing Technology 63 (1997) 364-369; PI S0924-0136(96)02648-9
26. D. Shaham, J. Rawers, E. Zolotoyabko ; *Structural transformation of iron powders mechanically processed in nitrogen;* Materials Letters 27 (1996) 41-45 ; May 1996; 1996 Elsevier Science B.V. All rights reserved SSDI 0167-577X(95)00274-X
27. Dominguez and J. Bigot; *MATERIAL TRANSPORT MECHANISMS AND ACTIVATION ENERGY IN NANOMETRIC Fe POWDERS BASED ON SINTERING EXPERIMENTS*; 096Ss9773(95)00199; Nanostructured Materials, Vol. 6. pp. 877-880.1995; Elsavier
28. Ugur Çavdar, Bekir Sadık Ünlü, Ahmet Murat Pinar , Enver Atik; *Mechanical properties of heat treated iron based compacts;* Materials and Design 65 (2015) 312–317; http://dx.doi.org/10.1016/j.matdes.2014.09.015
29. M.G. Bodas D.R. Dash and C.S. Sivaramakrishnan; *Oxidation of iron powder in a fluidized bed reactor;* Materials & Design. Vol. 17, No. 3, pp. 167-172, 1996 0 1997 Elsevier Science Ltd; PII: SO261-3069(96)00056-8
30. Laurine Choisez, Niek E. van Rooij, Conrad J.M. Hessels, Alisson K. da Silvaa, Isnaldi R. Souza Filhoa, Yan Maa, Philip de Goey , Hauke Springer, Dierk Raabea; *Phase transformations and microstructure evolution during combustion of iron powder;* Acta Materialia 239 (2022) 118261; https://doi.org/10.1016/j.actamat.2022.118261

31. Keqin Feng, Yi Yang, Mei Hongb, Jinling Wua, Shanshan Lana; *Intensified sintering of iron powders under the action of an electric field: Effect of technologic parameter on sintering densification*; journal of materials processing technology 208 (2008) 264–269; doi:10.1016/j.jmatprotec.2007.12.117
32. https://www.iqsdirectory.com/; access: June 2023
33. A.K. Eksi, A.H. Yuzbasioglu; *Effect of sintering and pressing parameters on the densification of cold isostatically pressed Al and Fe powders*; Materials and Design 28 (2007) 1364–1368; doi:10.1016/j.matdes.2006.01.018
34. R.K. Khatirkar, B.S. Murty; Structural changes in iron powder during ball milling; Materials Chemistry and Physics 123 (2010) 247–253; doi:10.1016/j.matchemphys.2010.04.004
35. M.G. Fillabi, A. Simchi, A.H. Kokabi; *Effect of iron particle size on the diffusion bonding of Fe–5%Cu powder compact to wrought carbon steels*; Materials and Design 29 (2008) 411–417; doi:10.1016/j.matdes.2007.01.004
36. Hussain Zuhailawati, Tan Chew Geok, Projjal Basu; *Microstructure and hardness characterization of mechanically alloyed Fe–C elemental powder mixture*; Materials and Design 31 (2010) 2211–2215; doi:10.1016/j.matdes.2009.10.034
37. A. Simchi; *Effect of C and Cu addition on the densification and microstructure of iron powder in direct laser sintering process*; Materials Letters 62 (2008) 2840–2843; doi:10.1016/j.matlet.2008.01.113
38. Wincenty Czerwiński; *Mechanika techniczna dla samouków*. Cz. 1, Wyd. 2 (2 nakł. podstawowy, 1 seria). - Warszawa : Państwowe Wydawnictwa Szkolnictwa Zawodowego, 1960.
39. PN-EN ISO 6892-1:2020-05 - wersja angielska; *Metale - Próba rozciągania - Część 1: Metoda badania w temperaturze pokojowej*; Data publikacji 26-05-2020
40. Waldemar Bachmacz; *Wytrzymałość materiałów: badania doświadczalne*; Politechnika Częstochowska. - Częstochowa : [s.n.], 1970.
41. N. M. Bielajew; *Wytrzymałość materiałów*; tł. z ros. Sylwester Kaliski. - Warszawa: Wydawnictwo Ministerstwa Obrony Narodowej, 1954.
42. Thomas Kalpakoglou, Stylianos Yiatros; *Metal foams: A review for mechanical properties under tensile and shear stress;* Sec. Mechanics of Materials Volume 9 - 2022; https://doi.org/10.3389/fmats.2022.998673

43. S.M. Tahir, A.K. Ariffin; *Fracture in metal powder compaction*; International Journal of Solids and Structures 43 (2006) 1528–1542; doi:10.1016/j.ijsolstr.2005.10.010
44. Anshuman Shrivastava; 3-Plastic Properties and Testing; Introduction to Plastics Engineering; Plastics Design Library 2018, Pages 49-110; https://doi.org/10.1016/B978-0-323-39500-7.00003-42
45. Chao Cai, Kun Zhou, *Chapter 7-Metal additive manufacturing*, Digital Manufacturing, The Industrialization of Art to Part 3D Additive Printing 2022, Pages 247-298, https://doi.org/10.1016/B978-0-323-95062-6.00005-X
46. Chee Kai Chua, Chee How Wong, Wai Yee Yeong; *Chapter Eight-Benchmarking for Additive Manufacturing*; Standards, Quality Control, and Measurement Sciences in 3D Printing and Additive Manufacturing 2017, Pages 181-212; https://doi.org/10.1016/B978-0-12-813489-4.00008-8
47. U. Ramamurty, *Mechanical Testing Methods of Fibers and Composites*; Encyclopedia of Materials: Science and Technology (Second Edition) 2001, Pages 5271-5274; https://doi.org/10.1016/B0-08-043152-6/00920-7
48. https://eu1.iam.3dexperience.3ds.com/; access January 2023
49. M.R. Wisnom; *Size Effects in Composites*; Comprehensive Composite Materials Volume 5, 2000, Pages 23-47, https://doi.org/10.1016/B0-08-042993-9/00035-8
50. Donald F. Adams, Thomas J. Whitney; 7.*2 Test Methods for Mechanical Properties*; Reference Module in Materials Science and Materials Engineering Comprehensive Composite Materials II Volume 7, 2018, Pages 4-37; https://doi.org/10.1016/B978-0-12-803581-8.10032-3
51. PN-EN ISO 4506:2018-05 - wersja angielska; *Węgliki spiekane - Próba ściskania*; Published Data 28-05-2018
52. Leandro R. Alejano & Antonio Bobet; *Drucker–Prager Criterion*; Rock Mechanics and Rock Engineering volume 45, pages995–999 (2012); Published: 18 July 2012
53. Leandro R. Alejano; Antonio Bobet; *Drucker–Prager Criterion*; Rock Mech Rock Eng (2012) 45:995–999; DOI 10.1007/s00603-012-0278-2
54. T. Yua, J.G. Teng, Y.L. Wong,S.L. Dong, *Finite element modeling of confined concrete-I*: Drucker–Prager type plasticity model; Engineering Structures; Available online 4 January 2010; Elsavier

55. Dragan M. Rakić1, Aleksandar S. Bodić, Nikola J. Milivojević, Vladimir Lj. Dunić, Miroslav M. Živković; *Concrete damage plasticity material model parameters identification*; Journal of the Serbian Society for Computational Mechanics / Vol. 15 / No. 2, 2021 / pp 111-122
56. Seungwook Seok, Ghadir Haikal, Julio A. Ramirez, Laura N. Lowes, Jeehee Lim; Finite element simulation of bond-zone behavior of pullout test of reinforcement embedded in concrete using concrete damage-plasticity model 2 (CDPM2); Engineering Structures Volume 221, 15 October 2020, 110984; https://doi.org/10.1016/j.engstruct.2020.110984
57. Xian-Xing (Lambert) Li; Parametric study on numerical simulation of missile punching test using concrete damaged plasticity (CDP) model; International Journal of Impact Engineering Volume 144, October 2020, 103652; https://doi.org/10.1016/j.ijimpeng.2020.103652
58. Bahar Ayhan, Erol Lale; *Modeling strain rate effect on tensile strength of concrete using damage plasticity model*; International Journal of Impact Engineering; Volume 162, April 2022, 104132; https://doi.org/10.1016/j.ijimpeng.2021.104132
59. Ryszard Kluszczyński; *Encyklopedia Powszechna*, ISBN 83-88080-13-X; Copyright Wydawnictwo, Kraków 2001
60. Henry Bessemer, Biography, Inventions, & Facts | Britannica
61. Aleksander S. Fiodorow; *Z historii metalurgii na Uralu*; Kwartalnik Historii Nauki i Techniki 22/4, 791-798; 1977
62. P. Ramakrishnan, *Automotive applications of powder metallurgy*; Indian Institute of Technology Bombay, India; Woodhead Publishing Limited, 2013; DOI: 10.1533/9780857098900.4.493
63. K.S. Narasimhan; *Sintering of powder mixtures and the growth of ferrous powder metallurgy*; Materials Chemistry and Physics 67 (2001) 56–65; PII: S0254-0584(00)00420-X
64. Peng Zhanga, Lin Zhanga, Kangxi Fua , Jingwu Caob, Cairang Shijiab, Xuanhui Qua; *Effects of different forms of Fe powder additives on the simulated braking performance of Cu-based friction materials for high-speed railway trains*; Wear Volumes 414–415, 15 November 2018, Pages 317-326; https://doi.org/10.1016/j.wear.2018.09.006

65. Xu Ma, Chenghua Luan, Shangwu Fan, Juanli Deng, Litong Zhang, Laifei Cheng; *Comparison of braking behaviors between iron- and copper-based powder metallurgy brake pads that used for C/C–SiC disc*; Tribology International 154 (2021) 106686; https://doi.org/10.1016/j.triboint.2020.106686
66. Sintering for production of shock absorbers. https://eurobalt.net/blog/2019/05/20/sintering-in-production-shock-absorbers/
67. Marouane Benaziz, Samuel Nacivet, Fabrice Thouverez; *A shock absorber model for structure-borne noise analyses*; Journal of Sound and Vibration Volume 349, 4 August 2015, Pages 177-194; https://doi.org/10.1016/j.jsv.2015.03.034
68. Shiying Li, Jun Xu, Xiaohui Pu, Tao Tao, Xuesong Mei; *A novel design of a damping failure free energy-harvesting shock absorber system*; Mechanical Systems and Signal Processing Volume 132, 1 October 2019, Pages 640-653; https://doi.org/10.1016/j.ymssp.2019.07.004
69. John Dixon; *Shock Absorber Handbook 2e*; September 2007, ISBN: 047051020X; John Wiley & Sons Inc;
70. https://www.sciencedirect.com/topics/engineering/shock-absorber; access June 2023
71. Praca zbiorowa, *Podstawy Konstrukcji Maszyn 2, Techniki wytwarzania i maszynoznawstwo*, Wydawnictwa Komunikacji i Łączności, wydanie 1 Warszawa 2012
72. Ran Zhang, Xu Wang, Sabu John*; A Comprehensive Review of the Techniques on Regenerative Shock Absorber Systems* Received: 28 March 2018; Accepted: 3 May 2018; Published: 7 May 2018 ; Energies 2018, 11, 1167 ; doi:10.3390/en11051167
73. Shock Absorber | 3D CAD Model Library | GrabCAD; access June 2023
74. Zawieszenie kolumnowe MacPhersona | Blog motoryzacyjny (gnapackaging.it); access June 2023
75. Układ kierowniczy - usterki - AutoZawieszenie.pl - o zawieszeniu samochodowym; access June 2023
76. IATF 16949:2016; *Wymagania względem systemów zarządzania jakości dla produkcji seryjnej oraz produkcji części serwisowych w przemyśle motoryzacyjnym*; Wydanie pierwsze 2016-10-01; International Automotive Task Force

77. Pulak Agrawal, K. M. Agarwal & R. K. Tyagi; *A review on Quality Management System in Automotive Sector and ISO/TS 16949*; International Journal of Advanced Engineering Research and Applications (IJA-ERA) ISSN: 2454-2377 Volume – 2, Issue – 8, December – 2016
78. Klaus Schwab; *Czwarta rewolucja przemysłowa*; ISBN 978-83-65068-81-1; 2016 by World Economic Forum
79. Marcin Lis, Sabina Ratajczak; *Six Sigma jako metoda doskonalenia jakości przedsiębiorstw w okresie rosnącej globalizacj*i; ZN WSH Zarządzanie 2014 (2), s.45-58
80. Ankesh Mittal, Pardeep Gupta, Vimal Kumar, Ali Al Owad, Seema Mahlawat, Sumanjeet Singh; *The performance improvement analysis using Six Sigma DMAIC methodology: A case study on Indian manufacturing company*; Heliyon; Volume 9, Issue 3, March 2023, e14625; https://doi.org/10.1016/j.heliyon.2023.e14625
81. Metal Powder Industries Federation; *MPIF 10 Method for Determination of the Tensile Properties of Powder Metallurgy (PM) Materials*; Standard Test Methods for Metal Powders and Powder Metallurgy Products; 2019 edition;ISBN 978-1-943694-24-2
82. https://www.imz.pl/pl/aktualnosci/Grupa_Badawcza__Badania_Wlasciwosci_i_Struktury/Maszyna_wytrzymalosciowa_Zwick_Roell_Z250__o/[30,291,,,,]; access June 2023
83. https://www.polsl.pl/rmt4/mts-10kn/; access June 2023
84. Barski Paweł, Stanula Agnieszka, Pilarczyk Wirginia: Analiza porównawcza zastosowania metody Rockwell'a oraz Vickers'a do pomiaru twardości komponentów wytworzonych za pomocą metalurgii proszków, TalentDetector'2021 Summer: Studencka konferencja naukowa, Gliwice, 25 czerwca 2021, Bonek Mirosław (red.), Prace Katedry Materiałów Inżynierskich i Biomedycznych, Politechnika Śląska, 2021, Politechnika Śląska, ISBN 978-83-65138-28-6, s. 1-13
85. PN-EN ISO 6508-1:2016-10 - wersja polska; *Metale -- Pomiar twardości sposobem Rockwella - Część 1: Metoda badania*; Data publikacji 17-08-2018
86. https://www.innovatest-europe.com/products/verzus-710rsb/; access June 2023

87. https://industry.nikon.com/en-us/products/industrial-microscopy/industrial-microscopes/inverted-eclipse-ma200/; access June 2023
88. https://www.imz.pl/pl/aktualnosci/Grupa_Badawcza__Chemia_Analityczna___BC/Analizator_zawartosci_wegla_i_siarki_CS600_firmy/[28,211]; access June 2023
89. https://pl.leco.com/product/744-series; access June 2023
90. IC-EM - Merlin Gemini II (ZEIS) (agh.edu.pl); access 2023
91. IC-EM - Titan Cubed 2 60-300 (FEI) (agh.edu.pl); access 2023
92. https://www.oshma.com.ar/producto/cast-n-vac-1000/; access 2023
93. https://www.mt.com/; access June 2023
94. Metal Powder Industries Federation; MPIF 42 Method for Determination of Density of Compacted or Sintered Powder Metallurgy (PM) Products; Standard Test Methods for Metal Powders and Powder Metallurgy Products; 2019 edition;ISBN 978-1-943694-24-2
95. M.M. Rahman, A.K. Ariffin, S.S.M. Nor , H.Y. Rahman; *Powder material parameters establishment through warm forming route*; Materials and Design 32 (2011) 264–271; doi:10.1016/j.matdes.2010.05.058
96. Yulong An, Guoliang Hou, Jie Chen, Xiaoqin Zhao, Guang Liu, Huidi Zhou, Jianmin Chen; *Microstructure and tribological properties of iron-based metallic glass coatings prepared by atmospheric plasma spraying*; Vacuum 107 (2014) 132e140; http://dx.doi.org/10.1016/j.vacuum.2014.04.021
97. Qiang Li, Biao Guo, Xiao Li, Yu Zhang, Jie Jian, Jinqing Ao, Qifeng Tang, Yun Lu; Fracture prediction of powder metallurgical Fe-Cu-C steel at elevated temperatures via finite element-aided hot tensile tests; Journal of Materials Research and Technology Volume 12, May–June 2021, Pages 423-436; https://doi.org/10.1016/j.jmrt.2021.03.008
98. S.M. Tahir, A.K. Ariffin; *Fracture in metal powder compaction*; International Journal of Solids and Structures 43 (2006) 1528–1542; doi:10.1016/j.ijsolstr.2005.10.010
99. Danrui Ni, Robert J. Cava; *Ferrites without iron as potential quantum materials;* Progress in Solid State Chemistry 66 (2022) 100346; https://doi.org/10.1016/j.progsolidstchem.2021.100346

100. Nadezda M. Talijan, Dusan S. Trifunovic, Dejan D. Trifunovic; *The influence of different iron powders on the friction properties of sintered friction materials based on iron*; Materials Letters 46 2000 255–260; PII: S0167- 577X 00 00181-6

Literature sources related to the topic of the work and not used in the dissertation

101. Adriaan B, SpieringsMark, VoegtlinThomas, BauerKonrad Wegener *Powder flowability characterisation methodology for powder-bed-based metal additive manufacturing.* Progress in Additive Manufacturing. (July 2015*)* .DOI: 10.1007/s40964-015-0001-4.

102. A. Stanula, W. Pilarczyk, *Combined carbon content assessment method for powder metallurgy*, Journal of Achievements in Materials and Manufacturing Engineering 2022; 114 (1): 15-21

103. J.Q. Bao, X. Long, K.H. Tan, C.K. Lee; *A new generalized Drucker–Prager flow rule for concrete under compression; Engineering Structures*; Volume 56, November 2013, Pages 2076-2082; https://doi.org/10.1016/j.engstruct.2013.08.025

104. M. Neuner, P. Hofer, G. Hofstetter; *On the prediction of complex shear dominated concrete failure by means of classical and higher order damage-plasticity continuum models;*Engineering Structures Volume 251, Part B, 15 January 2022, 113506; https://doi.org/10.1016/j.engstruct.2021.113506

105. Tsukada, K. Goto, Reo H. Yamamoto 2, M. Horio; *Metal powder granulation in a plasma-spouted/fluidized bed;* Powder Technology 82 (1995) 347-353; 032-5910195/$09.50; 1995 Elsevier Science S.A. SSDI 0032-5910(94)02934-G

106. Yongquan, Xiaoqiang Li, Zhun Cheng, Minai Zhang, Shengguan Q; The influence of sintering temperature and pressure on microstructure and mechanical properties of carbonyl iron powder materials fabricated by electric current activated sintering; Vacuum 137 (2017) 137e147; http://dx.doi.org/10.1016/j.vacuum.2016.12.044

107. C.Q. Yuan, Z. Peng, X.C. Zhou, X.P. Yan; *The characterization of wear transitions in sliding wear process contaminated with silica and iron powder*; Tribology International 38 (2005) 129–143; doi:10.1016/j.triboint.2004.06.007

108. Yongjian Li, Shiyun Dong, Shixing Yan, Xiaoting Liu, Peng He, Binshi Xu; *Microstructure evolution during laser cladding Fe-Cr alloy coatings on ductile cast*

iron; Optics and Laser Technology 108 (2018) 255–264; https://doi.org/10.1016/j.optlastec.2018.07.004

109. Rocco Lupoi, William M. Abbotta, Ramsankar Senthamaraikannanb, Sean McConnell, John Connollyc, Shuo Yina, Ramesh Babu Padamati; *Metal additive manufacturing via a novel composite material using powder and polymers formed in sheets;* CIRP Annals - Manufacturing Technology 71 (2022) 181-184; https://doi.org/10.1016/j.cirp.2022.03.012
110. S. Rebeyrat, J.L. Grosseau-Poussarda,U, J.F. Dinhut, P.O. Renault; *Oxidation of phosphated iron powders*; Thin Solid Films 379 2000 139 - 146
111. Amir Hadadzadeha, Mark A. Whitneya, Mary A. Wells, Stephen F. Corbinb; *Analysis of compressibility behavior and development of a plastic yield model for uniaxial die compaction of sponge titanium powder*; Journal of Materials Processing Technology 243 (2017) 92–99; http://dx.doi.org/10.1016/j.jmatprotec.2016.12.004
112. H. Kersten , P. Schmetz, G.M.W. Kroesen; *Surface modification of powder particles by plasma deposition of thin metallic films*; Surface and Coatings Technology 108–109 (1998) 507–512; P II: S0257-8972(98)00604-5
113. Andre Mussatto, Robert Groarke, Ahmed A-Hameed, Inam U.I. Ahad, Rajani K. Vijayaraghavan, Aidan O'Neill, Patrick McNally, Yan Delaure, Dermot Brabazona; *Evaluation via powder metallurgy of nano-reinforced iron powders developed for selective laser melting applications;* Materials and Design 182 (2019) 108046; https://doi.org/10.1016/j.matdes.2019.108046
114. Hao Liua,b, Jingbin Haoa, Zhengtong Hana, Gang Yuc, Xiuli Hec, Haifeng Yanga,; Microstructural evolution and bonding characteristic in multi-layer laser cladding of NiCoCr alloy on compacted graphite cast iron; Journal of Materials Processing Technology 232 (2016) 153–164; http://dx.doi.org/10.1016/j.jmatprotec.2016.02.001
115. L.A. Dobrzanski, M. Drak; *Hard magnetic composite materials Nd-Fe-B with additions of iron and X2CrNiMo-17-12-2 steel*; Journal of Alloys and Compounds 449 (2008) 88–92; doi:10.1016/j.jallcom.2006.02.092
116. B.V. Neamţu, F. Popa, T.F. Marinca, I. Chicinaş; *Soft magnetic composites based on Fe fibres and powders prepared by cold sintering process*; Journal of Alloys and Compounds 933 (2023) 167799; https://doi.org/10.1016/j.jallcom.2022.167799

117. Jae Hoon Jeong, Seung Kyu Ryu, Seong Jin Park, Hong Chul Shin, Ji–Hun Yu; *Analysis of iron powder design for compaction process*; Computational Materials Science 100 (2015) 21–30; http://dx.doi.org/10.1016/j.commatsci.2014.11.028
118. Jaroslav Čapek, Dalibor Vojtěch; *Microstructural and mechanical characteristics of porous iron prepared by powder metallurgy*; Materials Science and Engineering C 43 (2014) 494–501; http://dx.doi.org/10.1016/j.msec.2014.06.046
119. S. Kumar, V. Selvarajan; *Plasma spheroidization of iron powders in a non-transferred DC thermal plasma jet*; Materials characterization 59 (2008) 781 – 785; doi:10.1016/j.matchar.2007.06.011
120. Yu Bian, Junjie Ni, Chao Wang, Jinming Zhen, Hongguo Hao, Xiangjin Kong, Hui Chen, Jian Li, Xiaoqiang Li, Zhengfeng Jia, Wei Luo, Zhong Chen; *Microstructure and wear characteristics of in-situ micro/nanoscale niobium carbide reinforced copper composites fabricated through powder metallurgy;* Materials Characterization 172 (2021) 110847; https://doi.org/10.1016/j.matchar.2020.110847
121. S. Kumar , Hyuntaek Na , V. Selvarajan , Changhee Lee; *Influence of metal powder shape on drag coefficient in a spray jet;* Current Applied Physics 9 (2009) 678–682; d oi:10.1016/j.cap.2008.06.005
122. Yukai Zhuang, Xiaowan Su, Nilesh P. Salke, Zhongxun Cui, Qingyang Hu, Dongzhou Zhang, Jin Liu; *The effect of nitrogen on the compressibility and conductivity of iron at high pressure*; Geoscience Frontiers 12 (2021) 983–989; https://doi.org/10.1016/j.gsf.2020.04.012
123. S.T. Huang, Y.S.Duh, T.Y. Hsieh, Y.Y. Sun, J.M. Tseng, J.Z. Lin, H-C. Wu, C.S. Kao.*; Thermal analysis for nano powders of iron and zinc by DSC;* Procedia Engineering 45 (2012) 518 – 522; doi: 10.1016/j.proeng.2012.08.196; 1877-7058; 2012 Published by Elsevier Ltd.
124. Diayn M. Dimitrov, Desislava Mincheva , Stoyan D. Slavov ; *Influence of porosity to dynamic Young's modulus of sintered iron.* Bayesian approach; Materials Today: Proceedings 59 (2022) 1677–1682; https://doi.org/10.1016/j.matpr.2022.03.399
125. Cameron Barr, Aaron Pateras, Andrey Molotnikov, David Clarke, Milan Brandt; *Effect of composition on the tensile and corrosion performance of nickel aluminium bronze produced via laser powder bed Fusion*; Additive Manufacturing 54 (2022) 102771; https://doi.org/10.1016/j.addma.2022.102771

126. Shehdeh Ghannam, Husam Najm, Rosa Vasconez; Experimental study of concrete made with granite and iron powders as partial replacement of sand; Sustainable Materials and Technologies 9 (2016) 1–9; http://dx.doi.org/10.1016/j.susmat.2016.06.001
127. Kun Yue, Guofu Lian, Jiayi Zeng, Changrong Chen, Ruqing Lan, Linghua Kong; *An investigation on graphite behavior and coating properties in the molten pool based on different powder particle sizes;* Heliyon 9 (2023) e14222; https://doi.org/10.1016/j.heliyon.2023.e14222
128. Y akovleva S.P, Makharova S.N., Vasilyeva M.I., Ptitsyna A.V.; *Wear resistance factors of diamond-metal powder systems, obtained by explosive compaction*, Procedia Structural Integrity 20 (2019) 190–197; 2019 Published by Elsevier B.V
129. Anton Zhukova, Boris Barakhtina , Ivan Shakirova , Vitaliy Bobyra , Pavel Kuznetsova; *The Structure of Iron Powder Aggregation Obtained by Selective Laser Melting;* Procedia Structural Integrity 23 (2019) 305–309
130. Z. He, F. Xiong, S. Tan, X. Yao, C. Zhang, Q. An; *Iron metal anode for aqueous rechargeable batteries;* Materials Today Advances 11 (2021) 100156; https://doi.org/10.1016/j.mtadv.2021.100156
131. Mikhail S. Vlaskin, Anatoly V. Grigorenko, Alexander A. Gromov d , Vinod Kumar , Alexander O. Dudoladov, Olga V. Slavkina, Viktor I. Darishchev; *Methane pyrolysis on sponge iron powder for sustainable hydrogen production*; https://doi.org/10.1016/j.rineng.2022.100598
132. Govind S. Guptaa, S. Sarkarb, A. Chychkoc, L.D. Tengd, M. Nzottae and S. Seetharamand; *Process Concept for Scaling-Up and Plant Studies;* Treatise on Process Metallurgy, Volume 3; 2014 Elsevier Ltd.; http://dx.doi.org/10.1016/B978-0-08-096988-6.00040-7
133. Fredrik Persson, Christopher Neil Hulme, Par G. Jonsson, *Particle morphology of water atomised iron-carbon powders,* Powder Technology, Volume 397, January 2022, 116993; https://doi.org/10.1016/j.powtec.2021.11.037
134. P.Lindskog, P. Arbstedt; Iron Powder Manufacturing Techniques: A Brief Review; pages 14-19, Published online: 19 Jul2013; https://doi.org/10.1179/pom.1986.29.1.14

List of figures

List of tables

Agnieszka Stanula

Streszczenie

Celem naukowym rozprawy doktorskiej jest zbadanie wpływu składu chemicznego materiałów proszkowych, Fe-C, Fe-C-Cu na właściwości mechaniczne elementów spiekanych.

Na podstawie sformułowanej tezy określono następujące cele wdrożeniowe rozprawy:

1. Dobór materiału proszkowego w celu wyznaczenia właściwości wytrzymałościowych elementów spiekanych.
2. Redukcja dużej ilości badań prowadzonych w laboratorium poprzez zbudowanie odpowiedniej bazy wiedzy naukowej, oraz weryfikacja wdrażania nowych produktów.
3. Koncepcja *Digital Twin* – porównanie parametrów rzeczywistych i literaturowych użytych do analizy elementów skończonych MES.
4. Stworzenie odpowiedniego stanowiska badawczego w celu badania gęstości elementów spiekanych.

Zakres tematyczny rozprawy doktorskiej, w tym określenie problemu badawczego, obejmuje zdefiniowanie zależności pomiędzy zawartością miedzi i węgla a parametrem gęstości dla elementów spiekanych będących podzespołem zawieszenia pojazdu. Stosując odpowiedni skład chemiczny oraz proces technologiczny istnieje możliwość znalezienia zależności pomiędzy składem chemicznym, gęstością a właściwościami mechanicznymi komponentów (wytrzymałość na rozciąganie oraz ściskanie, granica plastyczności, wydłużenie oraz twardość).

Badania metalograficzne dostarczają informację o wpływie pęknięcia w elemencie spiekanym na potencjalną awarię w całym zawieszeniu samochodu. Obliczenie oraz określenie strat węgla w procesie produkcyjnym umożliwia obniżenie kosztów produkcji.

Zakres badań naukowych wymaga sprawdzenia:

1. Właściwości materiałów proszkowych
2. Struktury wytworzonych elementów spiekanych
3. Właściwości mechanicznych elementów spiekanych

W tym celu użyty został mikroskop optyczny, skaningowy oraz transmisyjny mikroskop elektronowy. Badania właściwości mechanicznych wymagają sprawdzenia twardości, wytrzymałości na rozciąganie i ściskanie oraz gęstości.

Wyniki prób ściskania oraz rozciągania były rozproszone z racji porowatości materiału. Aby określić zależności danych i wyników rozdzielono badania na analizę elementów spiekanych z materiału proszkowego 22 oraz analizę elementów spiekanych z pozostałych materiałów proszkowych Fe-C-Cu i Fe-C.

Symulacja prób wytrzymałościowych oraz szeroki zakres badań umożliwiły opracowanie bazy materiałowej.

Słowa Kluczowe: metalurgia proszków, konwencjonalna metoda spiekania, gęstość, właściwości mechaniczne

Agnieszka Stanula

Abstract

The scientific objective of the doctoral dissertation is examination of the impact of the influence of the chemical composition of iron-based powder materials, as Fe-C, Fe-C-Cu on the properties of sintered components.

Based on the formulated research postulate, the following implementation goals of the dissertation were determined:

1. selection of powder material to determine the strength properties of sintered components
2. reduction of large research amounts under laboratory conditions by the development of an appropriate scientific knowledge base and verification of the implementation of new powder metallurgy products
3. the Digital Twin concept - a comparison of real and literature parameters used for the finite element analysis (FEA)
4. design and construction of a suitable test stand to study the density of sintered components.

The thematic scope of the dissertation, including the definition of the research topic, includes defining the relationship between copper and carbon content and the density parameter for sintered components that are components of vehicle suspension. Using the right chemical composition and a technological process, it is possible to find relationships among the chemical composition, density and mechanical properties of the components (tensile and compression strength, yield strength, elongation and hardness).

Metallographic studies carry information about the effects of a crack in a sintered component on a potential failure in the entire car suspension system. Production costs may be reduced by the calculation and determination of carbon losses in the production process.

The scope of scientific studies requires verification of the following issues:

4. the properties of powder materials
5. the structures of manufactured sintered components
6. the mechanical properties of sintered components

For that purpose, an optical microscope, a scanning and a transmission electron microscope were used. Studies of mechanical properties require hardness, tensile and compressive strength tests and density.

The results of the compression and tensile tests were scattered due to material porosity. In order to determine the relationship of data and results, the tests were separated into the analysis of sintered components from powder material 22 and the analysis of sintered components from the other powder materials, i.e. Fe-C-Cu and Fe-C.

Strength test simulations and a wide range of tests made it possible to establish a material base.

Key words: powder metallurgy, conventional sintering process, hardness, mechanical propertiest

Agnieszka Stanula

List of achievements

Publikacje

1. Stanula Agnieszka, Pilarczyk Wirginia: Combined carbon content assessment method for powder metallurgy, Journal of Achievements of Materials and Manufacturing Engineering, International OCSCO World Press, vol. 114, nr 1, 2022, s. 15-21, DOI:10.5604/01.3001.0016.1479, 70 punktów

2. Stanula Agnieszka, Pilarczyk Wirginia: Konwencjonalna metoda spiekania materiału FC-0208, W: TalentDetector2022_Winter : Międzynarodowa Studencka Konferencja Naukowa, Gliwice, styczeń, 2022. T. 2 / Bonek Mirosław (red.), Prace Katedry Materiałów Inżynierskich i Biomedycznych, 2022, Politechnika Śląska, ISBN 978-83-65138-31-6, s. 711-723, 20 punktów

3. Stanula Agnieszka, Pilarczyk Wirginia: The correlation of the results after the static compression test for FC-0208 material sintered with the conventional method, W: Międzynarodowa konferencja naukowa Material Technologies in Silesia'2022, 12-15 czerwca 2022, Wisła / Bonek Mirosław (red.), 2022, Politechnika Śląska, ISBN 978-83-65138-32-3, s. 169-170

4. Barski Paweł, Stanula Agnieszka, Pilarczyk Wirginia: Analiza porównawcza zastosowania metody Rockwell'a oraz Vickers'a do pomiaru twardości komponentów wytworzonych za pomocą metalurgii proszków, W: TalentDetector'2021 Summer : Studencka konferencja naukowa, Gliwice, 25 czerwca 2021 / Bonek Mirosław (red.), Prace Katedry Materiałów Inżynierskich i Biomedycznych, Politechnika Śląska, 2021, Politechnika Śląska, ISBN 978-83-65138-28-6, s. 1-13, 20 punktów

5. Stanula Agnieszka, Pilarczyk Wirginia: In which situation to use transverse rupture strength or tensile properties in powder metallurgy, W: TalentDetector'2021 Summer : Studencka konferencja naukowa, Gliwice, 25 czerwca 2021 / Bonek Mirosław (red.), Prace Katedry Materiałów Inżynierskich i Biomedycznych, Politechnika Śląska, 2021, Politechnika Śląska, ISBN 978-83-65138-28-6, s. 494-499, 20 punktów

6. Stanula Agnieszka, Pilarczyk Wirginia, Wilk T., Villamana J.: A selection of methods to check the combined porosity control, W: Interdyscyplinarne Badania Młodych Naukowców / Bonek Mirosław [i in.] (red.), Prace Katedry Materiałów Inżynierskich i Biomedycznych,

Politechnika Śląska, 2020, Politechnika Śląska, ISBN 978-83-65138-26-2, s. 116-121, 20 punktów

7. Stanula Agnieszka, Pilarczyk Wirginia,Jager M., Wilk Tomasz: The influence of technological parameters as the handling and sintering process on the structure of iron based powders, W: METAL 2020 : 29th International Conference on Metallurgy and Materials, May 20-22, 2020, Brno, Czech Republic. Conference proceedings, Metal, 2020, Tanger, ISBN 978-80-87294-97-0, s. 880-885, DOI:10.37904/metal.2020.3626, 5 punktów

Udział w konferencjach:

1. III seminarium naukowo-techniczne " Materiały dla motoryzacji" organizowanym przez Wydział Inżynierii Materiałowej Politechniki Śląskiej, Katowice 22 styczeń 2020
2. 60. Międzynarodowa Konferencja Naukowa „Krzepnięcie i Krystalizacja Metali 2020" PAN (Polska Akademia Nauk) Komisja Odlewnictwa, Sekcja Metalurgiczna Komitetu Inżynierii Materiałowej i Metalurgii", Konferencja online 29-30.09.2020
3. TalentDetector 2021; Studencka Konferencja Naukowa; Katedra Materiałów Inżynierskich i Biomedycznych, Wydział Mechaniczny Technologiczny, Politechnika Śląska, Styczeń 2021
4. TalentDetector 2021 Summer; Studencka Konferencja Naukowa; Katedra Materiałów Inżynierskich i Biomedycznych, Wydział Mechaniczny Technologiczny, Politechnika Śląska, 25 czerwca 2021
5. 1st Interdisciplinary Annual PhD Conference on Material Science and Innovative Technologies InterMTS 2022; Kraków, 19-20 May 2022. Wystąpienie na konferencji: Agnieszka Stanula, Wirginia Pilarczyk, "*Structure of material Fe-C after SPS (Spark Plasma Sintering) process technology"*; ISBN 978-83-957026-4-8;
6. The 6th Stanisław Gorczyca European School on Electron Microscopy and Tomography; 12-15 July 2022, Kraków, Poland. Wystąpienie na konferencji: Agnieszka Stanula, Wirginia Pilarczyk *"SEM observation after static compression";*
7. Międzynarodowa konferencja naukowa Material Technologies in Silesia'2022; ISBN 978-83-65138-32-3; Wydawnictwo Politechnika Śląska. Wystąpienie na konferencji: Agnieszka Stanula, Wirginia Pilarczyk *"The correlation of the results after the static compression test for FC-0208 material sintered with the conventional method"*

8. APMME 2023 Applications of Physics in Mechanical and Material Engineering; Wystąpienie na konferencji: Agnieszka Stanula, Wirginia Pilarczyk, Sebastian Raczek, Mark Jager *"The compression test results for iron-based sinter component"*

Zgłoszenia patentowe:

1. *Powder Metallurgy material and method for producing the same* (nr P.441597), zgłoszenie o wynalazek złożone 29.06.2022r.

Nagrody i wyróżnienia:

1. Grant Projakościowy, będący wsparciem dla osób rozpoczynających działalność naukową w nowej tematyce badawczej pn" " Dostosowanie nowoczesnych metod spiekania do materiału zdefiniowanego"

2. Grant Projakościowy w kursie Nature Masterclasses w programie wspierającym zwiększenie zdolności młodych naukowców w zakresie publikowania w wysoko punktowanych czasopismach oraz ubiegania się o prestiżowe projekty międzynarodowe